On the lifetime of the First Mirrors in the diagnostic systems of the International Thermonuclear Experimental Reactor

Inauguraldissertation

zur
Erlangung der Würde eines Doktors der Philosophie

vorgelegt der
Philosophisch-Naturwissenschaftlichen Fakultät
der Universität Basel

von
Gregory De Temmerman
aus Tourcoing (France)

Basel, 2006

Genehmigt von der Philosophisch-Naturwissenschaftlichen Fakultät
auf Antrag von

Prof. Peter Oelhafen
Dr. Matej Mayer

Basel, den 16.10.2006

Dekan Prof. Dr. Hans-Peter Hauri

"If you want to look at someone's soul,
you have to look at their dreams."
E. Kusturica

Contents

Acknowledgements

It is always hard to write down acknowledgements on the paper, since it relates to something very personal. This part is not present in the text because it has to, but because I wish to. This work is the results of the collaborations (I would never have dreamt of so many...) with several top-leading institutions in this field which explains the length of this section.

First of all, I would like to thank Pr. Peter Oelhafen for giving me the opportunity to carry out this thesis. The initial subject of the thesis was not focused on mirrors but I had the freedom to make the initial direction evolve.

There are people that has (directly or indirectly) the power of communicating their passion and their enthusiasm taking you in their wake. I shall never forget the day I met Richard Pitts, when I gave a seminar in Lausanne shortly after the beginning of this work, and how it changed the way this work was going. His broad knowledge of the field and his ever-growing enthusiasm were a good example all along this thesis. Moreover he always found time on his extremely busy schedule to help me taking the good decisions for my personal future. I am also very thankful to Marek Rubel for all the efforts he made to include me in the mirror experiment at JET. Moreover, experiments in PISCES-B would never have been possible without him selling myself to the people there.

I shall not forget Andrey Litnovsky and the numbers of emails and phonecalls we exchanged to discuss experiments or exchange ideas about what happened to our mirrors... I can't remember how many parcels with mirrors I received from Jülich and the time I spent in a dark cellar to characterize them. I am also grateful to Peter Wienhold who initiated the mirror experiments in TEXTOR and kept his expert eye on what we were doing helping us with many useful comments.

I was given the opportunity of both visiting California and making experiments in PISCES-B by the combined efforts of Marek Rubel, Alberto Loarte and Russ Doerner. I spent there a unforgettable time coming back with a nice suntan as well as interesting results. Special thanks to Russ Doerner, Matt Baldwin and Tyler Lynch who did that this stay was going so smoothly. I shall of course not forget the barbecues organized on fridays behind the lab...

I would like to thank all the people I worked with during the past few years: Dmitry Rudakov, Manfred Lipa, Paul Coad, Guy Matthews, Daniel Matthys, ...

My special thanks also go to the members of the ESCA group in Basel: Teresa, Iris, Andriy, Laurent, Martin, Michael, Roland for the good working atmosphere. In particular I am very grateful to Teresa for the careful reading of the manuscript.

I also would like to associate my parents to this work, because without their support during my studies, none of the present work would have been possible.
I have the great chance of sharing my life with an exceptional woman, she has always been there when times got rough being always supportive and patient. I know how the redaction period was stressful for me and how difficult I should have been. I think this is fair to dedicate this work to her.

Abstract

Plasma diagnostic systems will be necessary tools for the future success of the International Thermonuclear Experimental Reactor (ITER) both to better understand the physics involved in magnetically confined burning plasma and for the protection of the device in case of disruptions etc. In contrast to conditions in today's tokamaks, a high level of radiation and neutrons is expected in ITER. To reduce the extent of the possible neutron leakage and to protect the optical components (windows, fibres) from the radiations it was proposed that the light of the plasma should be transmitted by mirror optics to diagnostics through a labyrinth embedded in shielding material.

The first elements of the plasma diagnostic systems in ITER will therefore be metallic mirrors called "First Mirrors". Being the closest element to the hot confined plasma they will suffer from intense radiation, from bombardment by energetic particles and possible deposition of impurities eroded from the plasma-facing components. They will have to maintain the required optical properties despite these extreme conditions. The question of the lifetime of these first mirrors (i.e. how long will they maintain their optical properties) is thus of the highest importance because any change in the reflectivity of the first mirror will affect the reliability of the spectroscopic or laser signal and thus the reliability of the diagnostic system.

The objective of this thesis was to improve the understanding of the effects of the plasma-wall interactions in a tokamak (material erosion, migration, and redeposition) on the optical properties of in-vessel metallic mirrors, with a view towards the parameters which may be optimized to extend their lifetime. This was achieved by a thorough participation in the mirror experiments carried out in several tokamaks (Tore Supra, TCV, TEXTOR, DIII-D and JET) through detailed optical and surface characterizations of the mirrors before and after their exposure, and by dedicated laboratory experiments.

Several important conclusions have been derived from these experiments. Under erosion conditions, the progressive increase in the surface roughness (due to the appearance of the crystallographic grains) results in a progressive decrease of the mirror reflectivity. To prevent such effects, the mirror crystallography should ensure that the roughness will always remain negligible in comparison with the wavelength of the light. This may be achieved in two different ways: either by using single crystal mirrors or by manufacturing the mirror in the form of a nanocrystalline coating (Rh or Mo) on a polished metallic substrate.

For mirrors located in deposition dominated areas (in the divertor for example), deposition of impurities on the mirror surface will lead to drastic changes of the reflectivity. The carbon deposition rate observed on the mirrors exposed in the DIII-D ($\sim$2 nm$\cdot$s^{-1}) divertor gives an idea of the extent of the problem. Carbon is expected to be the main impurity deposited on

mirrors located in areas remote from the plasma due to its long range migration. Mitigation of the carbon deposition has been achieved by heating the mirrors to about 200°C. This is a very promising result because such temperature is relatively moderate. However for mirrors in direct line-of-sight from the plasma, deposition of beryllium should also be taken into account. According to the experiments made in the PISCES-B linear device, deposition of Be containing layer will significantly modify the mirror reflectivity. Moreover, even if deposition of carbon can be mitigated during the co-deposition of Be and C, deposition of Be is not affected by the mirror temperature. The possible diffusion of beryllium in the mirror material (enhanced by the temperature) may complicate the possible in-situ cleaning of the mirrors.

Results from experiments made in Tore Supra, TCV, and in a laboratory stand in Basel have shown that the substrate material plays a role in determining the importance of the erosion/deposition mechanisms affecting the mirror reflectivity. In TCV, the deposition rate of carbon was found to be lower on a high-Z material (Mo) than on a low-Z material (Si). This may be explained by enhanced re-sputtering of the deposited carbon due to a higher particle reflection coefficient on Mo. From experiments made in Tore Supra and in Basel, it was observed that under simultaneous bombardment with deuterium and carbon, the sputtering of copper mirrors was enhanced by the presence of carbon. This leads to an anomalous effective sputtering yield for copper. Numerical simulations with the Monte Carlo code TRIDYN have shed some light on the results observed for molybdenum, stainless steel and silicon samples. However, such an approach failed to reproduce the phenomena observed for copper. It seems therefore quite likely that the chemistry of copper towards carbon plays a role in the observed increase erosion when carbon is present in the plasma.

Part I

First mirrors for nuclear fusion diagnostic systems

Chapter 1

Nuclear fusion

The world's economic growth over the past century has relied on the assumption of unlimited fossil fuels reserves for energy production. The current surge in oil prices and the growing concern about the exhaustion of the available resources [1] associated with the pollution (Greenhouse effect,...) resulting from the intensive use of such fuel have raised the necessity of modifying our relation towards energy. Improvements have been made in the efficiency of energy production but they are restricted by thermodynamic limitations (Carnot efficiency for example). An emerging fringe of economists see a possible solution in a radical change of our economic model [2] (economic degrowth), which is very unlikely to happen globally on a reasonably short timescale. Moreover, even the most optimistic forecasts [3] foresee a global increase of the world energy consumption.

A unique scenario for replacing the current dependency on fossil fuels does not exist. Different options are being considered (solar and wind energy, new generation of nuclear fission reactors,...) and may constitute what will be the future energy mix. Amongst these different approaches, nuclear fusion appears to be an attractive solution.

1.1 Basic principles

The fundamental idea driving the research in nuclear fusion is to reproduce on earth what makes stars shine. Basically nuclear fusion is the process by which 2 nuclei join together to form a heavier nucleus. This reaction is accompanied by a release of kinetic energy according to the equivalence between mass and energy formulated by Einstein. However, a substantial energy barrier arising from the mutual repulsion due to the positive charges of the nuclei, must be overcome for fusion to occur. The most accessible fusion reactions occur with isotopes of hydrogen because they only contain one single positive charge thus reducing the Coulomb barrier to be overcome. Eq. 1.1 shows the different fusion reactions possible with isotopes of hydrogen. In all cases, the fusion reaction results in the production of an energetic neutron. In

brackets are indicated the energy released by the given reaction.

$$\begin{aligned} D^2 + D^2 &\longrightarrow He^3 + n^1(+3.272\ MeV) \\ D^2 + D^2 &\longrightarrow T^3 + H^1(+4.03\ MeV) \\ D^2 + T^3 &\longrightarrow He^4 + n^1(+17.6\ MeV) \\ D^2 + He^3 &\longrightarrow He^4 + H^1(+18.3\ MeV) \end{aligned} \tag{1.1}$$

Fig. 1.1 shows the cross sections of the fusion reactions listed in eq. 1.1 as a function of the deuteron energy. As seen, the D-T reaction is the most attractive due to a higher reaction cross-section (i.e. a higher reaction probability) and a lower energy required to make the reaction possible. This is thus the reaction envisaged for a fusion reactor.

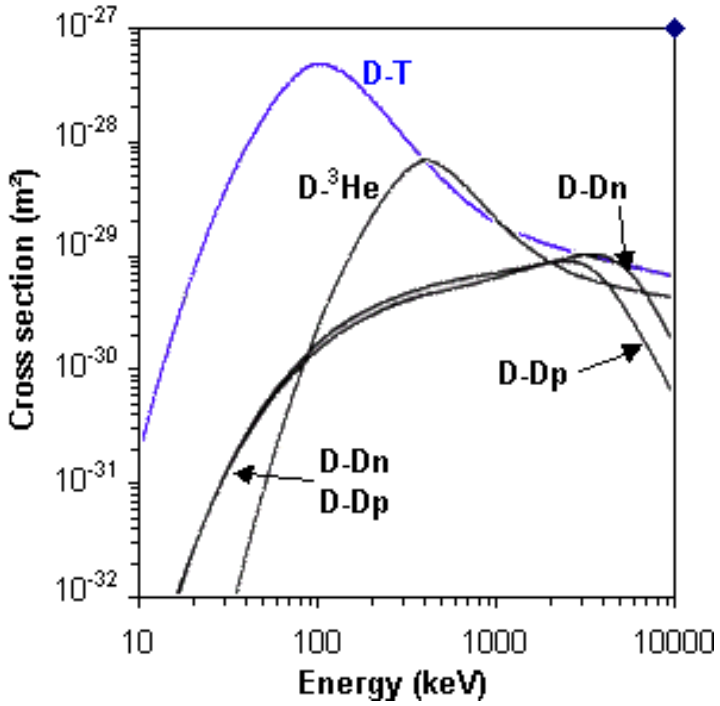

Figure 1.1: Cross section of different fusion reaction as a function of the deuteron energy

At the very high temperatures (about 10 keV) required for fusion reactions, the fuel (the mixture of deuterium and tritium) is fully ionized. The electrostatic charge of the nuclear ions is neutralized by the presence of an equal number of electrons and the resulting quasi-neutral gas is called a plasma.

The neutrons produced by the fusion reactions leave the plasma without interactions whereas the α particles (He^{2+}), which are charged, transfer their 3.5 MeV energy to the plasma through collisions and thus contribute to the heating of the plasma.

In a fusion reactor a continuous loss of energy is expected (due to radiation for example), the rate of energy loss, P_L, is characterized by an energy confinement time τ_E defined by the equation:

$$P_L = \frac{W}{\tau_E} \tag{1.2}$$

where W is the total energy of the plasma. The confinement time is the characteristic time the plasma would need to evacuate its whole energy due to losses only. So, if P_H is the additional power supplied by external heating to compensate the losses, the overall power balance can be written in the form:

$$P_L = P_H + P_\alpha \tag{1.3}$$

where P_α is the total α-particle heating. A measure of the efficiency of the reactor is given by the ratio, Q, of the thermonuclear power produced to the heating power supplied:

$$Q = \frac{P_\alpha}{P_H} \tag{1.4}$$

Break-even is reached when $Q = 1$. When the energy losses are entirely compensated by the energy provided by the α-particles without the need of additional heating ($P_{add} = 0$), i.e. when $Q \to \infty$, the *ignition* point is reached and the plasma is self-sustained.

The conditions for reaching ignition are described by the Lawson criterion [4], which is expressed in eq. 1.5 for a temperature of 10 keV:

$$n\tau_E \geq 10^{20}\ m^{-3}s \tag{1.5}$$

where n and τ_E are the plasma density and energy confinement time respectively. Two different approaches may lead to the satisfaction of the Lawson criterion:

- *magnetic confinement* working at low density ($\sim 10^{20}$ m^{-3}) and trying to obtain relatively long energy confinement time ($\sim$ 1 s) with a strong magnetic field ($\sim$ 5 T). This is the method currently envisaged for a fusion reactor, and will be described more in the next section.

- *inertial confinement* which works with extremely low energy confinement time ($\sim 10^{-11}$ s) and should therefore reach very high densities ($\sim 10^{31}$ m^{-3}) by compressing strongly the fuel with intense laser radiation. This approach is more oriented towards military applications (Laser Mégajoule in France for example).

1.2 Magnetic confinement: the tokamak

The term tokamak is a transliteration of a russian word meaning "toroidal chamber in magnetic coils". The tokamak [5] consists of a toroidal vacuum vessel inside which a strong toroidal magnetic field is generated by external poloidally wound magnetic coils (fig. 1.2). However, this field alone is insufficient to confine the plasma. Because of the toroidal geometry, the toroidal field (B_T) is not uniform within the major radius (R) of the tokamak ($B_T \propto R^{-1}$). The resulting $\bigtriangledown \mathbf{B} \times \mathbf{B}$ drift separates ions and electrons, thus producing a vertical electric field which leads to an outward collective motion of both the ions and electrons ($\mathbf{E} \times \mathbf{B}$ drift) making the plasma unstable. To prevent this, the magnetic field should be helical which is achieved by adding to the toroidal field a poloidal magnetic field produced by the plasma current itself. The plasma current is driven by transformer action using a solenoid passing through the torus

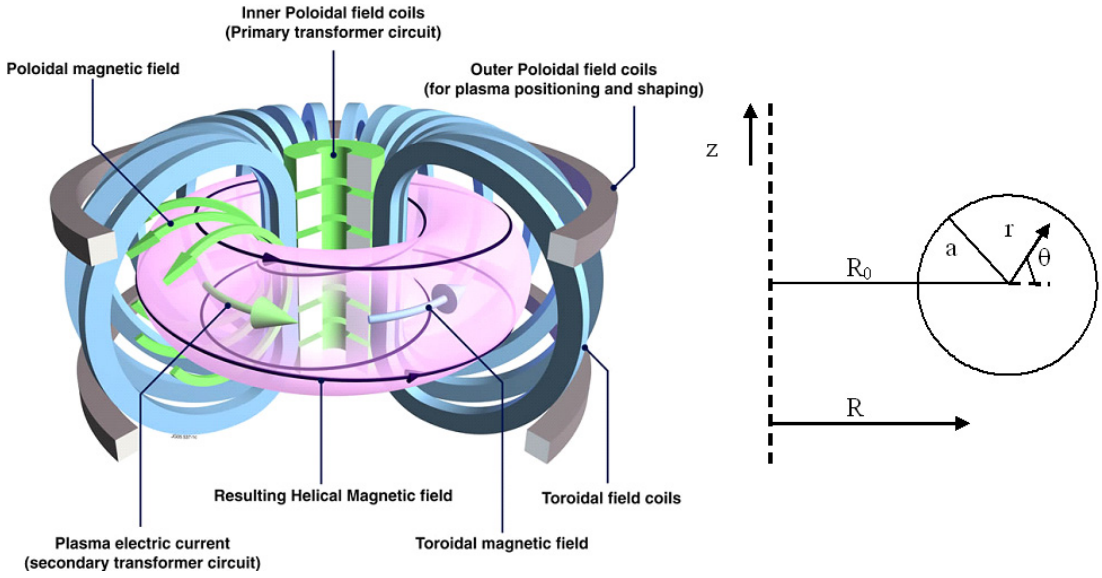

Figure 1.2: Schematic view of a tokamak. R_0 and a are the tokamak major and minor radius respectively.

centre as primary and using the plasma as secondary. Control of the plasma shape and position requires additional coils located at suitably placed positions.

As seen in chapter 1.1, it is necessary to bring the fuel mixture to very high temperature for fusion reactions to occur. In all tokamaks the initial heating comes from the ohmic heating generated by the plasma current. As the temperature increases, the collision frequency increases and the resistivity of the plasma falls, reducing the efficiency of the ohmic heating, hence the necessity of additional heating systems. Amongst the different methods envisaged, are the injection of energetic neutral beams and the resonant absorption of radio-frequency electromagnetic waves.

In present machines, magnetic fields of up to 5 T are produced either by normal coils or by superconducting coils. Plasma currents up to 7 MA have been produced in the JET tokamak.

1.3 Limiter and divertor

Hitherto we have not considered the strong interactions arising between the very hot plasma and the immediately surrounding material that constitute the plasma chamber. Ions, electrons and radiation from the plasma are incident on the surrounding material surfaces, heating them and producing neutral atoms and molecules of plasma and wall materials which return to the plasma and which both dilute and cool the plasma fuel.

Two different approaches exist to minimize and control the plasma material interactions in a tokamak. The first option is to materially limit the plasma radius by inserting a so-called *limiter* in the vacuum vessel (fig. 1.3). The limiter defines the *Last Closed Flux Surface* (LCFS), which is the boundary between the core plasma where all magnetic surfaces close back on themselves and the *Scrape-Off Layer* (SOL) plasma where field lines are open and

terminate on the surrounding material structures (called first wall). The other possibility to define the LCFS is to employ an external magnetic coil generating a current parallel to the plasma current. This parallel current results in the creation of an *X-point* where the poloidal magnetic field vanishes. This diverts the poloidal field lines, hence the name *divertor* (fig. 1.3), to toroidally symmetric plates: the divertor targets. A compressed tutorial on edge plasma physics can be found in [6], only some basic notions necessary for this work will be outlined here.

By definition, a limiter is very close to the confined hot plasma; the plasma-surface interaction being localized to the leading edge of the limiter. The limiter can therefore suffer from severe heating, melting and erosion. Moreover, the proximity to the confined plasma implies that any impurities released from the limiter can easily penetrate into the plasma and contaminate the core. When entering in the core plasma, the impurities can cool it down by radiation which is to be avoided to favour fusion reactions. Some modern tokamaks still use the limiter configuration like TEXTOR (Germany) and Tore Supra (France).

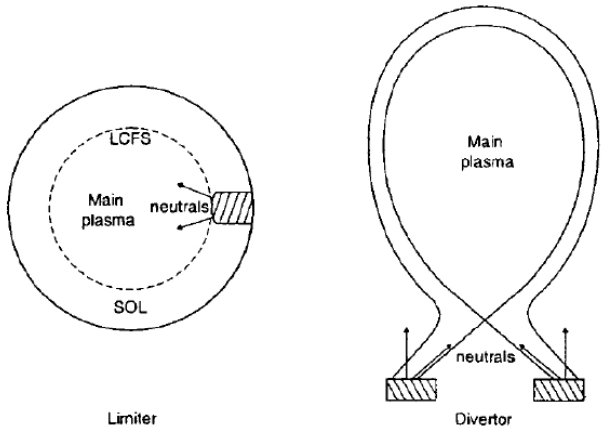

Figure 1.3: Poloidal cross-sections of a tokamak illustrating the limiter (left) and divertor (right) configurations (from [6])

Most modern tokamaks favour the divertor configuration, where the LCFS is defined solely by the magnetic field and plasma-surface interactions are localized near the divertor target plates (fig. 1.4). The impurities released from the target are ionized and may be swept back to the target by the plasma flow before they can enter the confined plasma. The region below the X-point and inside the separatrix is called the *Private Flux Region*, it contains a thin layer of plasma lying along the two separatrix arms and terminating at the target. The objectives of a divertor design are to:

- minimize the impurity content of the plasma by maintaining the plasma surface-interactions remote from the confined plasma, and preventing any impurities produced at the target to enter the confined plasma (by the divertor particle flow),

- remove the alpha particle power by heat transfer through a solid surface to a cooling fluid,

- produce a high helium neutral density region to ease exhaust of the helium ashes produced by the fusion reactions.

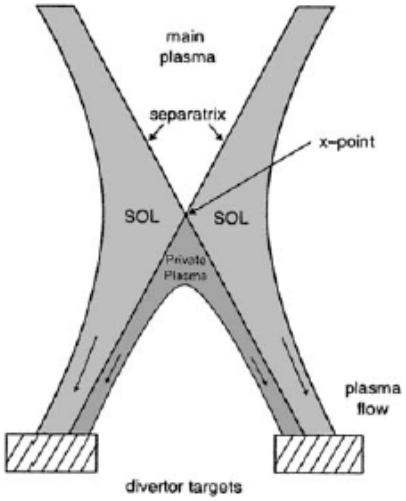

Figure 1.4: SOL and Private Flux Region (PFR) in a divertor configuration (from [6])

Due to the localization of the plasma-surface interactions near the target plates, erosion of the target surface, as well as significant power deposition on the target plates, can occur and be a serious problem for their lifetime. A possible approach to reduce this problem is to produce a "detached divertor plasma". For sufficiently high plasma density (which depends on the power input), a drop of the plasma temperature near the targets is observed. Temperature can drop low enough for electron-ion recombination to become important, thus removing charged particles and extinguishing locally the plasma flow. This is usually accompanied by a significant decrease in the incident power to the targets and plasma flux density.

Another advantage of the divertor configuration is the easier accessibility of a high confinement regime known as *H-mode*, discovered on the ASDEX tokamak in 1980's [7], occuring beyond a certain regime in heating power. In this mode, the energy confinement time is approximately 2 times higher than in the normal *L-mode* or "low confinement" regime. The majority of present large tokamaks are operating with a divertor configuration: DIII-D (USA), JET (UK), ASDEX-Upgrade (D), TCV (CH). It should be noted that most divertor tokamaks begin the plasma discharges by a limiter phase during which the current is ramped up, only after this phase is the diverted configuration established. The duration of this limiter phase depends on the machine but is likely to be about 100 s in a next-step device like ITER.

1.4 ITER

Most present tokamaks operate with deuterium fueled discharges because of the safety constraints associated with the use of tritium. However two large tokamaks, JET and TFTR (USA), were designed to study plasma operations with a fuel mix of deuterium and tritium.

Using a 1:1 ratio of tritium to deuterium, they both produce significant fusion power [8]. In TFTR, 10.7 MW of fusion power were produced with a fusion gain amounting to $Q \approx 0.27$ [9]. An extended phase of D-T operations was carried out at JET in 1997, 16.1 MW were produced from fusion reactions for a corresponding gain of $Q \approx 0.62$ [10]. Although these results represent a real breakthrough showing the possibility of substantial fusion reaction rated in a magnetically confined plasma, the Q ratio attained during these experiments are not sufficient to reach the break-even and very far from what would be necessary for a commercial reactor. Experimental scaling laws [11] have shown the dependency of the energy confinement time to (amongst other parameters) the size and aspect ratio of the tokamak. The possibility of producing energy from fusion at an industrial scale requires therefore a significant jump in terms of machine performances.

In November 1985, Premier Gorbachov of USSR, following discussions with President Mitterand of France, proposed to President Reagan of USA that an international project be set up to develop fusion energy for peaceful purposes. The ITER-project subsequently began as a collaboration between the former Soviet Union, the USA, the European Union and Japan. ITER is the acronym for International Thermonuclear Experimental Reactor, which also means "the way" in latin. The main goal of ITER is to demonstrate the scientific and technologic feasibility of energy production by fusion reactions. ITER should accomplish this objective by demonstrating high power amplification ($Q \geq 10$) and extended burn of deuterium-tritium plasmas ($\approx$ 500 s),with steady-state as an ultimate goal, by demonstrating technologies essential to a reactor in an integrated system, and by performing integrated testing of the high-heat-flux and nuclear components required to utilise fusion energy for practical purposes. The main parameters of ITER are listed in fig. 1.5. ITER should both demonstrate high plasma per-

Total fusion power	500 MW
Q - fusion power/additional heating power	$\geq$10
Average 14 MeV neutron wall loading	0.57 MW/m^2
Plasma inductive burn time	$\geq$ 400 s
Plasma major radius (R)	6.2 m
Plasma minor radius (a)	2.0 m
Plasma current (I_P)	15 MA
Toroidal field @ 6.2 m radius	5.3 T
Plasma volume	873 m^3
Plasma surface	678 m^2
Installed auxilliary heating/current drive power	73 MW

Figure 1.5: Main parameters of ITER as defined in [11]

formance with extended burn and elevated gain, but also test the availability and integration of essential fusion technologies and test the components for a future reactor (like the tritium breeding blanket) [12]. A schematic view of the ITER tokamak is shown in fig. 1.6, as well as a comparison of the plasma cross sections of ITER and present tokamaks, as seen JET, which is the world's largest tokamak, is barely two times smaller than ITER.

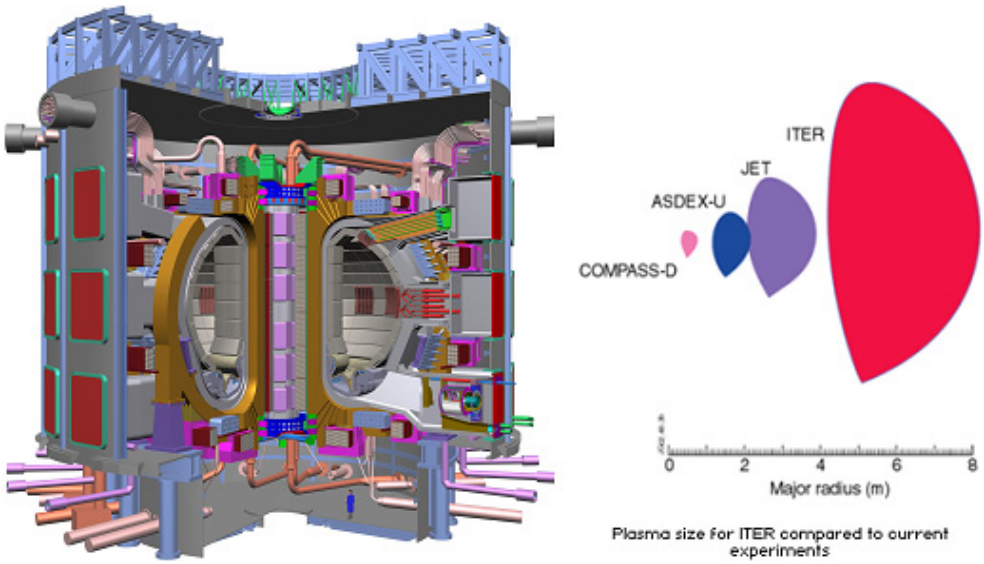

Figure 1.6: Schematic cutaway of the ITER tokamak and comparison of the expected ITER plasma cross section to that of present tokamaks.

The current participants to the project are the European Union (plus Switzerland), the USA, Japan, China, Russia, Korea and India (which joined the project in 2005). The total estimated costs for the projects amount to 10 billion euros of which 5 are for the construction. In June 2005, after a long negotiation process, the different parties agreed to build ITER in Cadarache, in southern France. The construction should start in 2006 and last for 10 years [13]. The first plasma is expected in 2016.

1.5 The diagnostic mirror problem

Even if one of ITER's principal goal is to demonstrate significant levels of energy production by fusion reactions, it is designed first of all to be an experimental device. In this sense, it should provide a better understanding of the physics involved in magnetically confined burning plasmas. To do so, a wide range of diagnostic systems will be necessary to control and understand the plasma performances [14]. About 40 individual measurements systems are being designed and installed on the machine. The basic principles of these systems are in many cases similar to those currently used in tokamaks. The full range of plasma parameters will be covered by the different types of diagnostics [15]: magnetics, neutronic, optical, bolometric, spectroscopic, microwave, electrostatic,...

Most present day tokamaks have pulse durations of few seconds and low levels of neutron productions whereas ITER is planned to maintain plasma discharges for up to several hundreds of seconds. This, associated with the significant scaling ITER should bring in terms of constraints on the in-vessel materials and to the high level of neutron production imply a strong modification of the diagnostic designs in order to ensure their compatibility with such harsh conditions [16].

In particular, optical spectroscopy is used to monitor the impurity concentations in the plasma, the species of interest being Be, B, C, N, O, W, ... coming both from the erosion of the first wall materials or from the background vacuum. These measurements are done by measuring the intensity of the line radiations emitted by the plasma. At the temperatures expected in ITER, most of the line radiation will occur in the Ultra-Violet (UV) and visible regions because they are due to electronic transitions. In current machines the plasma is observed through optical windows or optical fibres. In ITER however, all diagnostic systems will have to include effective neutron shielding in order to minimize neutron leakage. For the optical and spectroscopic diagnostic systems this will be done using optical periscopes embedded in shielding blocks [17]. The high levels of radiation lead to unacceptably high radiation-induced luminescence and absorption in refractive components such as windows [18] and so the first optical components will have to be metallic mirrors. These plasma facing mirrors (PFMs) are located close to the plasma (typically within ≤ 1 m) and are fully exposed to the plasma radiation (energetic ions, energetic neutrals, neutrons, gammas, and high levels of electromagnetic radiation). As a result, they can suffer erosion and/or deposition, nuclear heating and possibly structural changes. The possible degradation of the mirrors reflectivity as a result of these damaging effects represents a serious concern for the reliability and long-term usefulness of the spectroscopic characterization systems. A concerted effort within the tokamak community has been initiated recently to characterize the consequences of the damaging effects the mirrors will face on their optical properties, their possible lifetime (i.e. how long can they maintain the required optical properties), and seek mitigation methods. Results from these investigations will be the main topic of the work presented here.

Chapter 2

Implications of the plasma-wall interactions in a tokamak for mirrors

The previous chapter gave a general introduction about nuclear fusion and principles of the magnetic confinement and tokamak. The interactions of the hot plasma with the surrounding materials, as well as specific transient effects arising from magneto-hydro-dynamic phenomena, will be contributing to the degradation of the optical reflectivity of the first mirrors. This chapter will give the basic notions necessary to understand these effects and more particularly how they generate the "mirror problem".

2.1 Physical sputtering

Physical sputtering is the most fundamental erosion mechanism and a very well investigated problem. An extensive theoretical approach can be found in [19].

Sputtering is the removal of atoms from the surface of a solid as a result of impacts by ions or atoms. When an energetic ion or neutral atom is incident on a solid surface, it produces a collision cascade among the lattice atoms. Physical sputtering takes place when this cascade results in a surface atom receiving sufficient energy to overcome the surface binding energy. The sputtering yield (the number of atoms ejected per incident particle) is proportional to the energy deposited in elastic collisions within a near surface layer. Physical sputtering is thus a threshold process: at low particle energy, where the energy transferred to surface atoms is comprable with the surface binding energy, the sputtering yield decreases strongly and become zero below a threshold energy E_{th}. For light ions incident on heavy materials, the threshold energy is determined by the energy which can be transferred to target atoms and can be analytically approximated by [20]:

$$E_{th} = \frac{(M_1 + M_2)^4}{4M_1M_2(M_1 - M_2)^2} E_s \tag{2.1}$$

where M_1 and M_2 are the incident particle mass and target mass respectively. The energy dependence of the sputtering yield at normal incidence can be described empirically by the following equation:

$$Y = QS_n(E)\left(1-\frac{E_{th}}{E}\right)^2\left(1-\left(\frac{E_{th}}{E}\right)^{2/3}\right) \tag{2.2}$$

where $S_n(E)$ is the function for the energy dependence of the energy deposited in elastic collisions. Values of Q and E_{th} are tabulated for many ion-target combinations [21].

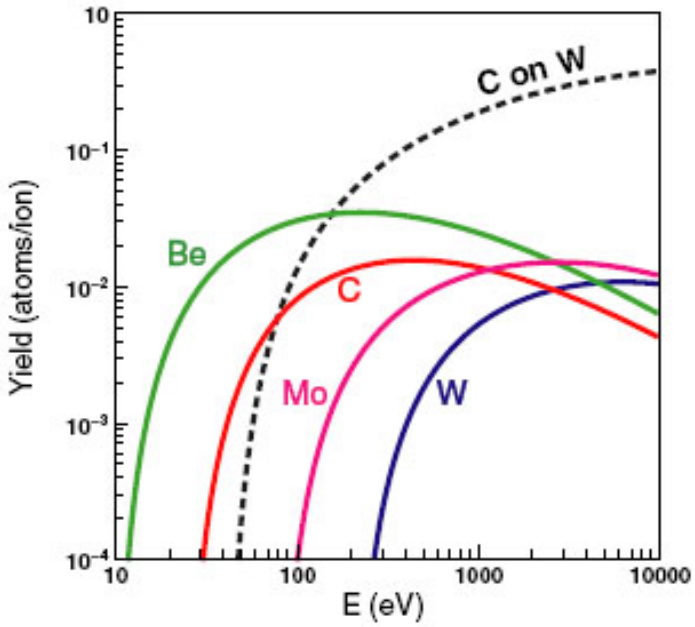

Figure 2.1: Energy dependence of the sputtering yield of various fusion relevant materials by deuterium ions with normal incidence from [22]. In addition data for the sputtering yield of C on W is shown.

As seen in fig. 2.1, above the energy threshold the sputtering yield increases, reaches a maximum and then decreases at high energies. This decrease in yield is due to the collision cascade taking place deeper in the solid so that there is a lower probability for the surface atoms to receive an energy sufficient to be sputtered.

The sputtering yield increases with the incidence angle, since the higher the incidence angle the more energy deposited within the near-surface layer [23]. Surface roughness tends to reduce the sputtering yield and its pronounced dependence on the angle of incidence [24]. It should also be mentioned that the sputtering yield of a given material depends on its crystallographic structure. The erosion yield of individual grains with different crystallographic orientations can vary by a factor of 2 on a broad energy range [25]. This is of particular importance for polycrystalline materials made by nature of grains with different orientations.

In a tokamak, ions reach the PFCs with a directed average enery (in eV) of $E_i \sim 3Z_iT_e + 2T_i$ comprising, respectively, the energy gained via acceleration through the electrostatic sheath and the thermal energy. The typical impurity ions expected to leave the confined plasma in a fusion device (Be, C, O,...) will be multiply charged and may thus impact the surrounding materials with significant energy. Moreover as described in section 1.2, the magnetic field configuration

in a tokamak and the gyration movement of the ions around the field lines imply that ions will not intersect the confining surfaces with a normal incidence.

Another important contribution to physical sputtering in a tokamak arises from the *charge exchange neutrals* (CXN). These particles are neutrals originating from the plasma-wall interactions which have experienced a charge exchange reaction with plasma ions, yielding a neutral with the local ion temperature. These neutral particles are not influenced by the magnetic field and can therefore penetrate deeply in the confined plasma region (where the ion temperature is high) and experience a succession of charge exchange processes. This process thus transforms a fraction of the recycling neutrals with energy of a few eV into very energetic particles. Some evidence of damages due to CXN on the vessel walls has been reported in JET [26] and ASDEX-Upgrade [27]. In ITER, the fluxes of CXN will be much higher than in current devices. Moreover, numerical simulations predict that the energy distribution will have a high energy tail which reaches the several keV range [28].
Since the mirrors will not be in direct line-of-sight of the plasma, erosion by CXN is expected to be the main sputtering effect for First Mirrors.

2.2 Chemical Sputtering

Carbon is currently used in present tokamaks as a first wall material as a result of its lack of a liquid phase which makes it extremely forgiving under strong transient heat loads. For this reason graphite is planned to be used for the divertor targets in ITER. In the case of carbon, not only physical suttering but also chemical sputtering contributes to the global erosion under hydrogen ions (or hydrogen isotopes) bombardment. Chemical reactions between carbon and incident hydrogen ions lead to the formation of volatile hydrocarbon molecules or to loosely bond hydrocarbon precursors which will be sputtered physically with a much lower threshold energy. The complete description of the mechanisms driving the chemical erosion is rather complex, but is determined basically by three processes [29] :

- the sp^2 carbon atoms of the graphitic planes are hydrogenated by reaction with the thermalized ions, forming CH_3C complexes with an sp^3 configuration. At temperatures above 400 K, CH_3 radicals can be released while at temperatures above 600 K, release of H_2 due to the molecular recombination of hydrogen at the surface reduces the chemical erosion yield [30].

- The thermal reaction is enhanced by radiation damage created from the kinetic energy tranfers from incident ions to lattice atoms. The damage created in the lattice results in open bonds for hydrogen attachment. This process, and consequently the chemical erosion yield, is dependent on the mass of the hydrogen isotope.

- At low surface temperature those carbon surface atoms not embedded in a perfect crystal lattice will be hydrogenated up to CH_3 with one remaining bond to the graphitic lattice, but no thermal release of hydrocarbon occurs. However, these fully hydrogenated groups are bound to the surface with much smaller binding energies (≈ 1 eV) than carbon surface atoms in their regular lattice environment (7.4 eV) and therefore have a much reduced

threshold energy for the physical sputtering by hydrogen ions. This effect is called ion induced desorption of hydrocarbon [31].

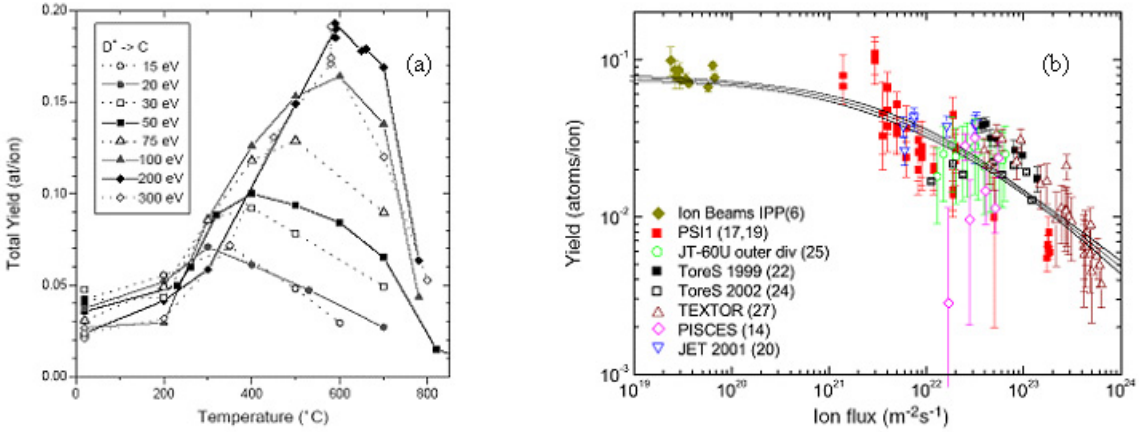

Figure 2.2: (a) Temperature dependence of the chemical erosion yield of pyrolitic graphite by deuterium ions at different energies from [32] and (b) chemical sputtering yield dependence on particle flux density from [33].

As mentioned, the reaction of the thermalized ions with the carbon surface implies that the chemical erosion yield is a function of the surface temperature with a defined maximum at a temperature T_{max} which depends on the energy of the incoming ions as illustrated in fig. 2.2a [32]. Systematic measurements of the chemical erosion yield (Y_{chem}) by *in-situ* spectroscopic measurements in both tokamaks and plasma simulators determined the flux dependence of the chemical sputtering yield [33] as shown in fig. 2.2b. The data were normalized to an incident energy of 30 eV and were taken near the maximum of the yield dependence on the surface temperature. There is a clear decrease of Y_{chem} with ion flux, with an extrapolated value of $5 \cdot 10^{-3}$ at ITER divertor relevant fluxes of 10^{24} $m^{-2}s^{-1}$. This decrease is explained by a saturation effect: when too much deuterium is offered to the surface, the surface is overloaded and the average residence time of the impinging deuterium in the surface becomes smaller. As a consequence the reaction rate of hydrocarbon decreases [31].

2.3 Erosion due to transient effects (ELMs)

The discovery of the H-mode described briefly in section 1.3 was accompanied by the observation of *edge localized modes* (or ELM). The increase of the energy confinement time (and of the particle confinement time) associated with the H-mode is mostly due to a reduction of the transport coefficients at the plasma edge region through the creation of a so-called *edge transport barrier*. Due to the reduced energy losses associated with the formation of the transport barrier, there is an increase in the plasma energy density and the formation of a strong gradient between the core plasma region and the SOL. This region is called the *pedestal*. When the pressure gradient in the pedestal exceeds a certain stability threshold, repetitive instabilities appear

at the plasma edge in the form of a quasi-periodic drop of the pedestal plasma density and temperature. These instabilities are the ELMs [34]. The increased particle confinement time is also valid for impurities and thus an increase of the impurity content (and consequently an increase of the energy losses due to line radiation of these impurities) is noticed during H-mode plasmas. In this sense, ELMs can be seen as a natural regulating mechanism which clamp the electron density and the line radiation and provide a very good technique for running H-mode discharges in steady-state [35]. The ELMy H-mode is currently envisaged as the baseline scenario for ITER.

ELMs lead to significant energy and particles fluxes being expelled from the confined plasma onto the PFCs protecting the vacuum vessel. These fluxes are observed by the large spikes in the divertor D_α emission line due to changes of excitation states in the local plasma and release of neutrals by recycling. The frequency of these ELMs (1-300 Hz) and their magnitude (1-8 % of the total plasma energy content) make them a serious concern for the lifetime of the PFCs. Extrapolations from results obtained in JET when studying power deposition on the divertor targets during ELMs (so-called type I ELM) lead to expected energy fluxes at the ITER divertor targets in the range 0.6-3.4 MJm^{-2} [36]. Such energy loads will lead to significant temperature rise of the divertor targets. Transient temperature peaks close to the melting (or sublimation for carbon) temperature may lead to significant increase of the material erosion yield.

2.4 Material migration and transport

The previous sections gave a brief survey of the mechanisms leading to material erosion in tokamaks. However a tokamak being a closed system all eroded materials have to be redeposited somewhere else, this mechanism constitutes the process of material migration and transport.

The transport of the impurities released by erosion through and by the plasma and their deposition and/or re-erosion consitute the process of material migration. Re-deposition of the eroded material may occur close to the point of erosion or at remote areas. Material migration is dependent on material type, plasma configuration, machine geometry,... In limiter tokamaks, the erosion of limiters is the main impurity source. Most of the eroded material is redeposited on these surfaces due to their proximity to the confined plasma. In divertor machines, atoms sputtered from the target plates are ionized and are either promptly redeposited on the target plates or transported through the divertor plasma [22] primarily under the influence of the ion temperature gradient force, which drives impurities out of the divertor, and friction with the flow of deuterium into the divertor which returns them to the plates. Prompt redeposition occurs typically for high-Z impurities which are easily ionized and have comparatively large larmor radii, the impurities being redeposited within the first gyration, reducing the gross erosion rate [37] and limiting the possibility of long-range migration of high-Z impurities. The situation is more complex in the case of carbon where the possible formation of neutral hydrocarbons through chemical erosion leads to longer range migration.

In most modern tokamaks, significant effort is being pursued to understand the migration phenomenon and its implications (for tritium retention in the redeposited layers for example). A common feature of several divertor tokamaks is the strong assymetry in carbon deposition

between the inner and outer divertors [38, 39]. The inner divertor is a region of net deposition while the outer is a zone of net erosion or neutral erosion/deposition. Thus the carbon deposition found in the divertor must have originated from erosion of the main chamber wall or the outer divertor (which is a zone of net erosion in tokamaks) and driven to the divertor by the large SOL flows (measured by means of Mach probes [40, 22]). An additional contributor to the asymmetries in material deposition between outer and inner divertors may be due to the lower electron temperature measured in the inner divertor [41].

Another striking feature found in many tokamaks is the intense co-deposition of carbon and deuterium in regions which are shaded from ion flux but lie near carbon surfaces receiving high ion flux [42]. Since ions cannot access these surfaces, this carbon deposition can only be due to carbon (or hydrocarbon) neutrals arising from chemical erosion followed by molecular dissociation [38]. The same mechanism would not apply for metals since metals are eroded by physical sputtering as atoms which are then ionized and redeposited on surfaces intersecting the field lines.

Different tools are used to study the issues of erosion/deposition and material migration. One can make the distinction between the in-situ methods allowing measurements on a shot by shot basis and post-mortem analysis. The latter consists in inserting a dedicated material component for a complete experimental campaign and to retrieve it at the next vacuum break (typically several months later). Ion beam surface analysis and optical microscopy are subsequently used to determine the changes in the material induced by the long term exposure [43] with the major drawback of integrating in the results a large number of discharge types and configurations. To study material migration on a shorter period, injection of a tracer gas (^{13}C labelled methane $^{13}CH_4$) is performed via gas puffing at a given location during a series of identical discharges [44]. The experiments are performed at the end of experimental campaigns so that first wall and divertor tiles may be extracted for ion-beam analysis sensitive to the isotope [45]. Measurement of neutral and low ionization states of atoms and molecules entering the plasma after being sputtered by optical emission spectroscopy gives a qualitative idea of the erosion suffered by the PFCs. Measurement of material deposition can be made on a shot by shot basis using quartz micro-balances (QMB) located at various locations in the vacuum vessel [46]. Other diagnostic techniques are being developed to enlarge the in-situ erosion/deposition measurement capabilities [47, 48].

2.5 Material choice for ITER

ITER will represent a major upscale from present machines in terms of duty cycle, stored energy, power exhaust, and plasma duration. The completion of the ITER engineering design in 2001 has brought a complete design of the machine with an innovative choice of plasma-facing materials [50]. A cutaway showing the configuration chosen for ITER is shown in fig. 2.3. The selection of the plasma facing materials was driven primarily by the requirements of plasma performance, i.e. a minimization of the plasma contamination by impurities, and component lifetime.

Beryllium is used as a first wall material (total area ~ 700 m^2) because it has the advantage

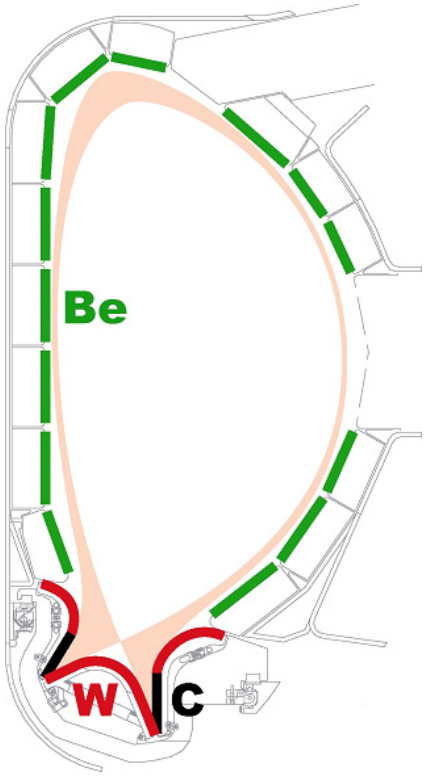

Figure 2.3: Cutaway showing the layout of Plasma Facing components in ITER with the different selected materials

of being of low-Z material with a good thermal conductivity and a strong affinity for oxygen (free energy for oxide formation -581 kJ· mol^{-1}) making it a very good oxygen getter [49]. However its main drawbacks are a high sputtering yield and a low melting point (1560 K) limiting its power handling capabilities. It can also be toxic (when present in the form of dust) although the safety precautions to be taken are similar to those induced by the presence of tritium in the vacuum vessel.

Tungsten as a high-Z material with a low sputtering yield and a high melting temperature (3695 K) will be used for the baffle regions (where high fluxes of CXN are expected) of the target and the surface of the divertor dome (total area $\sim$ 100 m^2). Finally, Carbon Fibre Composite (CFC) is chosen for the divertor target plates as a result of its high thermal shock resistance owing to its lack of a melting phase (it simply sublimes) making it extremely forgiving under the strong transient heat loads expected during ELMs. However, the use of carbon can lead to tritium retentium by co-deposition with carbon, and since nuclear licensing limits the T-inventory in ITER to 350 g for safety reasons [50], removal techniques would have to be employed to recover the trapped tritium. Moreover CFC materials suffer from severe degradation of their mechanical and thermal properties under high fluence neutron irradiation [51] at fusion neutron energies.

Since the main chamber wall of ITER will likely be an area of net erosion (see chapter 2.4), the eroded beryllium will be transported to the divertor, and concentration of Be in the SOL plasma is expected to be in the range 1-10 % [52]. Mixed-material effects will occur that

could lead to strong modifications of the physical properties of the divertor materials. The formation of tungsten beryllides (alloy Be/W) due to the bombardment of a tungsten target by Be containing plasma has been observed experimentally [53]. These alloys have a much reduced melting temperature ($\sim$ 1500 K) thus limiting the power handling capability of the material.

Chapter 3

First mirrors for diagnostic systems in ITER

3.1 Motivation

As described in chapter 1.5, optical diagnostic systems in modern tokamaks view the plasma through optical windows or optical fibres. Considering the design and expected performances of ITER, fast neutron fluxes of $\approx 3 \times 10^{13}$ and $\approx 2\times 10^{13}$ $\mathrm{m^{-2}s^{-1}}$ are expected at the first wall and just outside the ports, respectively [55]. In addition, the γ radiation flux will be 10^4 $\mathrm{Gy.s^{-1}}$, and intense UV and x-ray radiations are expected (up to 500 $\mathrm{kW}\cdot m^{-2}$). Silica-based windows are sensitive to radiation-induced absorption (RIA), decreasing substantially their transmittance for wavelengths below 800 nm [56]. Materials with otherwise superior radiation tolerance such as sapphire suffer from radiation-induced luminescence (RIL) after high fluence of γ radiations [57]. To reduce the extent of these problems and their effects on the diagnostic signals it was proposed that the light from the plasma be transmitted by mirror optics through a labyrinth embedded in shielding material. This has the advantage of recessing the vacuum windows or the optical fibres located at the end of the labyrinth some metres away from the zone of intense radiation and to shield them by reducing substantially the levels of neutrons they will be facing to typically 10^{-4} of the flux at the first wall [58].

The first element of the plasma diagnostic systems in ITER will therefore be metallic mirrors called First Mirrors (FM). Being the closest element to the confined plasma they will suffer from the intense radiations mentioned above and also from bombardment by CXN and possible deposition of impurities eroded from the plasma-facing components. They will have to maintain the required optical properties despite these extreme conditions. According to the design of the ITER spectroscopic systems the wavelength range of interest is 0.05-1000 nm [59], while some diagnostics such as the infrared laser polarimetry system will work with lasers of wavelength 9.27 and 10.6 μm [60] and the poloidal polarimeter will have an operating wavelength of 118 μm [61]. The choice of the first mirror material should thus be made by taking into account the wavelength range of interest for the system and the resistance of the material to the degradation mechanisms to be encountered. For this, since the wavelength range is fixed by the system, an assessment of the effects of the different processes on the optical properties is required.

3.2 Integration of metallic mirrors in the current design of ITER diagnostic systems

Figure 3.1 illustrates the approximate locations and sizes of the first mirrors to be installed in ITER. Mirrors will be installed in a large variety of locations with different distances between the mirror surface and the plasma. Depending on their locations, the mirrors will be subject to different levels of radiations and particle fluxes. Moreover, depending on the diagnostic system, the mirrors will be more or less open to the plasma. Three examples of the integration of first mirrors in the current design of the diagnostic systems will be reviewed in the following sections to expose the differences in their arrangements and illustrate the importance of the first mirrors in the diagnostic systems.

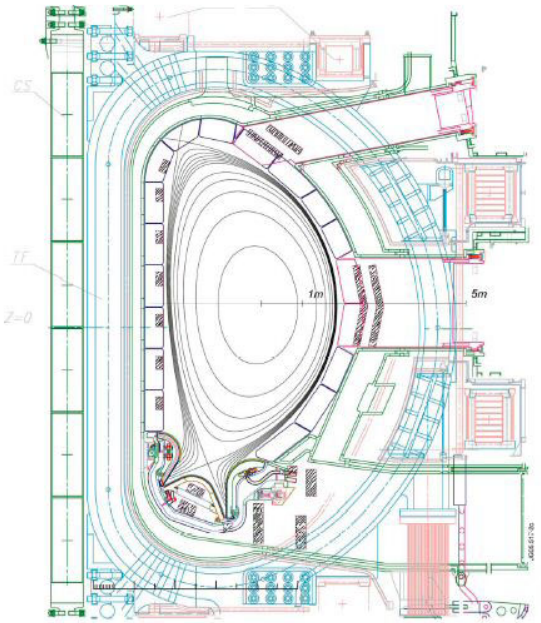

Figure 3.1: Cross section of ITER showing the locations of the first mirrors in the vacuum vessel. Mirrors appear as textured rectangles.

3.2.1 LIDAR Thomson Scattering

In Thomson scattering, radiation from a high power laser is injected into the plasma and the radiation scattered incoherently by the electrons is corrected and spectroscopally analysed [16]. Measurements of the intensity and spectral width of the scattered signal allow electron temperature and density to be respectively determined. The approach chosen for ITER is known as light detection and ranging (LIDAR) technique [62]. In this case, the input beam and the collection beam follow the same optical path, the backscattered radiation is measured and spatial distribution is obtained by the time of flight principle.

Fig. 3.2 shows a view of the ITER LIDAR system design, with the arrangement of the mirrors. The first mirror, with dimensions 320x240x34 mm^3 will be located at a distance of

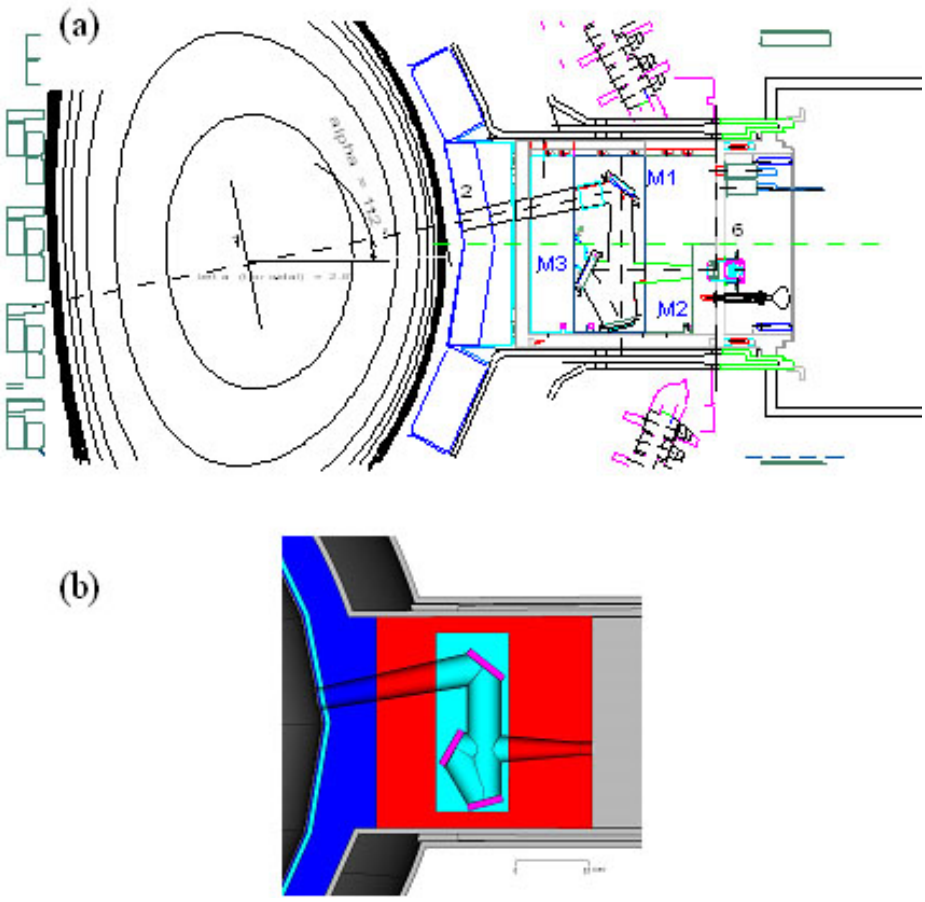

Figure 3.2: (a) Cross-section of ITER showing the arrangement of the LIDAR mirrors (M1 is the first mirror) and (b) closer view of the mirror setup (pictures courtesy of M. Walsh).

about 1.8 m from the LCFS, thus reducing the level of charge-exchange neutrals arriving at the mirror surface. The mirror will also have to transport the high power laser beam, whose working wavelength is 800 nm, and will be actively cooled.

3.2.2 H_α spectroscopy

The main role of the H_α spectroscopy system is to monitor ELMs and transitions from L to H-mode [59]. The system measures Balmer lines (transitions of principal quantum number from n= 3-8 to n= 2) emitted from hydrogen isotopes in the wavelength range 370-660 nm. The light from the plasma (fig. 3.3) is collected by a concave mirror which observes the plasma over a wide angle through a small conical pupil. The light reflected from the first mirror is then transmitted through an optical labyrinth to an optical fiber bundle. The signal is then analyzed with a high dispersion spectrometer located in the remote diagnostic room.

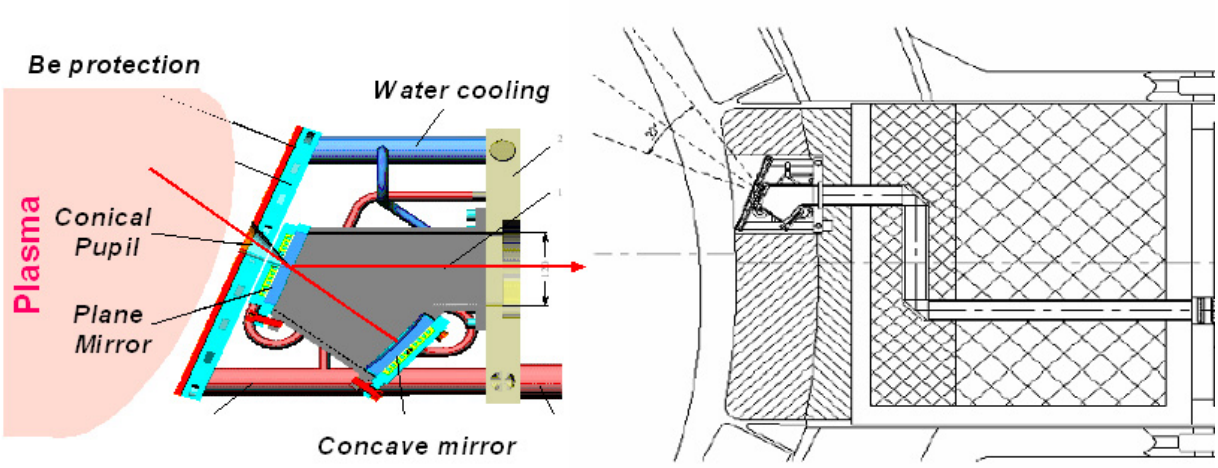

Figure 3.3: Arrangement of the mirrors in the labyrinth system of the H_α spectroscopy system.

3.2.3 Divertor Impurity monitor

Identification of the impurity species arriving at the divertor targets and measurement of their distribution and fluxes will be made by spectroscopic measurements in the wavelength range 200-1000 nm. According to the materials used for the plasma-facing components, the expected impurities are carbon, tungsten and beryllium, as well as seeded (extrinsic) impurities (N_2, Ar, Ne, Kr).

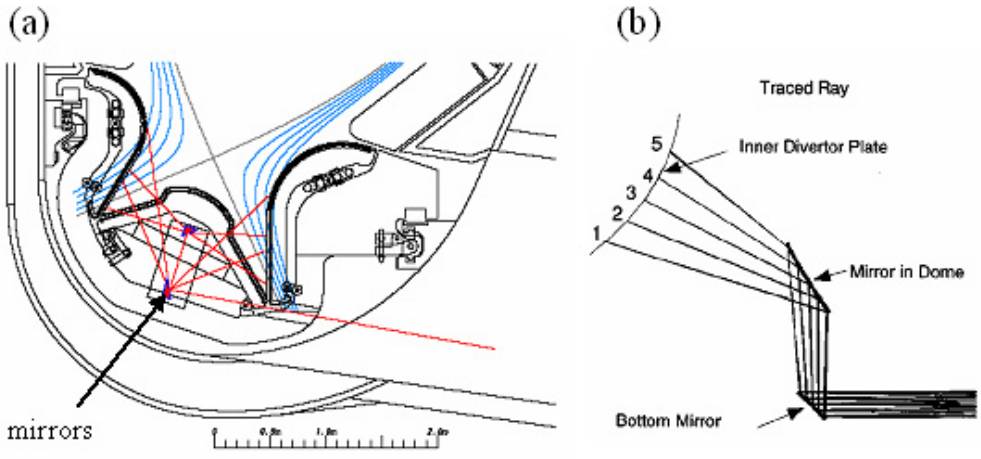

Figure 3.4: (a) Locations of the mirrors in the ITER divertor for the impurity monitor system, (b) line of sight of the inner divertor target using two mirrors, the same system (with two other mirrors) is used to observe the outer target [63].

The inner and outer divertor regions will be observed using metallic mirrors located at the bottom of the divertor cassette and just under the dome (fig. 3.4). In addition, lines of sight through the gap of 10 mm between the divertor cassettes will be provided to observe the

divertor leg and the X-point region. Baffle plates will be installed in front of the mirrors to reduce the solid angle of exposure to the plasma and thereby reduce the number of particles impinging on the mirrors.

3.3 Specific issues related to the first mirrors

As described in the previous section, the first mirror will be a key element of the diagnostic systems in ITER, since any modification of its reflectivity will have an impact on the spectroscopic signal. The material to be chosen should therefore ensure the highest resistance to the damaging effects it will have to face. The main damaging effects are expected to be due to the neutron flux (causing mainly volumetric modifications and possible transmutation) and to bombardment by CXN (causing modification of the mirror surface). In terms of reflectivity the latter is the most dramatic. Depending on the mirror location and its relative distance to the plasma, bombardment by CXN will either result in sputtering of the mirror surface or in deposition of impurities. Both effects will influence the surface reflectivity.

Sputtering of the mirror surface by CXN or plasma ions may result in an increase of the surface roughness and thereby a decrease of the reflectivity. A qualitative evaluation of the relation between the surface roughness and the specular reflectivity at normal incidence of a mirror is given by Bennett's formula [64]:

$$R_s = R_0 \; exp\left(\frac{-(4\pi R_{RMS})^2}{\lambda^2}\right), \tag{3.1}$$

where R_s is the measured specular reflectivity, R_0 is the reflectivity of an ideally smooth surface of the same material, R_{RMS} is the surface RMS roughness (in nm) and λ the wavelength of the light (in nm). This relation imposes both a technological requirement (for the mirror preparation) and a limit to the mirror surface roughening the diagnostic system could cope with. To ensure that the reflectivity loss does not exceed 5 % of the initial reflectivity a necessary condition is that R_{RMS} remains lower than $\lambda/50$. However according to eq. 3.1, this limit is more restrictive in the UV and visible region, while the reflectivity appears to be less sensitive to the surface roughness in the infrared region of the spectrum.

Investigations of the effect of surface roughening due to deuterium ion bombardment on the reflectivity of mirrors from different materials have been made in laboratory experiments [65, 67]. The main findings are summarized in fig. 3.5. The degradation of the reflectivity appears to be a linear function of the eroded thickness. Moreover the degradation rate of the reflectivity (and so the increasing rate of the roughness) is strongly dependent on the material type and crystallographic form. Polycrystalline materials exhibit a very pronounced decrease of their reflectivity under ion bombardment. Indeed such materials are made of crystallographic grains with different orientations and thus different sputtering yields (chapter 2.1); under ion bombardment the initially polished surface is transformed into a stepped structure [66, 69] revealing the morphology of the different grains. On the contrary, the degradation rate of the reflectivity of single crystal mirrors is much slower, the surface being sputtered quite homogeneously by the impinging ions. The differences found in fig. 3.5 between crystals with different orientations is due to their different sputtering yield.

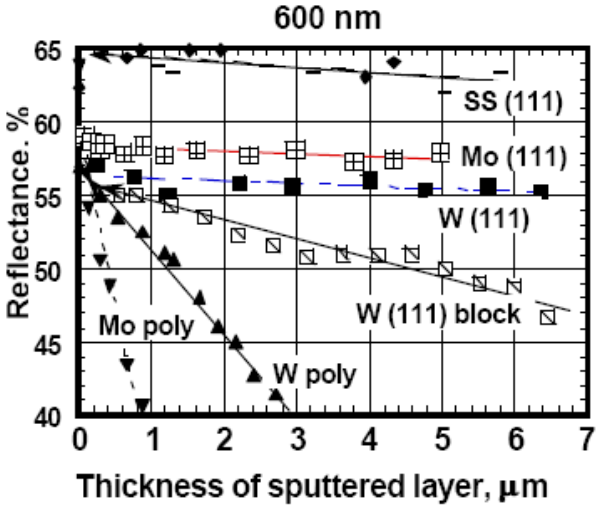

Figure 3.5: Reflectance of mirrors from different materials and with different crystallographic structures at 600 nm as a function of the thickness of the layer eroded by deuterium ions, from [68].

If the energy of the particles impinging on the mirror surface is below the sputtering threshold, the mirrors may become coated by a film made of material eroded from the plasma-facing components. This effect has already been observed for the windows used for optical and laser diagnostics in several tokamaks, their transmission being reduced by the formation of a thin film on their surface [70]. The effect of impurities on the reflectivity of the first mirrors will be even more pronouced because the reflected light crosses the deposited film twice (in case of transmission the film is crossed only once by the light).

Calculations[1] of the influence of an amorphous hydrogenated carbon (a-C:H) film on the reflectivity of a molybdenum mirror are shown in fig. 3.6 for two different types of film typically found in fusion devices [71] (at normal incidence):

- soft (or polymer-like) films with a refactive index of 1.6 at 632.8 nm and $H/C \approx 0.8$,
- hard (or diamond-like) films with a refractive index of 2.4 at 632.8 nm and $H/C \approx 0.3$.

The optical properties (refractive index n and extinction coefficient k) of a-C:H films can be accurately described with a Cauchy relation of the form:

$$\begin{aligned} n(\lambda) &= n_0 + 10^2 \frac{n_1}{\lambda^2} + 10^7 \frac{n_2}{\lambda^4} \\ k(\lambda) &= k_0 + 10^2 \frac{k_1}{\lambda^2} + 10^7 \frac{k_2}{\lambda^4} \end{aligned} \tag{3.2}$$

where n_i, and k_i are fitting parameters. The films are considered as homogeneously deposited on a semi-infinite substrate, and the roughness of both the film and the substrate are neglected. Results from the calculations show that even a very thin carbon film modifies strongly the reflectivity of a metallic mirror. A 20 nm thick soft film already reduces the reflectivity at

[1]Performed with the Sentech Spectraray 2 software

350 nm by 20 % (fig. 3.6a). Moreover after a certain thickness is reached the reflectivity spectrum is modified by the appearance of interference effects. The positions of the maxima of the reflectivity are defined by the relation:

$$2dn = k\lambda \tag{3.3}$$

where k is an integer and d is the film thickness. These effects are most pronounced in the UV and visible range and almost vanish in the near infrared. In the case of diamond-like films (fig. 3.6b): interference effects appear already for a film thickness of 40 nm, due to the higher refraction index.

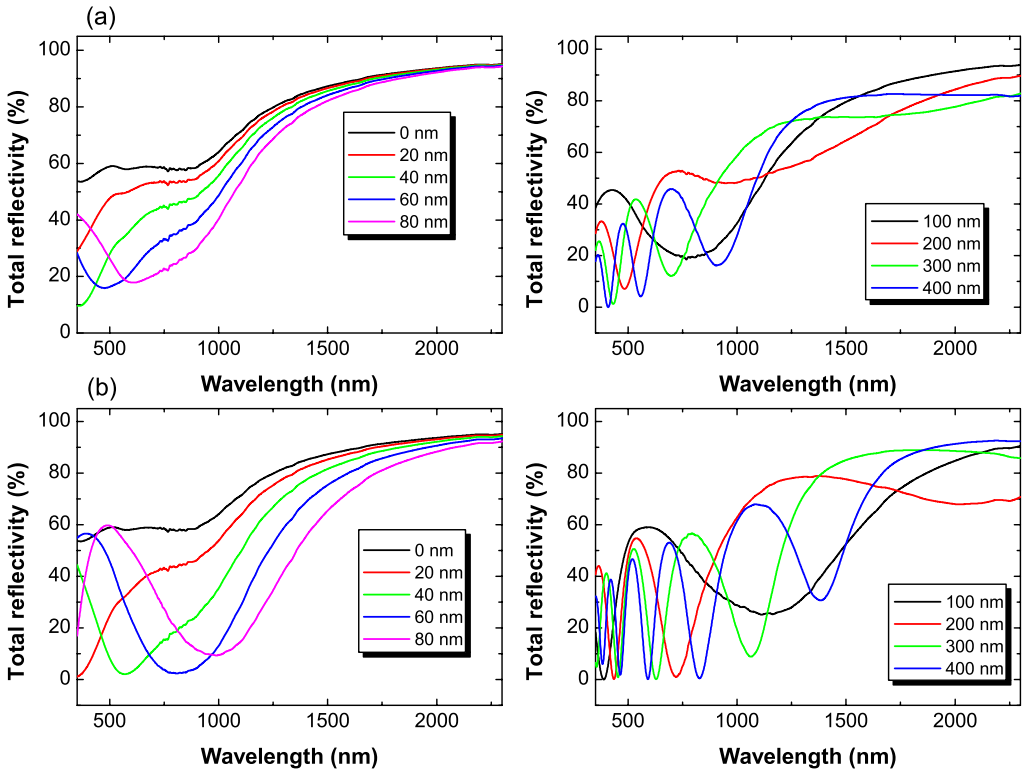

Figure 3.6: Evolution of the reflectivity of a molybdenum mirror as a function of the thickness of the a-C:H film for (a) a soft polymeric film and (b) a hard diamond-like film. The legends on the graphs indicate the thickness of the deposited film.

In ITER, deposition of metallic impurities like Be may also occur for some mirrors. Since metals have a higher extinction coefficient than a-C:H films, the light will not penetrate as deep in the layer and after a certain thickness (about 20 nm for pure Be) the reflectivity of the mirrors will be driven by the reflectivity of the deposited layer, and the substrate will be invisible to the light.

Removal of deposited layers, consisting mainly of carbon, on diagnostic windows in present

machines has been achieved by in-situ laser ablation [72, 73]. However, the efficiency of such techniques for metal-containing layer on a metallic substrate has still to be demonstrated.

3.4 Particle fluxes

The extent of the phenomena described hitherto, and their consequences for the mirror lifetimes, will mainly depend on the flux and energy of the particles arriving at the mirror surface. Extrapolations from the numbers estimated in present machines are quite uncertain. However some estimations can be obtained by numerical simulations. Description of the codes used for such simulations is far beyond the scope of this work. Interested readers are referred to [74] and references therein for more details. Usually such simulations are made to evaluate the erosion at the first wall [28]. In case of mirrors some assumptions have to be made concerning the reduced solid angle due to the recessment of the mirrors behind the first wall surface.

Such calculations were done recently [75] using the B2-Eirene simulation code with the latest non-linear neutral model [76]. In these calculations, the plasma consists of deuterium (no distinction is made between deuterium and tritium), helium and carbon ions and atoms, and D_2 molecules. The source of carbon in the simulation is the sputtering of the target plate, and a fixed sputtering yield is applied to take into account both physical and chemical sputtering, although any flux dependence of the chemical sputtering yield is neglected. The plasma parameters are calculated for a predefined computational grid whose outer limit is the SOL plasma and thus does not extend to the walls. Assumptions must be made for the plasma parameters in the region between the outer edge of the grid and the wall. It is assumed [28] that the particle fluxes are conserved in this region (no recycling) and that the electron and ion temperatures decay exponentially with 3 cm fall-off length until they reach 10 eV and stay constant at this level further out (or stay constant at this level if less than 10 eV at the grid edge). The locations, collimation angles and viewing directions of the mirrors investigated are shown in fig. 3.7 and 3.8. The solid angle is taken as 3 times the collimation angle.

As seen from the results listed in table 3.1, both the fluxes of incoming particles to the mirrors and their energy are strongly position-dependent and can (at least for the fluxes) differ by several orders of magnitude. Mirrors located at positions 6,8,9 and 13 will encounter fluxes of deuterium particles with an average energy well above the physical sputtering threshold of the possible candidate materials, while mirrors at locations 5 and 11 will see higher particle fluxes but with lower average energy and may be rather subjected to deposition of impurities. These estimates are quite crude and may be wrong by an order of magnitude, but nevertheless allow some interesting conclusions to be drawn. First of all the beneficial effect of the recessment of the mirrors behind the first wall surface and the small solid angle is rather obvious. Indeed the particle flux at the location 1 is four orders of magnitude lower than the flux at location 2 (corresponding to the first wall). Secondly, these calculations indicate that the fluxes of helium with low energy impinging on the mirror surface will be rather low. This is important because formation of blisters and bubbles have been reported for metallic mirrors exposed to high fluences ($\approx 10^{26}$ ions $\cdot$ cm^{-2}) of low energy helium ions [77]. The situation is quite different for mirrors located under the divertor dome (location 14). According to the simulations (and to

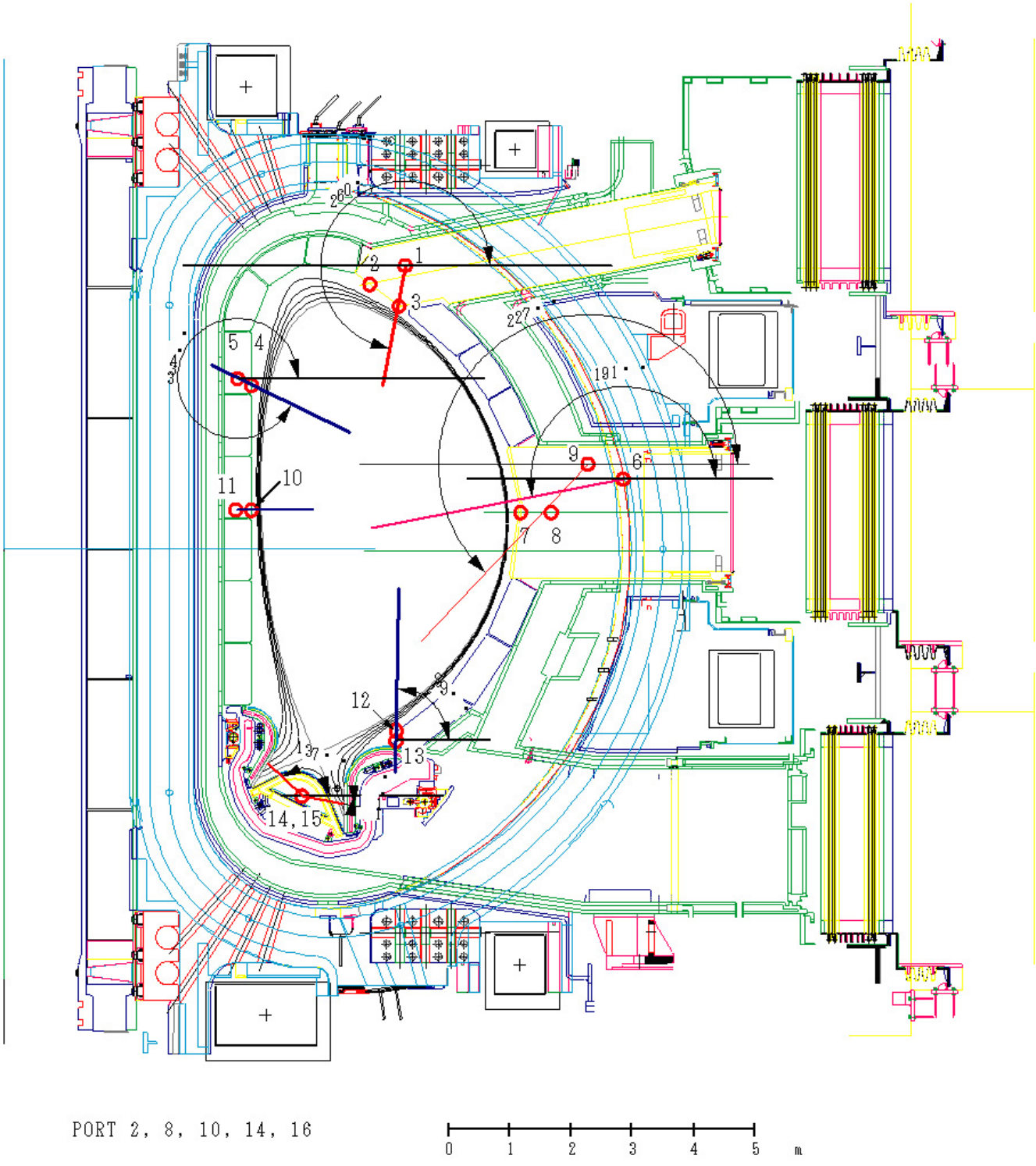

Figure 3.7: Selected mirror positions and viewing directions for the estimates of the particle fluxes on the mirrors.

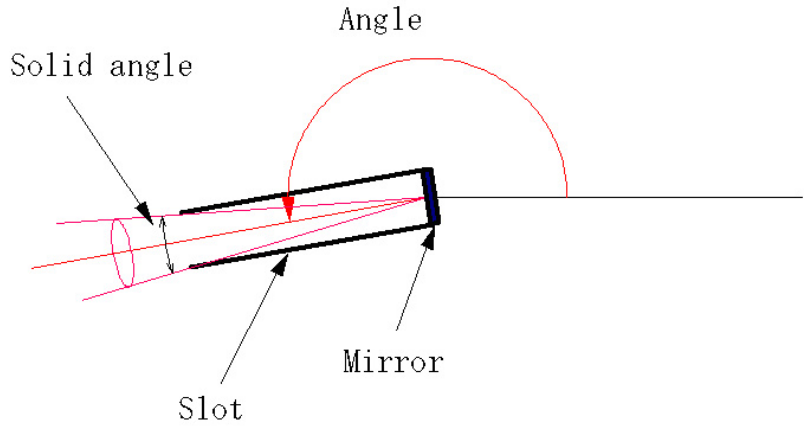

Figure 3.8: Definitions of the solid and collimation angles for the flux estimates.

observations in present machines), only particles with energy lower than 5 eV will be present in the private flux region and arrive at the mirror surface. Furthermore, high fluxes of He, D_2 and C are expected, leading to the conclusion that these mirrors will likely suffer from deposition.

Position	**1**	**5**	**6**	**8**	**9**	**11**	**13**	**14**
Solid angle	0.1	0.15	0.02	0.1	0.1	0.15	0.15	0.02
Flux D	7.4E+17	1.5E+19	2.6E+17	1.3E+18	2.6E+17	1.0E+19	1.0E+18	4.4E+17
Energy D	52.9	15.3	326	329	251	31.2	222	0.1
Flux D2	9.6E+15	3.0E+16	7.9E+13	1.8E+15	3.3E+13	1.7E+16	2.3E+15	7.8E+20
Energy D2	2.07	0.87	20	16.7	11.4	1.05	11.5	0.1
Flux He	1.1E+15	2.4E+16	9.8E+15	4.9E+16	9.8E+15	2.4E+16	5.1E+16	1.0E+21
Energy He	2.85	1.03	3.06	3.88	4.64	1.29	21.2	0.1
Flux C	6.5E+15	1.1E+17	1.0E+16	5.2E+16	1.0E+16	7.4E+16	4.5E+16	1.0E+20
Energy C	2.5	0.8	0.1	0.1	6.1	0.8	14.3	0.1

Table 3.1: Estimated fluxes of particles in ITER (m^2s^{-1}) with energies higher than 5 eV at the selected mirror locations, average energy of each species (eV) as well as the solid angle are also indicated. For D, He and C the fluxes include both ions and neutrals. For position 14 (mirrors under the divertor dome), the indicated flux corresponds to particles with energy lower than 5 eV (the flux of particles with energy above 5 eV being negligible).

3.5 Candidate materials for first mirrors in ITER

Following the previous observations, a good candidate material for first mirror in ITER should meet the following requirements:

- high optical reflectivity,
- chemical stability in the specific ITER environment,

- stability under high neutron fluxes (no transmutation),
- high thermal conductivity (for efficient cooling),
- low sputtering yield.

Taking these requirements into account leads to a list of a few materials whose use may be appropriate: copper, stainless steel (SS), tungsten, molybdenum and rhodium. The reflectivity of these materials in the range 250-2000 nm is plotted in fig. 3.9 and was calculated using the optical properties indicated in [78]. Each of these materials have interesting features and

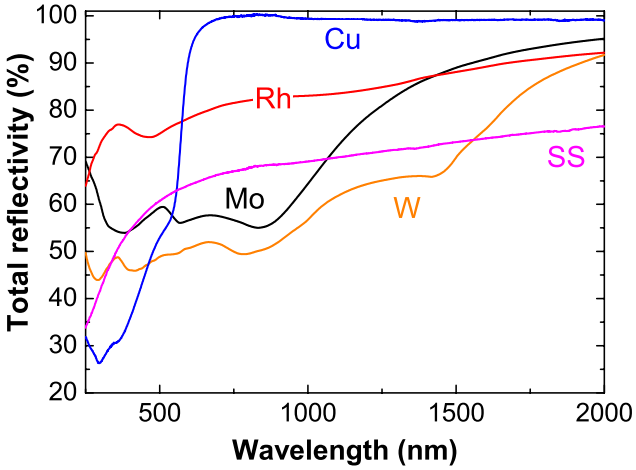

Figure 3.9: Reflectivity of the different candidate materials for first mirrors in ITER.

drawbacks. Stainless steel is a relatively well known material with good resistance to neutrons, is easy to manufacture but has a rather low reflectivity. Copper has a very high reflectivity after 500 nm but very low below and is sensitive to sputtering. Tungsten and molybdenum are high-Z materials with a low sputtering yield by D. It has been shown in laboratory experiments [54] that single crystal mirrors from these materials may preserve their reflectivity after several microns have been eroded. However, tungsten has a relatively low reflectivity and manufacturing large single crystals (some mirrors in ITER will have a diameter higher than 30 cm) remains challenging from a technological point of view. Finally, rhodium has a very good reflectivity over the UV-Vis-NIR range and is a high-Z material. However, the price of the raw material (one of the most expensive) implies its use only as a coating on a metallic substrate thus adding further complications to the problem since an excellent adhesion of the coating should be ensured despite the possible thermal loading the mirror may endure. In addition the coating technology to be used should produce coating with negligible (if any) amount of impurities and optical properties as close as possible to the theoretical values. Recent investigations were made by electrodeposition of Rh on various substrates [79] showing problems in the reproducibility of the method and reflectivity lower than the reference values. Moreover, the question of the

compatibility of such deposition method with the vacuum requirements in ITER has still to be addressed because of the impurity content in the Rh layers.

3.6 Aim of this work

Basic knowledge of the degradation mechanism is not sufficient to predict the mirror lifetime. Indeed in a system such as a tokamak (and a fortiori in ITER), erosion and deposition are not separate and independent phenomena. Even if a mirror is submitted to a flux of high energy ions, erosion can turn to deposition provided a certain level of impurities in the plasma is reached [80]. Moreover, these effects may depend on the mirror temperature (as in the case of chemical sputtering) on the mirror location and on the plasma configuration and parameters.

Laboratory experiments in well controlled conditions, though necessary to understand the influence of some parameters and much easier to realize, can not reproduce the inter-dependence of the plasma-wall interactions in a tokamak. These two different aproaches are nevertheless essential.

The aim of this work is to improve the understanding of the effects of the plasma wall interactions in a tokamak on the optical properties of metallic mirrors and to determine which parameters may be optimized to extend the lifetime of these mirrors (i.e. the time they will maintain their optical properties). This has been done by a thorough participation in the mirror experiments carried out in different tokamaks (Tore Supra, TCV, TEXTOR, DIII-D, and JET) through detailed optical and surface characterisations of the mirrors before and after their exposure, and by dedicated laboratory experiments. The importance of the mirror crystallography was stressed by comparing single crystal and polycrystalline mirrors under erosion conditions. The effect of impurity deposition on the reflectivity of the mirrors was studied in DIII-D and TCV for carbon films and in the linear plasma machine PISCES-B for Be/C mixed layers. These experiments also allowed a mirror temperature regime where carbon deposition may be mitigated to be identified.

Part II

Methodology

Chapter 4

Mirror tests in tokamaks

As outlined in section 3.6 this work is articulated around two approaches. First, experiments in several existing tokamaks were made to simulate one precise condition expected to be faced in ITER. However, since dedicated sessions for mirror exposure are not always possible, these experiments are sometimes integrated over the duration of an experimental campaign. This implies that the mirrors are exposed to a variety of plasma configurations and one has to average the experimental conditions over this duration. Therefore when more controlled conditions were needed, simulation experiments were made in the laboratory. A flow chart describing the methodology applied in this work is shown in fig. 4.1. As seen, some particular points were investigated through experiments in different machines. For ease of reading, the different tokamaks in which experiments were carried out will first be described, as well as the associated experimental setups. Then a description of the laboratory experiments will be given. Finally, since these experiments are only meaningful if supported by robust surface analysis, chapter 6 will described the analysis techniques used. Part III will detail the different experimental results and make references to this section for the experimental details.

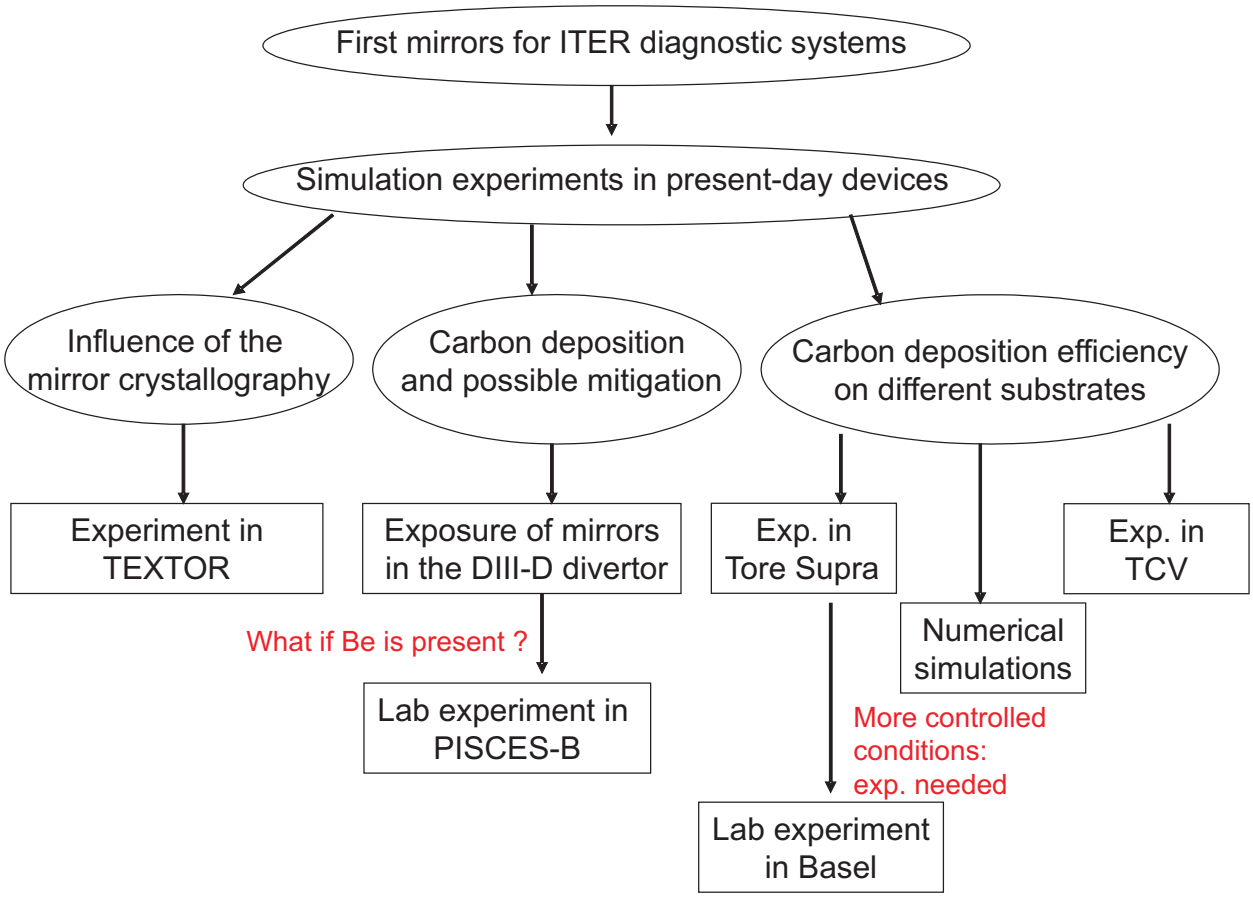

Figure 4.1: Methodology followed during this work.

4.1 Exposure of metallic mirrors in the SOL of TEXTOR

4.1.1 The TEXTOR tokamak

TEXTOR [95] is the Tokamak EXperiment for Technology Oriented Research in the field of plasma wall interactions. It is a medium size tokamak with a circular plasma section (R=1.75 m, a=0.46 m, B=3 T) with an excellent diagnostic access to the plasma boundary. An inside view of TEXTOR is shown in fig. 4.2. The limiters are made of graphite and the vacuum vessel of stainless steel. Regular boronizations are used for wall conditioning. The dynamic ergodic divertor (DED) was recently installed, increasing the graphite coating to $\sim 30\%$ of the total plasma-wetted area surface of the machine. TEXTOR is located in Forschungszentrum Jülich, Germany. Operation and scientific exploitation started in 1983. TEXTOR is now operated jointly by a cooperation of three EURATOM associations: Germany, Belgium and The Netherlands.

A large programme of mirror research is ongoing at TEXTOR, in close collaboration with the University of Basel. These studies started in 2003 with the exposure of large polycrystalline molybdenum mirrors in the erosion and deposition dominated areas of the SOL plasma [96].

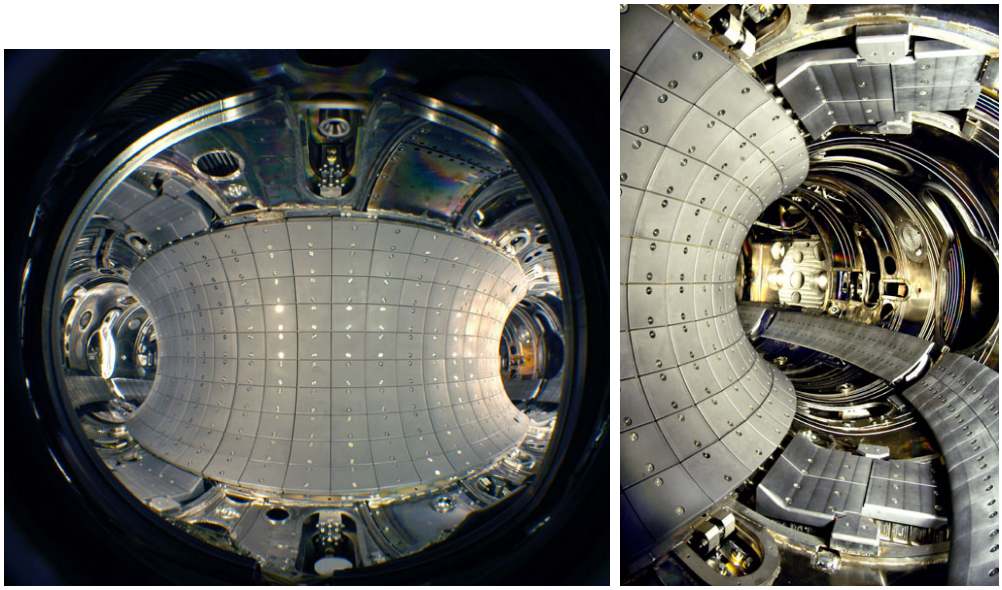

Figure 4.2: Inside view of TEXTOR showing the graphite limiters protecting the liner and shaping the plasma. On the right picture are shown the bumper limiter (left), the main limiters (top and bottom) and the toroidal limiter belt ALT-II (right).

4.1.2 First mirror tests in TEXTOR

Experiments at TEXTOR aim at simulating the effects of erosion due to charge exchange neutrals. Indeed the experimental conditions are such that the average ion energy corresponds to the average energy of the CXN expected to cause erosion of mirrors in ITER [28]. Moreover, the ion flux in the SOL of TEXTOR is much higher than the expected CXN on the first wall of ITER, therefore it is possible in one experimental day to simulate the effect of hundreds of ITER discharges.

Introduction of the mirrors in the SOL plasma is made using the so-called "limiter lock" system [97] allowing a flexible positioning of the mirrors at any position inside the SOL. One of the main features of the limiter lock concept is the good access for spectroscopic and optical observation in the horizontal as well as in the vertical direction, allowing the measurements of plasma parameters in close proximity to the probe head. In the present experiment, mirrors were introduced from the top of the machine.

To date only laboratory tests were conducted to check the resistance of metallic mirrors to erosion under pure deuterium plasma. Though informative, these experiments cannot reproduce the conditions met in a tokamak. The SOL plasma in a tokamak contains impurities coming from the erosion of the limiters and from residual impurities due to the base pressure. The direct comparison of single crystal and polycrystalline mirrors in a tokamak environment was needed to get closer to ITER-relevant situation and allow a better quantification of the lifetime of metallic mirrors submitted to erosion solely.

Three mirrors were used for the experiment [98, 99]: a polycrystalline molybdenum mirror (pc Mo), a single crystal molybdenum mirror with (110) orientation (sc Mo) and a single crystal tungsten mirror with (111) orientation (sc W). The single crystal mirrors were manufactured in

Russia and supplied by the Kurchatov Institute. The polycrystalline mirror was manufactured and polished at the Forschungszentrum Jülich. All three mirrors were placed in a row on the sample holder made from TZM (alloy containing 99 % Mo, 0.5 % Ti and 0.1 % Zr). A part of each mirror was protected with the cover plate of the holder. The holder with mirrors was inclined with an angle of 20° with respect to the toroidal direction.
Fig. 4.3a shows schematically the experimental setup. The leading edge of the holder was

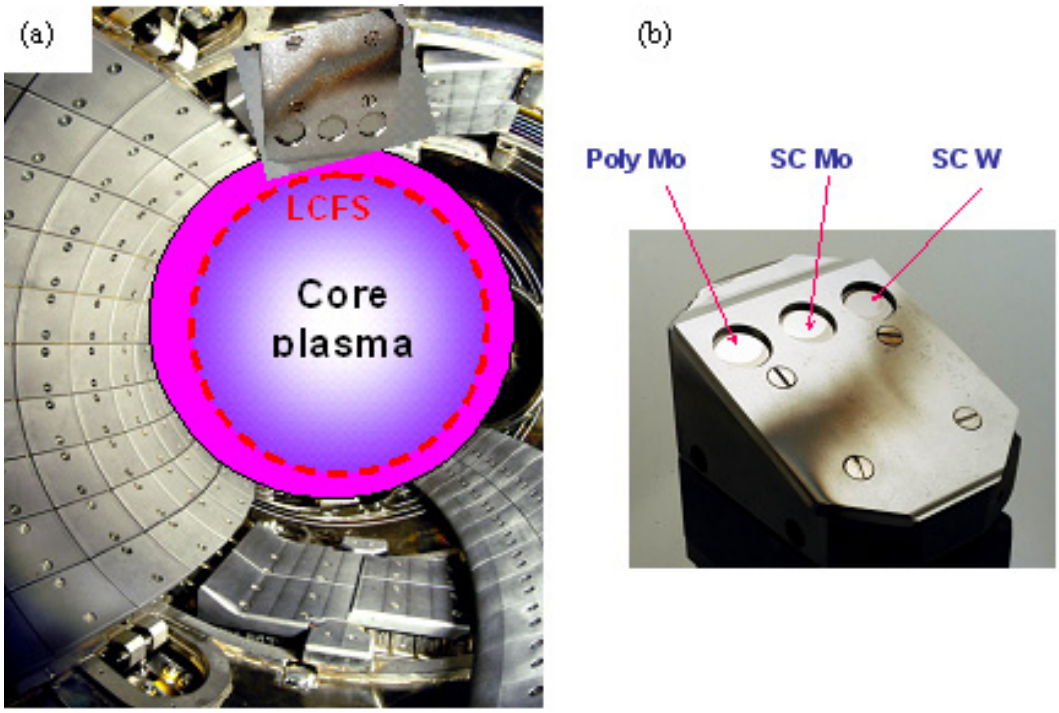

Figure 4.3: (a) Inside view of TEXTOR showing schematically the mirror exposure in the SOL plasma, and (b) mirror holder with inclined cover plate (20° and the three circular mirrors (22 mm diameter) after exposure in TEXTOR.

located at about 13 mm from the LCFS. The mirrors were exposed to 36 Neutral-Beam Heated identical plasma discharges for a total plasma duration of 210 s. Optical pyrometers were used to monitor the mirror temperature. The temperature of the holder was measured with thermocouples and was found to vary between 200 and 270 °C during the exposure. Electron density and temperature were measured with He beam diagnostic. The energy of D^+ ions impinging the surface of the mirrors was in the range 200-250 eV. Ion flux density was $2.4 \cdot 10^{18}$ ions$\cdot$cm$^{-2}\cdot$s^{-1} which is aprroximately 1000 times larger than the expected charge-exchange neutral flux on the ITER first wall [28]. The total fluence averaged over the mirror surface ($\approx$ 2.5 cm^2) amounts to $1.7\cdot10^{20}$ ions$\cdot$ cm^{-2} corresponding to about 200 ITER discharges. The appearance of the holder with the mirrors after exposure is shown in fig. 4.3b.

Before and after the mirror exposure in TEXTOR detailed characterizations of the mirrors were carried out at the University of Basel. Ellipsometry and spectrophotometry were used to determine the optical properties. Measurements were made at 4 different locations on the mirror surface to improve the statistics and check the homogeneity of the optical properties along

the mirror surface. In addition, elemental composition of the mirror surface was investigated by XPS and surface morphology was studied by SEM. SIMS depth profile and profilometry measurements were carried out at the Forschungszentrum Jülich.

During the pre-characterization, the reflectivity of the single crystal molybdenum mirror was found to be significantly lower than the values recommended in [78], with a drop of about 30 % at 250 nm. XPS revealed that the surface was covered with a 16 nm thick MoO_3 film, the thickness being known from ellipsometry. Removal of this oxide was made by cleaning the mirror in a hydrogen glow discharge. Details of the cleaning procedure may be found in [100].

4.2 Tests of molybdenum mirrors in DIII-D divertor

4.2.1 The DIII-D tokamak

The DIII-D tokamak [101] is located in San Diego, California, and is operated by General Atomics. The device features a large, highly elongated plasma (plasma major radius R=1.66 m and plasma minor radius a=0.67 m, plasma height up to 2.7 m). This geometry allows large size low aspect-ratio plasma to be formed as well as providing space for open divertor configurations using the top and especially the bottom surface as divertor targets (fig. 4.4). Graphite is the sole plasma facing material in DIII-D.

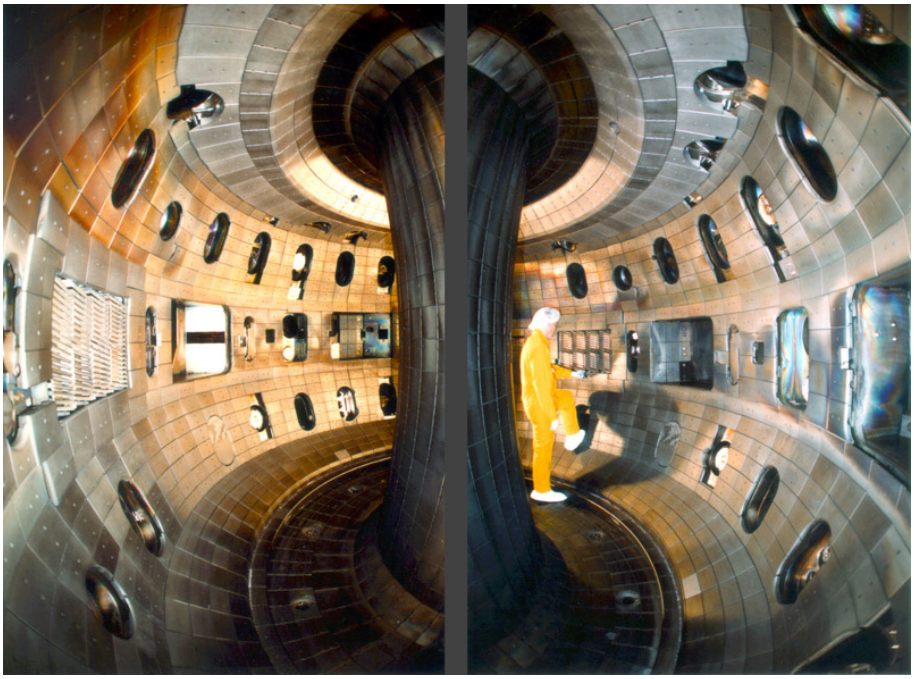

Figure 4.4: Composite view of the inside of the DIII-D tokamak (the width of the central column is distorted). Most visible are the graphite protection tiles and the access ports.

Plasma-material interactions in the lower divertor of DIII-D are studied using the Divertor Material Evaluation System (DiMES) [102] allowing insertion of material samples into the lower

divertor floor and their exposure to either a single plasma discharge or a series of reproducible discharges (to increase the total exposure time).

4.2.2 Exposure of molybdenum mirrors in DIII-D divertor

Mirrors located in the ITER divertor will likely be subjected to deposition of impurities eroded from the graphite divertor targets. Of particular interest is the Private Flux Region (PFR) where mirrors under the divertor dome will be located. Dedicated experiments were made in DIII-D where molybdenum mirrors were exposed in the divertor region to evaluate the carbon deposition rate under ITER-relevant conditions and to test mitigation methods [103, 105]. The experiment was made as a joint effort of Forschungszentrum Jülich, DIII-D team and the University of Basel.

Mirrors were exposed on a specially designed mirror holder mounted onto DiMES (fig. 4.5). The holder was made of stainless steel and equipped with a built-in heater and a thermocouple. The base of each mirror was held by three stainless steel clamps, one of which had an extended flap which masked an area of about 3×8 mm. This protected spot was used for reference during the analysis of the exposed mirrors. The mirrors were made of single crystal molybdenum with the reflective surface roughness of less than 10 nm. The mirrors were 4 mm thick; the diameters of the base and reflective surface were 22 mm and 18 mm, respectively.

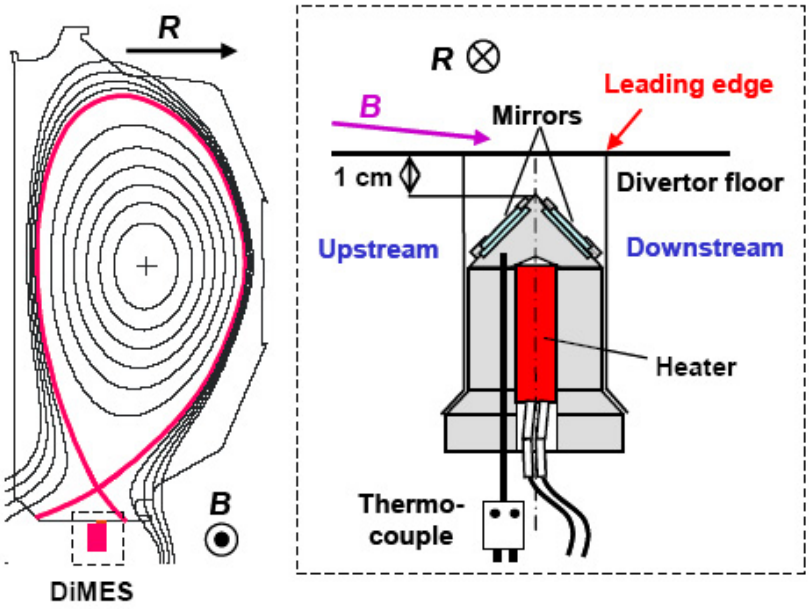

Figure 4.5: Scheme of the mirror exposure in the DIII-D tokamak.

The geometry of the mirror exposure is illustrated in fig. 4.5. The mirror holder was inserted into the divertor floor so that its top edge was 1 cm below the divertor floor surface. The top edge was oriented perpendicular to the magnetic field, so that the two mirrors faced opposite toroidal directions. The mirrors were exposed in lower single null magnetic configuration discharges and located in the private flux region during the exposure. The plasma

flow to the divertor was in the direction of **B** shown in fig. 4.5 (as confirmed by Mach probe measurements). The mirror facing the toroidal field direction will be referred as "upstream", the mirror turned back from the toroidal direction will be referred to as "downstream" mirror. The incidence angle of the plasma flux on the floor surface at the DiMES radial location was less than 1°.

Two sets of mirrors were exposed on two consecutive days. The exposure consisted of a series of reproducible ELMy H-mode discharges in deuterium. The discharge parameters were: toroidal magnetic field, B_T=2 T, plasma current, I_p = 1.1 MA, NBI heating power P_{NBI}=6.6 MW, line average density $\bar{n}_e = 8 \times 10^{19}$ m^{-3}. The divertor was detached and plasma parameters in the PFR were $T_e \approx 0.5 - 2$ eV and $\bar{n}_e \approx 4 - 8 \cdot 10^{20}$ m^{-3}. When helium glow discharge conditioning was applied in between the shots, the mirror holder was retracted to about 10 cm below the divertor floor.

The first exposure was made of 6 plasma discharges for a total exposure time of about 25 s. No active temperature control was used, but the holder and the mirror were heated by the plasma radiation and CXN fluxes. At the beginning of the exposure the holder temperature was 23°C and increased by $3 - 7$°C after each shot, and then decreased slowly during the He glow discharge. By the end of the exposure the holder temperature was at 41°C.

The second set of mirrors was exposed to 17 plasma discharges with plasma parameters similar to those of the first exposure, the total exposure time being 70 s. Mirrors were heated during the experiment to investigate the effect of mirror temperature on deposition mitigation. The target temperature was 400°C but due to a failure of the heater the temperature before the first shot was only 140°C. According to heat transfer modelling [103, 104] and taking into account the heating of the mirrors by radiation during the plasma discharge (about 3-7°C), the mirror temperature should have been in the range 176-199°C during the experiment.

For this experiment the single crystal molybdenum mirrors were supplied by Forschugszentrum Jülich. Optical measurements and surface analysis (SEM, XPS) before and after exposure were carried out in Basel.

4.3 Long term mirror exposure in Tore-Supra

4.3.1 The Tore Supra Tokamak

Tore Supra is a medium size limiter tokamak with a major radius of 2.25 m and a minor radius of 0.70 m. It has a circular shaped plasma. It is located in Cadarache, France, and operated by the Commissariat à l'Energie Atomique (CEA). Fig. 4.6 shows an inside view of the vacuum vessel and the graphite toroidal pump limiter.

Its main features are (i) superconducting NbTi magnetic coils cryogenically cooled by superfluid helium at 1.8 K, (ii) actively cooled graphite based (CFC) plasma-facing components brazed on copper alloys tubes actively water cooled, (iii) long pulse operations. Due to its unique features, a plasma duration of 6 min 18 s was recently achieved with an injected/extracted energy of about 1 GJ [106].

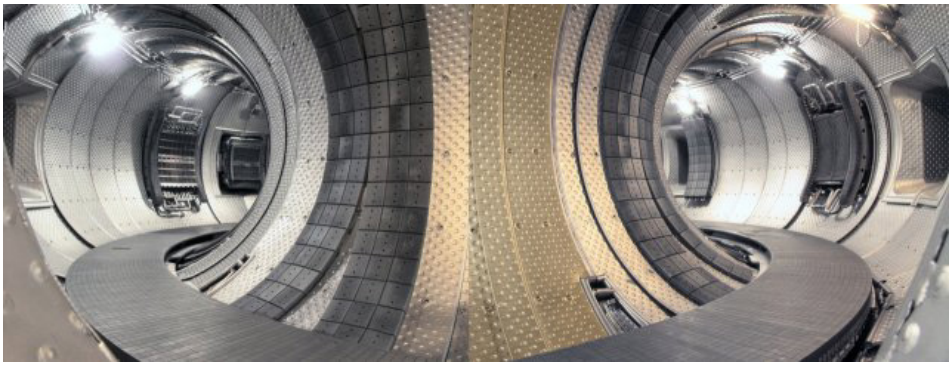

Figure 4.6: Inside view of the Tore Supra tokamak

4.3.2 Experimental setup

Metallic mirror samples (22 mm diameter, 4 mm thick) made of single crystal molybdenum (110), stainless steel (an analogue of the AISI 316 grade), and polycrystalline oxygen-free copper were installed in Tore Supra for long-term exposure during the experimental campaign 2003 – 2004 [107]. The mirrors were prepared and supplied by IPP Kharkhov, Ukraine. They were made from Russian materials.
Two mirrors of each material were installed in two sets on the high field side of the Tore Supra vessel at a poloidal angle of $\Theta = 15.4°$ (set A) and 7.6° (set B) out of the equatorial plane ($R = 2421$ mm, $r \approx 880$ mm) and positioned approximately 140 mm from the LCFS (Last Closed Flux Surface). The reflecting surfaces of all mirrors were oriented parallel to the toroidal direction and their surfaces located radially 5 mm behind the assembly structure which allowed a contact cooling via the first wall panels (Fig. 4.7). The mirrors were not protected by any shutter during plasma operations.

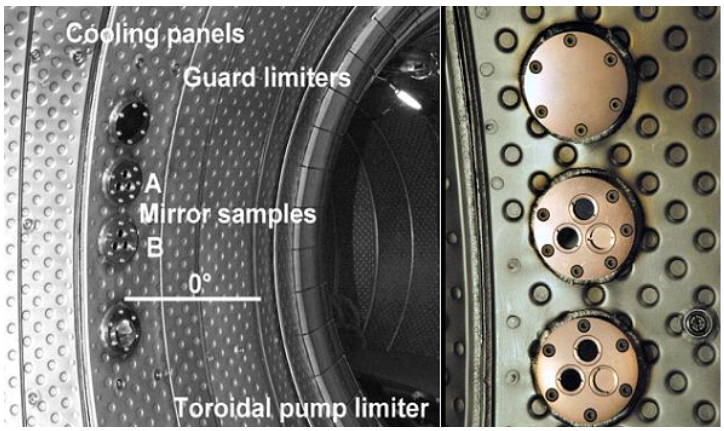

Figure 4.7: Location of the two sets of mirrors installed on the first wall of the Tore Supra tokamak

During about one year of exposure, about 1400 plasma pulses (mainly D_2) with plasma current $I_p \geq 200$ kA ($n_{eo} \approx 2{-}4{\cdot}10^9$ m^{-3}) have been performed with a cumulated pulse duration of about 26000 s (7 h and 10 min). In addition during the campaign, wall conditioning by glow

discharges in He (t = 362 h, $I = 7\mu$ A·cm^{-2}, U$_{anode}$ = 300 V, p=0.3 Pa), in D_2 (t=606 h, I=7 μA·cm^{-2}, U$_{anode}$ = 400 V, p=0.3 Pa) and 13 h of boronization have been performed in between plasma operation.

Baking cycles of the vacuum vessel structure were performed at temperatures around 200°C. According to 2D-thermohydraulic calculations the mirror temperature did not exceed 150°C during plasma operations.

A third set of mirrors was kept in air during the experiment and was used for reference measurements on virgin mirrors. Surface roughness of all mirrors (exposed and virgin) have been measured by confocal microscopy. Surface morphology and topography were investigated with SEM, and depth profile elemental analysis of the samples was made using SIMS. Optical measurements (total and diffuse reflectivity, ellipsometry) as well as chemical analyses of the mirror surfaces by means of XPS were made in Basel. All measurements were compared with those obtained on the virgin reference mirrors.

4.4 Exposure of different mirror materials in the TCV divertor

4.4.1 The TCV tokamak

The Tokamak à Configuration Variable (TCV) [108] is a compact tokamak with a distinctive rectangular vacuum vessel geometry: R=0.88 m with an internal height of 1.54 m and a minor radius of 0.25 m (fig. 4.8). It is capable of producing a wide variety of magnetic equilibria with limited or diverted configurations. Graphite is used as a plasma-facing material with about 90 % of the internal surface covered with isotropic polycrystalline graphite tiles [109]. The TCV tokamak is located in CRPP[1] Lausanne, Switzerland. The first tokamak shot was achieved in 1992.

4.4.2 Design of the sample manipulator

Assessment of the conditions expected for mirrors in the ITER divertor can only be made if mirrors are exposed in present machines at relevant locations. The experiment made in DIII-D gave a good indication of what to expect for mirrors located in the PFR. Moreover, a very comprehensive test is presently ongoing at JET where mirrors are exposed at several locations in the divertor (inner, outer, and base) and on the first wall [110], but the very long timescale of the experiment calls for experiments in smaller and more flexible divertor devices. Amongst the reasons driving the choice of TCV are its location (relatively close to the University of Basel), its flexibility (allowing exposure and retrieval of samples at short notice) and its full graphite first wall. However, since no tool was available for exposure of samples without breaking the torus vaccum, a dedicated sample manipulator has been designed and installed, and will be described in the following section.

The manipulator should provide the possibility to expose samples in the divertor region of TCV for later surface analysis, and provide a future option for other edge physics experiments (e.g. electrostatic analysis in the divertor region). Insulation of the sample holder from the main vacuum chamber is made by a UHV valve to allow sample exposure and retrieval without requiring a torus vent (fig. 4.9a). A manually operated linear drive is used to insert the sample head into the divertor floor region and to precisely adjust the position of the samples with respect to the top surface of the divertor target tiles. The turbopump attached to the system is only used for pumping down the insertion chamber. When the pressure is sufficiently low the valve is opened and the pump removed, so that the manipulator is pumped through the tokamak pumping system. This is done to avoid having the manipulator turbo pump too close to the strong magnetic field during tokamak operations when the samples are being exposed. The sample holder has a diameter of 29 mm and allows the simultaneous exposure of 2 samples with size of 14×10 mm^2 (fig. 4.9b).

Conditioning helium glow discharges are executed for 5 minutes between each tokamak discharge and for longer periods at the start of each operational day or after vessel boronisation cycles. Due to the absence of a shutter in the system and the impossibility of

[1]Centre de Recherche en Physique des Plasmas

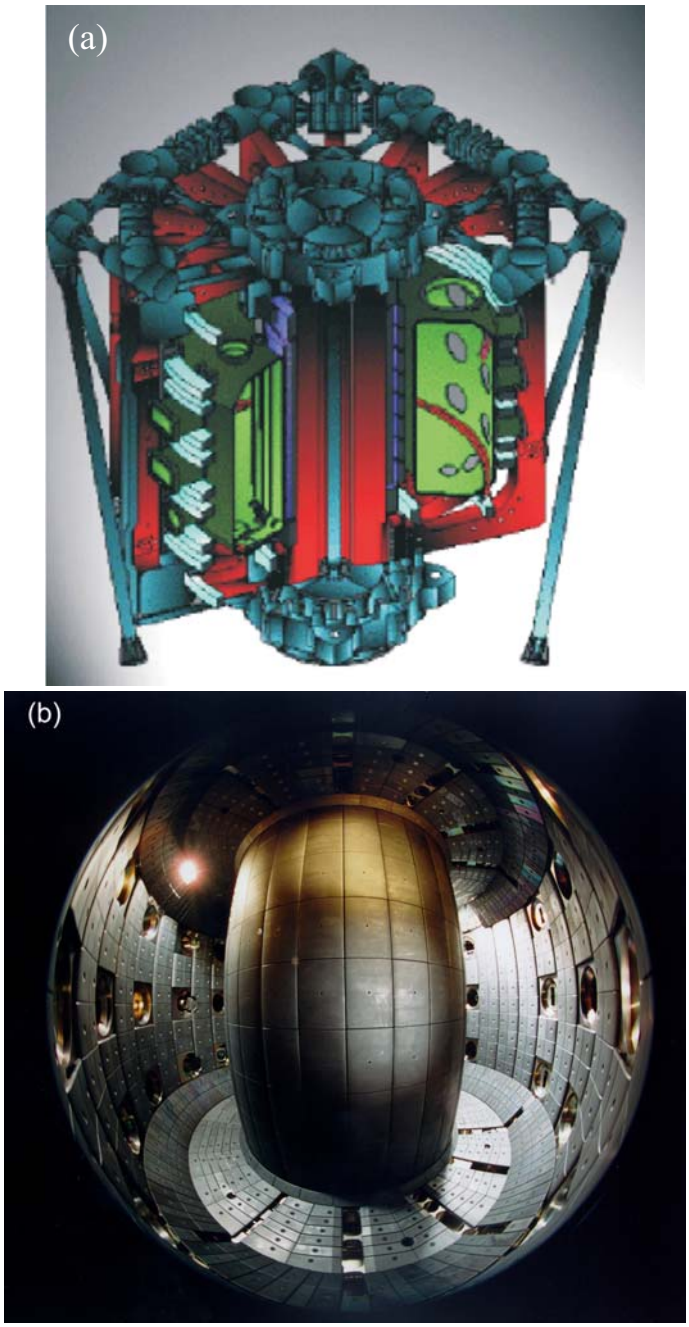

Figure 4.8: (a) Schematic view of the TCV vacuum vessel, (b) inside view of the TCV tokamak showing the graphite coverage of the vacuum vessel

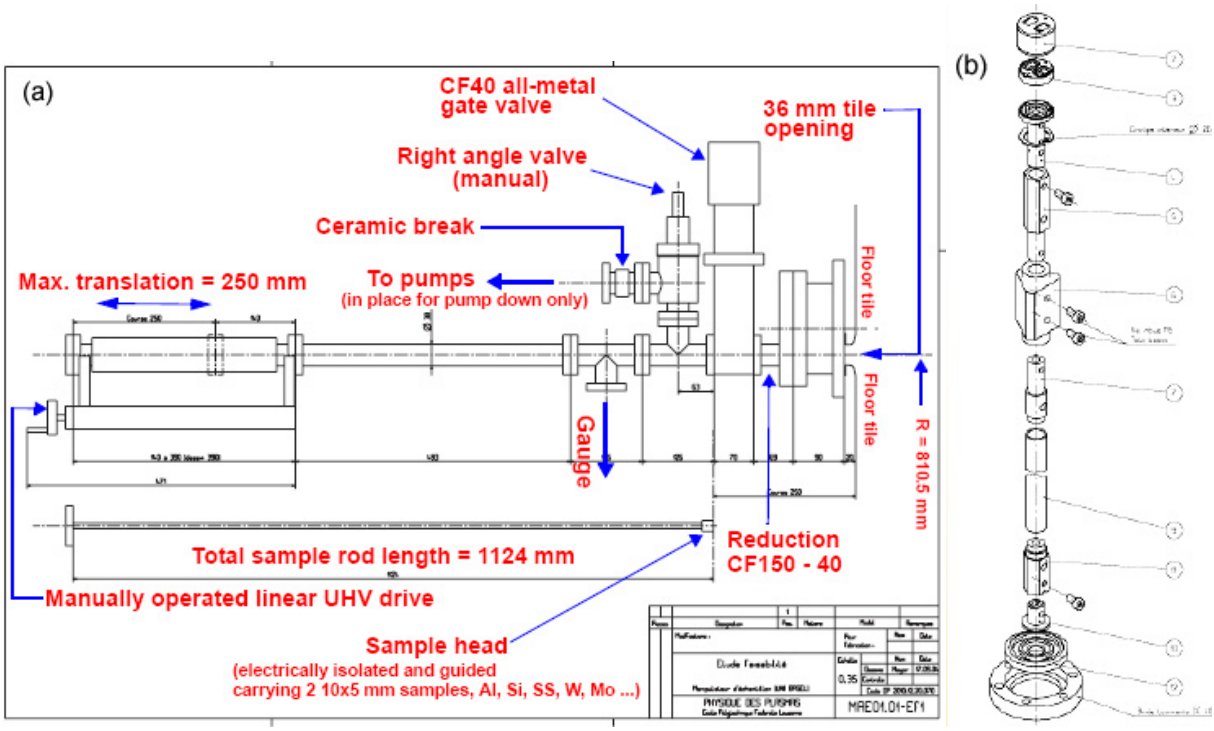

Figure 4.9: (a) Plane view of the manipulator design showing the manual linear drive and the valves used to insulated the manipulator from the torus, (b) isometric view of the sample head.

retracting the manipulator head during glow discharges, the sample holder is electrically insulated from the rest of the torus and hence maintained at the local floating potential established during the glow discharges. This minimizes the energy of the helium ions impinging on the mirror surface and avoids the ∼400 V cathode fall present elsewhere on the first wall.

The manipulator location (radial location for the centre of the manipulator head R=0.8105 m) places the samples underneath the far outer divertor SOL of the standard TCV single null lower discharge used as a fiducial shot at the start of each operational day to study the long-term evolution of wall conditions [111]. The choice of the sample locations is a compromise between the necessity of getting enough deposit to be meaningful and not exposing the samples to too high heat fluxes (ITER divertor mirrors will not be near high heat flux regions). Moreover, the samples should see impurity outflux from plasma-wall interaction in the main chamber but should never experience direct interaction with the plasma. Fig. 4.10 illustrates the insertion of the sample holder into the TCV divertor floor. As seen from fig. 4.10a, TCV has an open divertor geometry. Samples are recessed behind the front surface of the graphite tiles to avoid direct plasma impact; the linear drive system allows the recessment distance to be varied. Special chamfering is provided on the tiles around the sample entrance hole (fig. 4.10b) to prevent strong plasma-surface interactions in the sample vicinity and especially enhanced re-deposition of carbon sputtered locally from the leading edge of the graphite tile. With such an arrangement, during the "standard" shot, the incidence angle of the plasma flux on the tile above the sample holder is barely 1°, so that the ions interact with the tile only on the

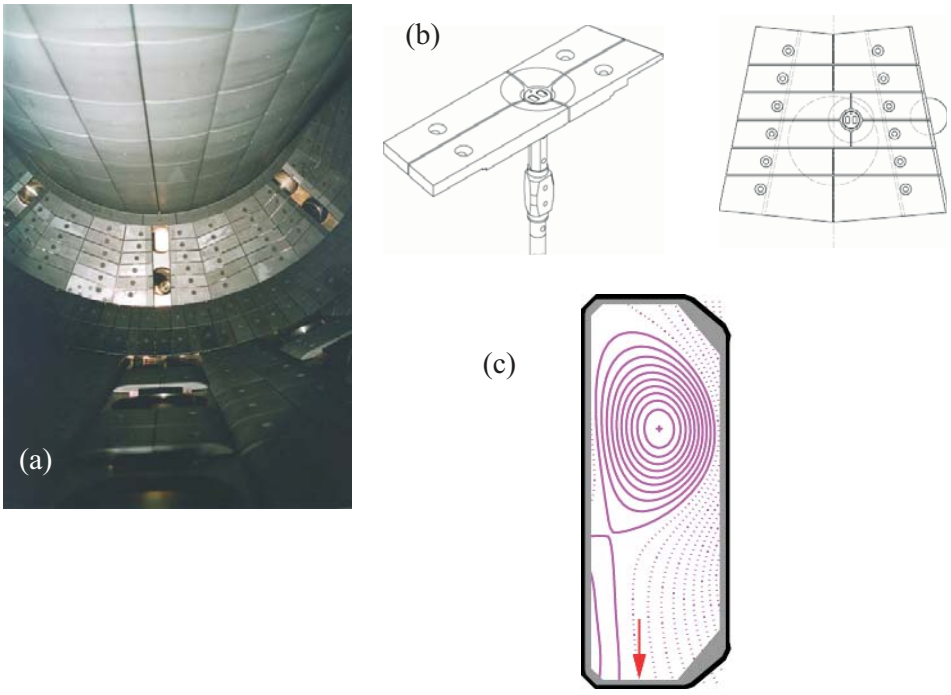

Figure 4.10: (a) Photo of the TCV floor showing the open divertor geometry, (b) schematic drawing showing the installation of the sample manipulator in the TCV vessel floor, and (c) magnetic equilibrium of the TCV standard single null diverted discharge (the red arrow indicates the mirror location).

chamfered edge. Fig. 4.10c, illustrates the location of the samples in the magnetic equilibrium of a "standard" shot.

4.4.3 Mirror exposure in TCV: experimental conditions

The large variety of magnetic equilibria studied on TCV and the absence of any shutter system protecting the samples means that most exposures are integrated across short experimental campaign periods of 2-3 weeks including regular helium glow discharge conditioning. Experiments have been made with different mirror materials (Mo, W, Si, Rh), different recessment distances and different exposure times [112, 113]. A dedicated experimental session was also made during which the samples were exposed to 19 ohmic L-mode discharges at $I_p = 320$ kA and $\bar{n}_e \approx 6 \times 10^{19}$ m^{-3} using the same configuration as the "standard" discharge.

Before and after each sample exposure, optical measurements and surface analysis are performed at the University of Basel. Spectroscopic ellipsometry is used to determine the optical properties of the samples and the deposited layer thickness, whilst XPS and SEM provide information on the layer composition and morphology. Depth profile measurements with SIMS have been made on some samples to study the homogeneity of the deposited layer. A stylus profilometer is used to confirm the estimation of the deposited thickness.

Chapter 5

Laboratory experiments

5.1 Exposure of mirrors to deuterium glow discharge containing methane

Mirrors made from stainless steel (SS) and polycrystalline copper have been exposed to a deuterium glow discharge with controlled partial pressure of methane in the gas mixture. Experiments are performed in a high vacuum plasma chamber located in the Institute of Physics at the University of Basel (CH). A schematic drawing of the system is shown in fig. 5.1. The chamber is pumped down to a base pressure of about 10^{-7} mbar using a conventional turbomolecular pumping system.

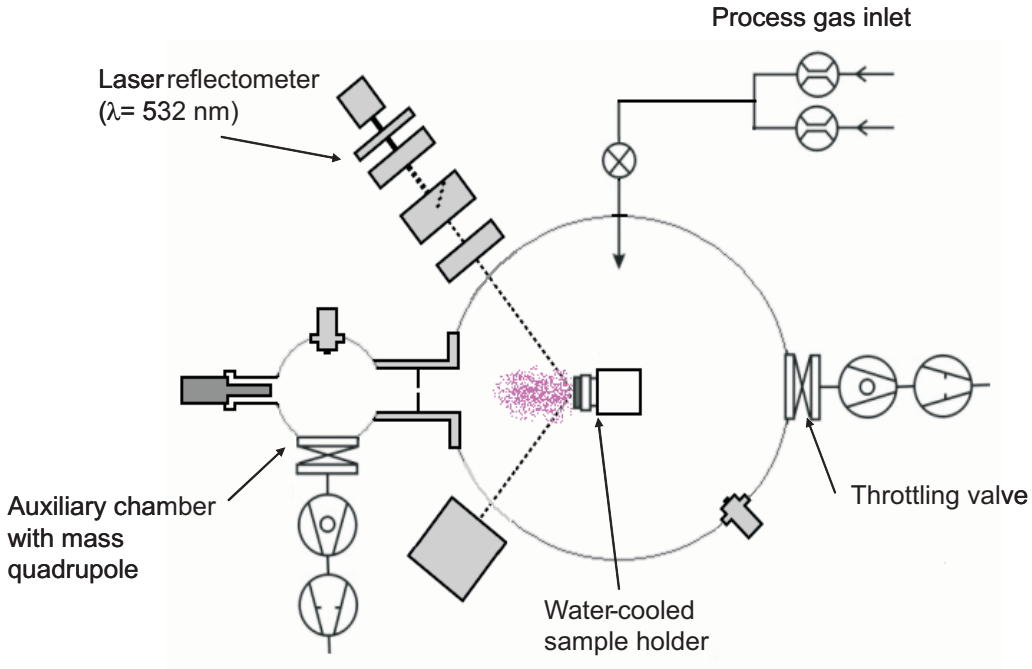

Figure 5.1: Schematic drawing of the XPS analysis chamber and the transfer system.

Monitoring of the partial pressures of D_2 and CH_4 during the plasma exposure is achieved

using a mass spectrometer[1] located in an auxiliary chamber connected to the main plasma chamber through a 100 μm diameter pinhole. The pumping system of the auxiliary chamber is independent of that from the main chamber. The necessity of this installation is due to the impossibility of the mass spectrometer to work at pressures higher than 10^{-5} mbar. From mass spectrometry measurements when the plasma is running, one can determine f_{CH_4}, the fraction of methane in the gas mixture.

The mirrors were mounted on a water-cooled sample holder. A negative bias of -200 V applied on the mirror controls the impinging ion energy. Ion fluxes are determined by measuring the current passing through the sample, neglecting secondary electron emission. Deuterium and methane are introduced into the chamber through mass flow controllers. The working pressure ($5 \cdot 10^{-2}$ mbar) is adjusted by a throtling value to the pumping system. Plasma parameters ($n_e \approx 10^{15}$ m^{-3} and $T_e = 13$ eV) were measured by means of a Langmuir probe.

The major drawback of the mirror experiments made in laboratory stands and described for example in [67] is that the mirrors have to be taken out of the plasma chamber regularly so that the reflectivity can be measured. An ideal approach would be to follow *in-situ* the development of the reflectivity over a wavelength range as a function of the incoming ion flux. An alternative solution has been chosen here, reflectivity data for s-polarized light are measured using a real time laser reflectometer, description of the system can be found in [89]. The light source is a solid state laser[2] with a working wavelength of 532 nm and a beam diameter of 1 mm. The main components of the system are a chopper, a beam splitter for the detection of a reference signal, a polarizer, two photodiodes for light detection and lock-in amplifiers for the sampling of incident and reflected beams. An incidence angle of 52° was used here.

The mirror samples were prepared in IPP Kharkov, Ukraine. The stainless steel mirrors were made from an analogue of the AISI316 grade (C0.04Cr18Ni11Mo3Ti) which is an austenitic steel. Copper samples were made from polycrystalline oxygen-free copper. All samples were cut using arc cutting in kerosene, washed by acetone and exposed for 20 minutes to low energy ions (50 eV) from a hydrogen ECR plasma. Since copper is very sensitive to oxidation in air, the samples were cleaned again for 5 minutes in a deuterium plasma (ion energy 200 eV) before the experiment.

Total and diffuse reflectivity measurements as well as ellipsometry were made before and after plasma exposure. Scanning Electron Microscopy (SEM) is used to study the surface morphology and Energy Dispersive X-Ray analysis (EDX) to check the surface chemical composition. Weight measurements of the mirrors before and after plasma exposure together with stylus profilometer measurements allow the eroded/deposited depth to be determined. For the calculations of the sputtered depth, density values of 8 and 8.92 g·cm^{-3} were assumed for stainless steel and copper respectively.

[1] Stanford Reasearch System RGA 200

[2] Laser 2000, LCM-T-01-ccs

5.2 Experiments in PISCES-B: study of deposited Be/C layers on mirror surfaces

PISCES-B[3] is a linear plasma plasma device located at the University of California at San Diego (UCSD). It is dedicated to studying plasma-material interactions for fusion relevant ma-

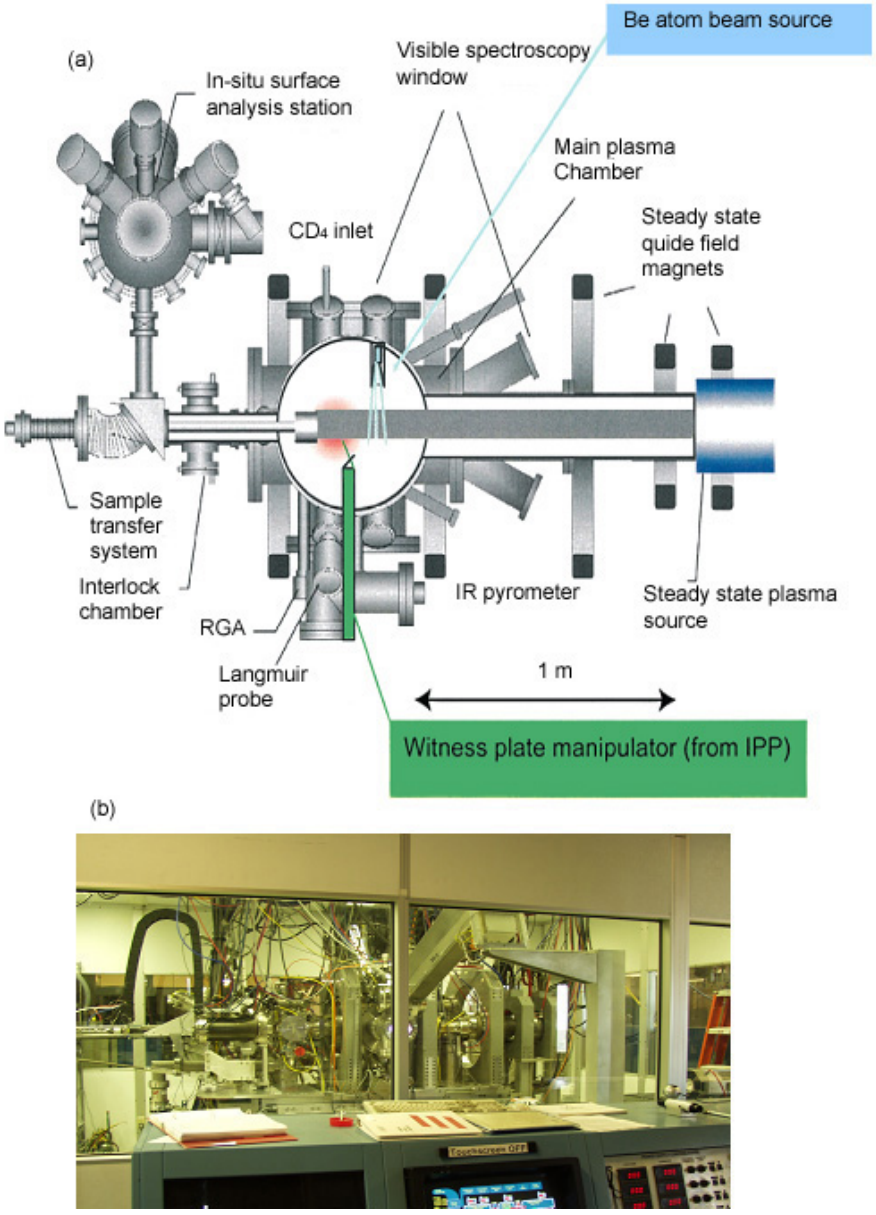

Figure 5.2: (a) Schematic top view of the PISCES-B device and (b) picture of the machine in the isolated contained air enclosure (the computer screen at the bottom gives an idea of the dimensions of the machine).

terials and plasma parameters [90]. The intense plasma flow generated in PISCES-B simulates

[3]Plasma Interaction Surface Component Experimental Station

the scrape-off layer plasma flow into the ITER divertor. The plasma is generated by an arc discharge initiated with a heated LaB_6 cathode. The anode and axial magnetic field define a cylindrical plasma with a radius of about 40 mm and axial length greater than 1 m. An *in-situ* surface analysis station with Auger Electron Spectroscopy (AES), XPS and Secondary Ion Mass Spectrometry (SIMS) is attached to the main plasma chamber (fig. 5.2a). The machine is installed in an airtight enclosure to allow safe operations with beryllium (fig. 5.2b).

Due to the combination of material planned to be used in ITER and the choice of beryllium as a first wall material in the main chamber, the SOL plasma flow in the ITER divertor may contain Be fraction in the range 1-10 % [52]. Recent results obtained in Pisces-B [91, 92] have shown that even with very low Be content in the plasma (≈ 0.1 %), at the plasma parameters relevant for ITER, a graphite target becomes coated with a beryllium layer that reduces its erosion by the plasma. In turn, Be re-erodes and leads to Be-rich deposited layer in line-of-sight locations from the target [93]. Even though the possible effects of ELMs on the Be layer deposited on the divertor targets are not yet known, these results suggest that beryllium, and not carbon, may be the main deposited impurity in the divertor region. Therefore it is of interest to determine what effect a mixed Be/C layer will have on the reflectivity of a metallic mirror. Hence, dedicated experiments have been initiated to study the deposition of material re-deposited on metallic mirrors due to erosion of a graphite target by a beryllium containing deuterium plasma.

Fig. 5.3 shows schematically the experimental arrangement used [93]. ATJ graphite targets are exposed to a high-flux ($\approx 3 \cdot 10^{22}$ deuterium ions$\cdot m^{-2}s^{-1}$) plasma. A Be impurity flux is generated through the use of an evaporative atomic beam source[4]. The emerging atom beam [91] is oriented in such a way that the beam travels perpendicular to the magnetic axis of PISCES-B. Because of a slow thermal velocity, evaporated beryllium atoms are rapidly ionized in the plasma through collisions. The beryllium ions thus created are entrained by the plasma flow and directed towards the graphite target. The concentration of beryllium ions is controlled by varying the temperature of the evaporator oven.

A region of the plasma column extending from the target to just beyond the beryllium injection zone (fig. 5.3) is observed spectroscopically. The determination of the concentration of Be ions in the plasma is made from the intensity of the BeII line (467 nm), the calibration of the BeII photon flux being done with a calibrated white light source. A complete description of the method is given in [94]. The plasma parameters (temperature, density) are measured using a reciprocating langmuir probe.

The mirrors were installed on a movable witness plate manipulator (see fig. 5.3) to collect redeposited material during the graphite target exposure. They are shielded from cross-field plasma transport so that only particle fluxes from sputter erosion and reflection from the target contribute to deposition/co-deposition. The witness plate can be independently heated in the temperature range 300-700 K and is fully retractable into a vacuum interlock chamber to allow rapid replacement of the sample without breaking the PISCES-B vacuum. However during the exposure, the mirrors are heated by the plasma radiation (about 100 K for one hour exposure time).

[4]VEECO/APPLIED EPI Molecular Beam Source

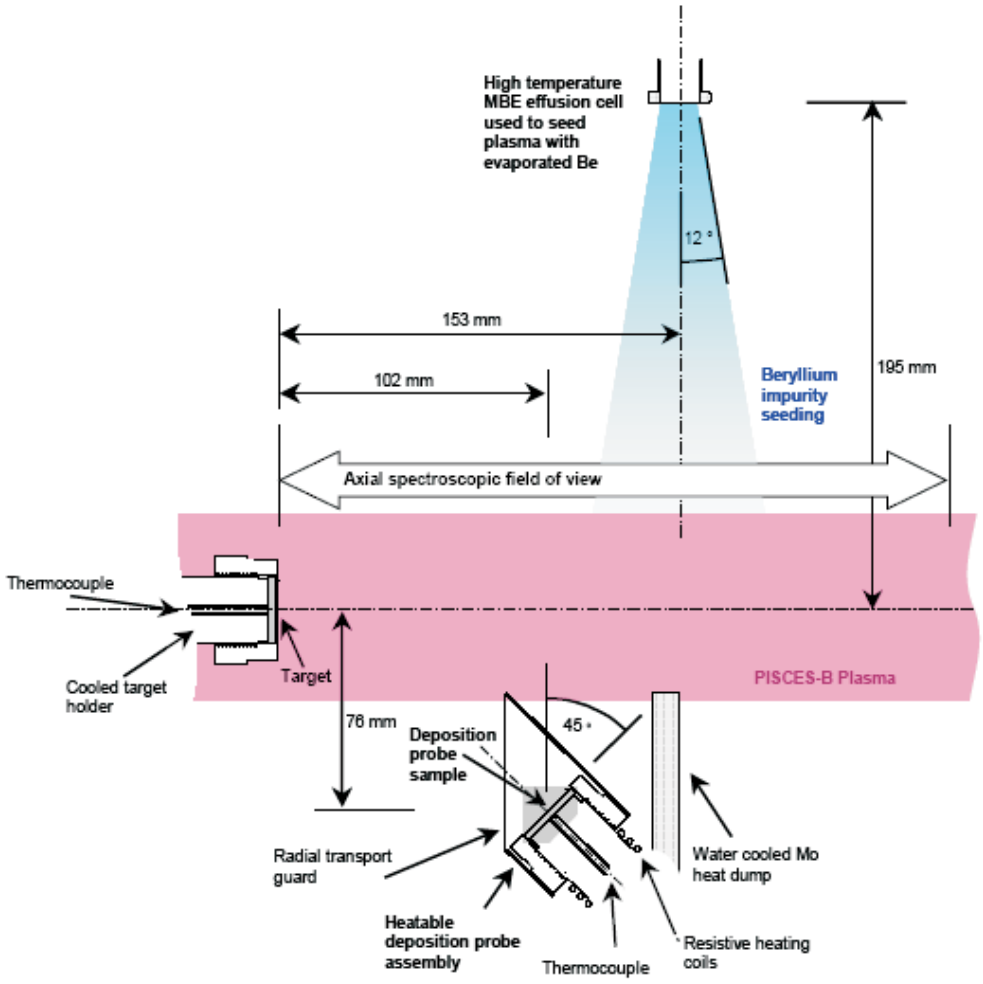

Figure 5.3: Arrangement used to collect deposited/codeposited material during exposure of target materials in PISCES-B.

12 mirrors (2 cm diameter, 2 mm thick) from polycrystalline molybdenum and copper were prepared and polished in the University of Basel. After polishing they were rinsed in an ultrasonic bath with acetone and alcohol and their reflectivity was measured using the spectrophotometer.

The optical equipment available in Basel is not compatible with Be handling. Therefore, in the present case a simple reflectance measurement system, housed inside the PISCES-B closed air environment, was used. A schematic drawing of the setup is shown in fig. 5.4. After being taken out from the machine, the mirror to measure is installed on a sample holder located inside the enclosure parallel to the window. Outside the enclosure, a calibrated white light source illuminates the sample with an angle of incidence of about 10°. The reflected signal is measured by an optical fibre terminated by a focusing lens and connected to a diode array spectrometer[5]. Measurements are done in the range 450-950 nm.

To avoid the necessity of using a calibrated sample for the determination of the absolute

[5]Ocean Optics HR2000

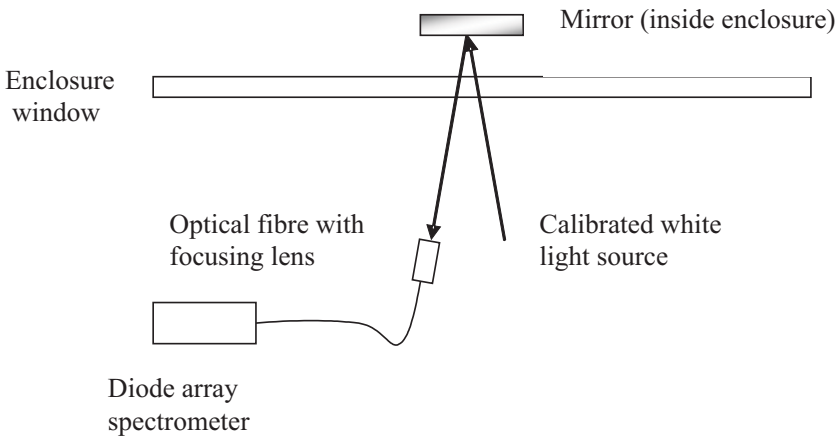

Figure 5.4: Schematic drawing of the setup used for reflectivity measurements on mirrors exposed in PISCES-B.

reflectance it was decided to measure the relative reflectivity of the exposed mirrors which can be defined by:

$$R_{rel}(\lambda) = \frac{I_{exposed} - I_{background}}{I_{virgin} - I_{background}} \tag{5.1}$$

where $I_{exposed}$ is the signal measured when an exposed mirror is placed on the sample holder, I_{virgin} is the same measurement made with a virgin mirror from the same material. The background in measured by blocking the incident light by a shutter.

Surface analysis on the exposed mirrors were made in IPP Garching, by depth-sputter XPS and Nuclear Reactions Analysis (NRA).

Chapter 6

Surface characterization techniques

This chapter will described the analytic tools used during this work to characterize the mirrors exposed in different conditions. Only the theoretical notions necessary to understand the measurement techniques will be given.

6.1 Reflectivity measurements

6.1.1 Some notions about optics

At the interface between two media with different optical properties, an incident plane electromagnetic wave is splitted in a reflected and a transmitted part (fig. 6.1). For the reflected

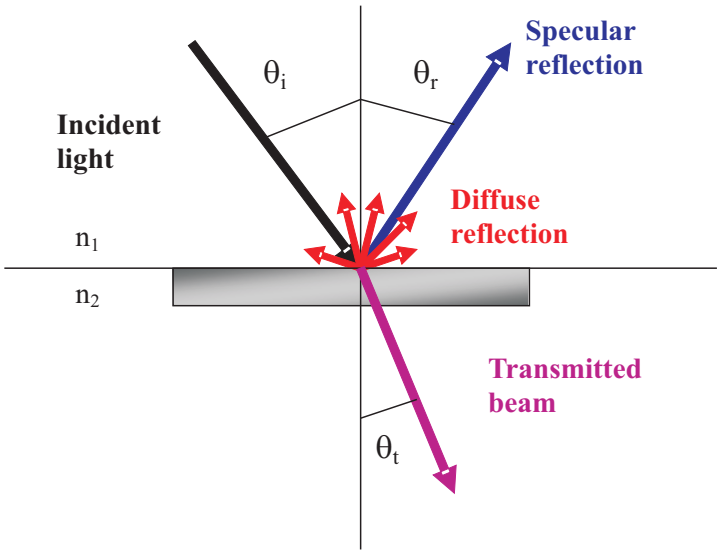

Figure 6.1: Description of the behaviour of the light at the interface between two media. θ_i, θ_r, and θ_t are the angle of incidence, of reflection and of transmission respectively.

beam the angle of reflection is equal to the angle of incidence ($\theta_r = \theta_i$). For the transmitted beam, according to the Snell's law one can write:

$$n_1 sin\theta_i = n_2 sin\theta_t \tag{6.1}$$

with n_1 and n_2 the absolute refractive index of the two media.

We assume that the two media in fig. 6.1 are linear, homogeneous and isotropic. The application of the boundary conditions for the electric field at the interface between the two media leads to the complex Fresnel coefficients for the reflected beam for the parallel (p) and perpendicular (s) components of the electric field.

$$\begin{aligned} r_s &= -\frac{sin(\theta_t - \theta_i)}{sin(\theta_t + \theta_i)} =\mid r_s \mid e^{j\delta_s} \\ r_p &= \frac{tan(\theta_t - \theta_i)}{tan(\theta_t + \theta_i)} =\mid r_p \mid e^{j\delta_p} \end{aligned} \tag{6.2}$$

In case of an absorbing medium the refractive index is a complex and can be written:

$$\tilde{n} = n - jk \tag{6.3}$$

where k is the absorption coefficient. The reflectivity of the medium 2 is defined as the ratio of the intensities of the incident and reflected beam, similarly to the description made in eq. 6.2 one can write:

$$\begin{aligned} R_s &= \left(\frac{sin(\theta_t - \theta_i)}{sin(\theta_t + \theta_i)}\right)^2 =\mid r_s \mid^2 \\ R_p &= \left(\frac{tan(\theta_t - \theta_i)}{tan(\theta_t + \theta_i)}\right)^2 =\mid r_p \mid^2 \end{aligned} \tag{6.4}$$

The reflectivity R observed for a natural or unpolarized light (containing an equal mix of s and p-polarisations) is given by:

$$R = \frac{(R_s + R_p)}{2} \tag{6.5}$$

For normal incidence ($\theta_i = 0$), the distinction between both polarizing components disappears and one has for the reflectivity:

$$R = \left(\frac{n_1 - n_2}{n_1 + n_2}\right)^2 \tag{6.6}$$

The reflectivity of a surface for oblique incidence is a function of the angle of incidence.

6.1.2 Different components of the reflectivity

The description made in section 6.1.1 is only valid for a perfect surface. When the surface roughness is not negligible compared to the wavelength of the light, part of the light bounces off in all directions (fig. 6.1), this is called diffuse reflection. The reflection described by the Fresnel's equations is called the specular reflection: it denotes the ability of the surface to transmit an image.

The angular distribution of the diffusely reflected light depends on the structure of the material, a common description is the Lambertian reflectance in which the light is reflected with equal luminance in all direction. The diffuse (resp. specular) reflectivity is defined as the ratio of the intensity of light reflected diffusely (resp. specularly) to the intensity of the incident

light. The total reflectivity (also called hemispherical reflectivity) is defined as the sum of both components:

$$R_t = R_s + R_d \tag{6.7}$$

where R_t, R_s and R_d are the total, specular and diffuse reflectivities respectively. As mentioned in chapter 3.3, the specular reflectivity is linked to the surface roughness through the Bennett's law.

6.1.3 Reflectivity measurements: the spectrophotometer

Reflectivity measurements are carried out using a UV-Vis-NIR spectrophotometer (Varian Cary 5). A calibrated PTFE standard is used as a reference sample allowing to determine absolute values of the sample reflectivity. The absolute reflectance of the sample to measure is therefore calculated with the formula:

$$R_{\%}(\lambda) = C(\lambda) \times \frac{I_{sample} - I_{background}}{I_{reference} - I_{background}} \tag{6.8}$$

where C is the absolute reflectance of the PTFE reference. From eq. 6.8 it is seen that measurements are made in three steps. First, a measurement of the background ($I_{background}$) is made by blocking the incident light, then the reference plate is measured ($I_{reference}$). The spectrophotometer is thus calibrated and the sample can be measured (I_{sample}).

The spectrophotometer is equipped with a 110 mm diameter integrating sphere (also called Ulbricht's sphere) in the wavelength range 250-2500 nm. The sphere is coated with PTFE (Poly Tetra Fluoro Ethylene or Teflon) which has a reflectivity close to 100 % over the whole working wavelength range [81] and is assumed to have a perfect lambertian diffuse reflectivity. The geometry of the integrating sphere allows to measure either the total or the diffuse reflectivity. For the total reflectivity, the incident light beam arrives on the sample with an incidence angle of $\approx 3°$ and strikes the inner wall of the sphere after reflection on the samples. On the contrary, for the determination of the diffuse reflectivity solely, the incident beam arrives on the surface with a normal incidence so that the direct reflected beam comes out of the sphere without being measured. Only the diffuse component is detected.

6.2 Spectroscopic ellipsometry

Ellipsometry is a widely used non-destructive method for the determination of the optical properties of materials and for the determination of thin film thickness. The first ellipsometer was designed by Rothen in 1945 [82] although studies about the polarization of light and its changes after reflection (or transmission) were initiated a long time earlier.

When a plane-polarized light beam is incident on the interface between two media at some oblique incidence, the reflected light beam is generally elliptically polarized. Ellipsometry measures the change in the polarization state of the light and interpretes it in terms of the physical properties of the media involved [83]. Using the notations defined previously and considering the material as absorbing (the refractive index being defined as in eq. 6.3), the

ratio $\rho = \frac{r_p}{r_s}$ is a complex number. Ellipsometry is based on the measurement of this quantity which is generally written in terms of 2 parameters ψ and Δ such that:

$$\rho = tan(\psi)exp(j\Delta) \tag{6.9}$$

Since r_p and r_s are complex numbers, eq. 6.9 can be written:

$$\rho = \frac{\mid r_p \mid}{\mid r_s \mid} expj(\delta_{rp} - \delta_{rs}). \tag{6.10}$$

giving

$$\begin{aligned} tan(\psi) &= \frac{\mid r_p \mid}{\mid r_s \mid} \\ \Delta &= (\delta_{rp} - \delta_{rs}). \end{aligned} \tag{6.11}$$

Thus, $tan(\psi)$ represents the relative attenuation of the p- and s-polarized components whilst Δ represents the relative phase shift introduced by the reflection on the surface.

Usually, it is not possible to compute directly the optical properties of the studied material from the measured ratio ρ. Instead, an optical model has to be employed and an iterative fitting procedure used [84, 85]. In the present study, for example, a virgin mirror will be modelled by a semi-infinite substrate, a deposited layer (carbon for instance) on a mirror surface will be modelled as a homogeneous and isotropic material on a semi-infinite substrate, etc. Some parameters in the model are set as free parameters and are varied during the fitting procedure (a least-squares regression usually but other methods may be employed) to minimize the following error function [83]:

$$G = \sum_{i=1}^{M} \left[(\Delta_i^m - \Delta_i^c)^2) + (\psi_i^m - \psi_i^c)^2 \right] \tag{6.12}$$

where M is the number of measurements, Δ_i^m, ψ_i^m are the values measured by the ellipsometer, and Δ_i^c and ψ_i^c are derived from the fictive model used to describe the material. Those parameters which produce the minimum value of G are assumed to be the "correct" optical constants of the materials. However, as pointed out in [86], obtaining a good fit of the model to the experimental data does not ensure that the model corresponds to reality. As a consequence, ellipsometry should be used in conjunction with other techniques to establish a suitable interpretation of the ellipsometric data.

The ellipsometer used in the laboratory is a Variable Angle Spectroscopic Ellipsometer (VASE) whose basic schematics are given in fig. 6.2. It is equipped with both a rotating polarizer and analyzer. A xenon lamp and a CCD spectrometer are used for measurements in the visible range while a Fourier transform spectrometer is used for measurements in the near infrared. The total wavelength range is therefore 350-2300 nm. The incident angle can be varied between 40 ° and 80 °. In addition, since the polarization of the incident light can be adjusted by the rotating polarizer, it is possible to study the reflectivity of the sample for a given polarization state of the incident light.

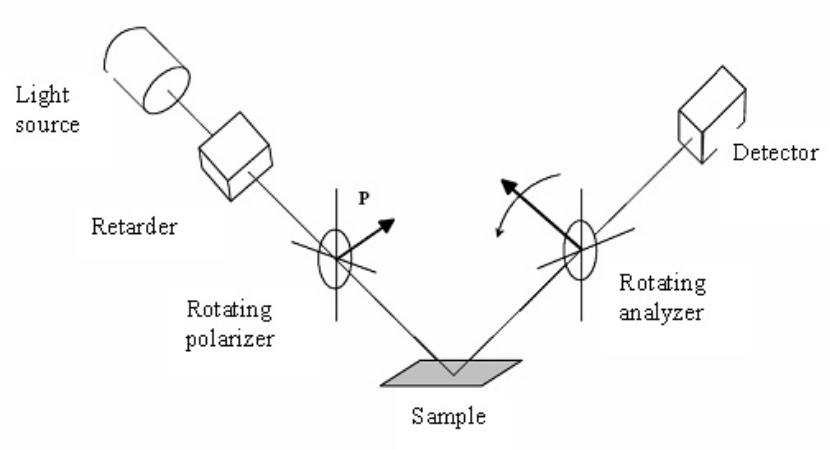

Figure 6.2: Basic principle of a spectroscopic ellipsometer

6.3 X-Ray Photoelectron Spectroscopy (XPS)

The X-ray photoelectron spectroscopy also called Electron Spectroscopy for Chemical Analysis (ESCA) is a very accurate method to investigate surface composition from both a quantitative and a qualitative point of view. The basic principles of the method will be described in this section.

6.3.1 Principle

The interaction of an X-Ray photon with a sample leads to the ejection of photoelectrons due to the photoelectric effect. The determination of the kinetic energy of the outgoing electron is the cornerstone of photoelectron spectroscopy. If the energy of the impinging photoelectron hν, the kinetic energy of the photoelectron E_{kin} and the sample's workfunction Φ are known, it is possible to calculate the original binding energy E_B of the photoelectron.

$$E_B = h\nu - \Phi - E_{kin} \tag{6.13}$$

The work function is the minimum energy (usually measured in electron volts) needed to remove an electron from a solid to a point immediately outside the solid surface.

The process of the photoemission can be described by the so-called *three-step model* [87] which is a simplification of the actual problem but has proven to be very fruitful for the interpretation of experimental data. In the first step of optical excitation, a photon is absorbed and the respective electron is excited into an unoccupied state in a direct or indirect transition. During their way to the surface (step 2) some of the electrons suffer energy losses due to interactions with the solid, e.g. plasma excitations, inelastic electron-electron and electron-phonon scattering. Finally, the electrons have to traverse the surface region to leave the sample and therefore to overcome the work function Φ (step 3).

The binding energy of the photoelectrons is an intrinsic material property and will not change with the X-ray source photon energy, but will show slight variations for a particular

element and energy level depending on the exact chemical environment of the atom, molecule or ion. This effect is called the *chemical shift* and is the reason for the other appelation of XPS: ESCA (Electron Spectroscopy for Chemical Analysis).

XPS is a surface-sensitive technique. The emission of photoelectrons (I_d) as a function of depth is predicted by the well-known Beer-Lambert equation [88]:

$$I_B = I_\infty \cdot (1 - e^{-d/\lambda sin\theta}) \tag{6.14}$$

where I_d is the intensity from a layer of thickness d at the surface, I_∞ is the intensity from an infinitely thick layer, λ is the inelastic mean free path (i.e. the mean distance travelled by an electron without energy loss), and θ is the take-off angle relative to the sample surface. From eq. 6.14 it follows that 63 % of the total signal originates in the outer 1λ of the specimen, and 95 % from within 3λ. While naturally no absolute cut-off can be given, it is reasonable to consider that most of the photoelectrons are emitted from within a layer thickness of 3λ. This depth is considered as the *information depth* of the method. The depth of analysis of XPS is generally quoted as being in the range of 2-5 nm [88].

6.3.2 Apparatus

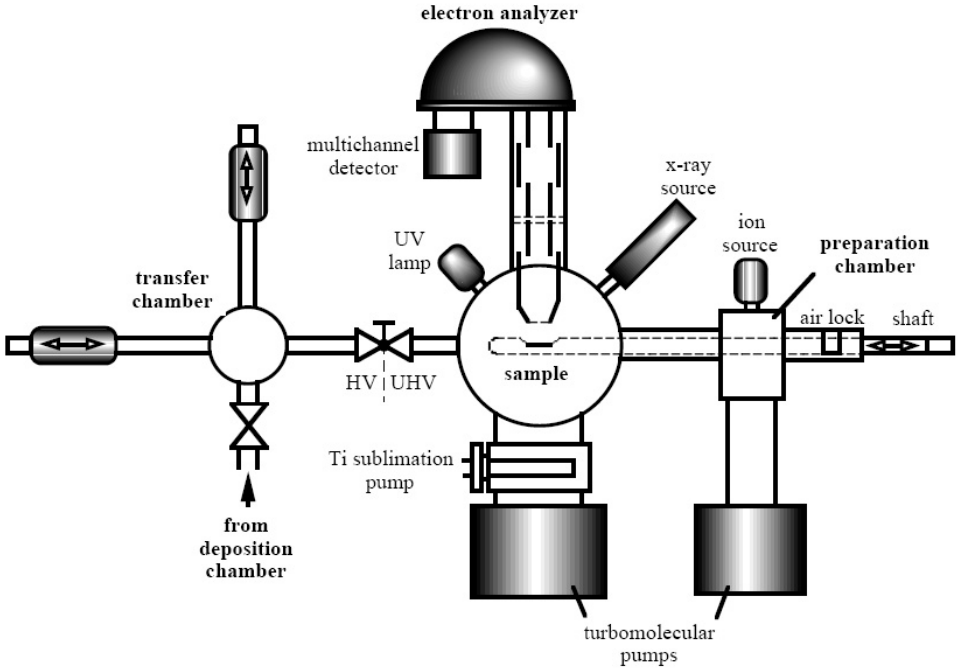

Figure 6.3: Schematic drawing of the XPS analysis chamber and the transfer system.

XPS measurements are made in a Ultra High Vacuum (UHV) chamber whose schematic drawing is shown in fig. 6.3. UHV is a prerequisite for XPS measurements because of the limited mean free path of the electrons in the residual gas of a HV system. Moreover higher pressures may result in the formation of adsorbates onto the surface which, given the thin

information depth of XPS, may mask the signal from the substrate. The typical background pressure in the analysis chamber is about $2 \cdot 10^{-10}$ mbar. The analysis chamber is attached to a plasma chamber by a transfer system that allows to tranfer the sample from one chamber to the other without exposing it to air. An additional load lock is available for the study of *ex situ* samples and was used for the study of mirrors exposed in a tokamak.

The electron detection consists of a spherical energy analyzer and a multichannel electron multiplier. The analyzer is operated in the constant pass energy mode. In this mode the spherical deflection unit, which acts as a narrow band pass for the electrons, is held at a constant pass energy. The electron energy is selected by biasing the whole deflection unit, including its entrance slit and the detector. The resolution of the analyzer is constant over the whole kinetic energy range which is necessary for reliable evaluation of the spectra.

For the XPS photon excitation a monochromatized Al Kα source at hν=1486.6 eV is used. For the electron binding energy calibration, a gold sample with the Au $4f_{7/2}$ line at 84.0 eV is used. The spectral resolution of the system is 0.5 eV.

XPS measurements were used to obtain information on the chemical composition of the mirror surface and link it to the evolution of the mirror reflectivity.

6.4 Observation of the surface morphology

Observation of the surface morphology are done by Secondary Electron Microscopy (SEM) using a Hitachi S-4800 microscope capable of high resolution imaging. Resolution of 2 nm at 15 kV can be reached with proper sample preparation. To improve the electrical contact between the mirror and the sample holder a silver paste is used.

Measurements of the surface roughness are made using a step profilometer (α-step, Tencor Instruments).

Part III

Experimental results

Chapter 7

Effect of the mirror crystallography: direct comparison of polycrystalline and single crystal mirrors under erosion conditions in TEXTOR

7.1 Changes in the optical properties induced by the exposure

In this chapter the results of the exposure of polycrystalline and monocrystalline mirrors under erosion condtions in the SOL plasma of TEXTOR will be described, details about the experimental setup may be found in chapter 4.1.2.The appearance of the single crystal molybdenum mirror after exposure in TEXTOR is shown in fig. 7.1. Apart the area which was covered

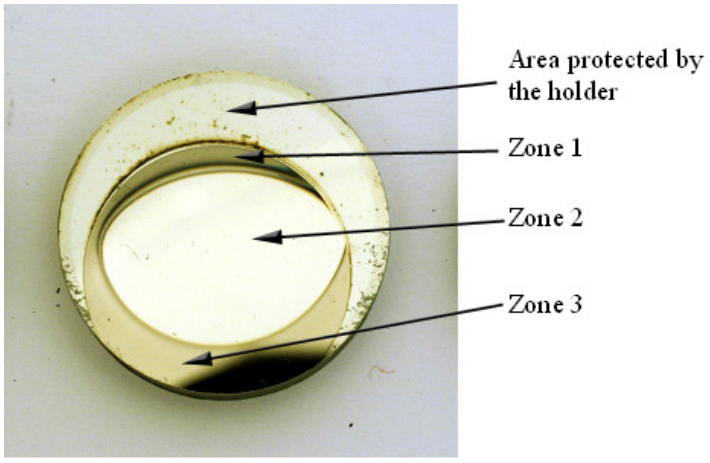

Figure 7.1: Appearance of the single crystal molybdenum mirror after exposure in TEXTOR. See text for details about the zones denoted 1,2 and 3.

(and protected) by the sample holder, three different zones can be distinguished. The shiny

metallic (zone 2) region corresponds to the area eroded by the incoming plasma ions. Whilst the deposits formed in zone 1 and 3 have different natures and origins. Due to the inclination of the sample holder, a local shadowing of the zone 3 from the plasma was created favouring deposition of a hydrocarbon film [38, 114]. The deposit in zone 1 was formed due to carbon particles reflected or re-eroded from the upper protecting part of the TZM holder as well as from re-deposition of the material eroded from the holder [99]. In the following we will focus on the analysis made in the zone 2 which suffered from pure erosion by the plasma ions.

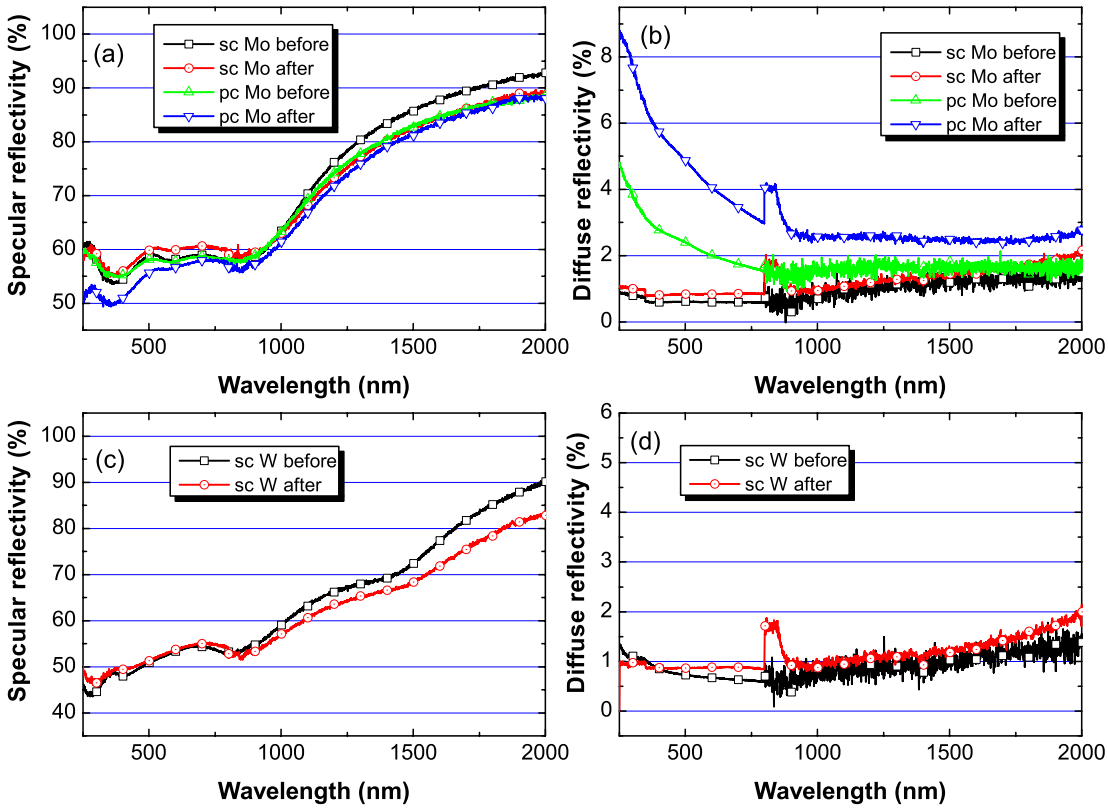

Figure 7.2: (a) and (b) specular and diffuse reflectivity of the single crystal (sc) and polycrystalline (pc) molybdenum mirrors before and after exposure in TEXTOR. (c) and (d) are the specular and diffuse reflectivity measurements made on the single crystal tungsten mirror. The peak near 800 nm, observed on some graphs, has a technical origin and is due to a detector change at this wavelength in the spectrophotometer.

Optical measurements were made at the same locations on the mirrors before and after exposure. The specular reflectivity of the single crystal (sc) Mo mirror is only weakly affected by the exposure (fig. 7.2a), a slight decrease (within 3 %) is noticed in the near infrared range. On the other hand, a pronounced decrease of the specular reflectivity of the polycrystalline (pc) Mo mirror is observed, with a fall of about 10 % at 250 nm. The diffuse reflectivity of

the sc Mo mirror remains very low after exposure (below 1 %), and no evolution induced by the plasma exposure is noticed (fig. 7.2b). For the pc Mo mirror, the diffuse reflectivity before exposure was already higher than that measured for the single crystal sample but a significant further increase is observed after plasma exposure with a maximum value of 9 % at 250 nm. The observations made for the single crystal tungsten mirror are similar to those made for the single crystal molybdenum mirror, namely a non-affected diffuse reflectivity and a slight decrease of the specular reflectivity in the near infrared range.

The advantages of the single crystal mirror under erosion conditions is really clear when comparing the specular reflectivities of sc and pc molybdenum mirror after their exposure in TEXTOR (fig. 7.3). One should keep in mind that the ion fluence bombarding the mirrors during the exposure ($1.7 \cdot 10^{20}$ $ions.cm^{-2}$) is roughly equivalent to the fluence impinging on the ITER first wall during 200 pulses [98], and to about 1000 pulses for a mirror recessed at the position 9 defined in fig. 3.7.

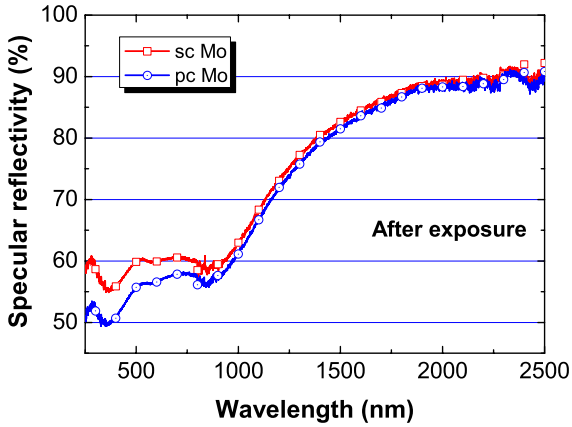

Figure 7.3: Comparison of the specular reflectivity of the single crystal and polycrystalline molybdenum mirrors after exposure in TEXTOR.

7.2 Surface morphology of the mirrors after exposure

Investigations of the surface morphology allow to explain the optical measurements described above. From the reflectivity measurements it is possible to determine values of the RMS (root mean square) roughness using Bennett's formula (Eq. 3.1) which can be re-written as follows:

$$ln(\frac{R_{spec}}{R_{tot}}) = \left(\frac{-(4\pi R_{RMS})^2}{\lambda^2}\right) \tag{7.1}$$

As seen from Eq. 7.1, a plot of $ln(\frac{R_{spec}}{R_{tot}})$ as a function of $(\frac{1}{\lambda^2})$ gives a linear curve whose slope is proportional to the square of the surface RMS roughness. Using this method the roughness of the three mirrors was evaluated before and after exposure, the results are listed in table 7.1.

According to what was observed for the diffuse reflectivity, the roughness of the single crystal

Mirror	**R_{RMS} before (nm)**	**R_{RMS} after (nm)**
sc Mo	1	1
pc Mo	5	9
sc W	2	2.5

Table 7.1: RMS roughness of the mirrors before and after their exposure in TEXTOR evaluated from Bennett's formula.

mirrors is not affected by the plasma exposure. On the contrary an increase of the surface roughness is found for the polycrystalline mirror.

Observations of the surface morphology were carried out with SEM on the zone 2 of the three mirrors. Surface of the single crystal mirrors (fig. 7.4a and c) remains very smooth after

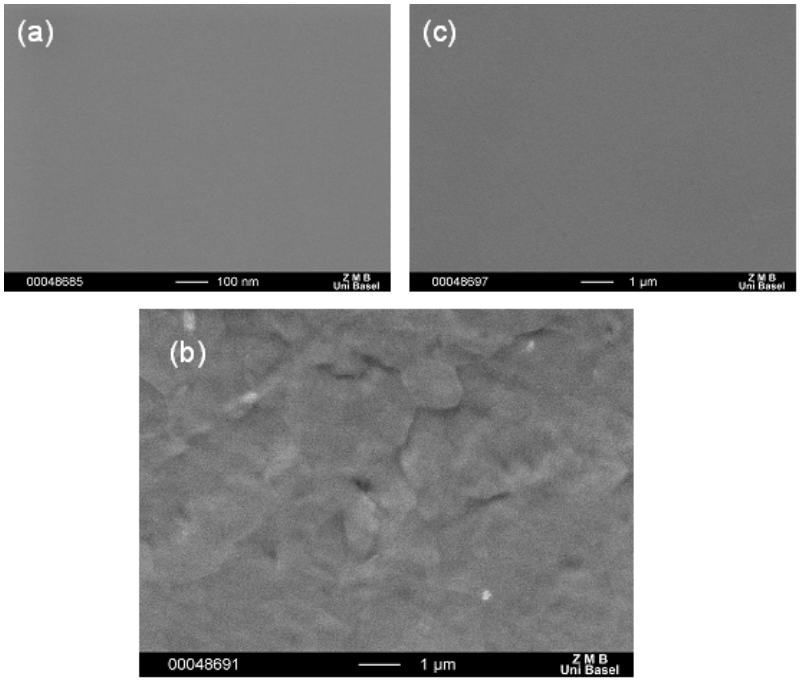

Figure 7.4: SEM picture of (a) single crystal molybdenum, (b) polycrystalline molybdenum and (c) single crystal tungsten mirrors after exposure in TEXTOR. Note the higher magnification for picture (c).

exposure and no evidence of deterioration is found by SEM even at very high magnification. This is consistent with the values of the surface roughness calculated from the Bennett's formula. On the other hand, the development of a microrelief is observed on the surface of the polycrystalline mirror after plasma exposure (fig. 7.4b), which was not visible before the exposure. The development of the surface relief is due to the appearance of the differently oriented crystallographic grains the material is made of. The surface of a polished metallic material is covered with a plastically deformed layer (known as Beilby layer) [115] created by abrasion of

the crystallographic grains by the polishing medium. When submitted to sputtering by plasma ions, this layer is gradually removed and since crystallographic grains with different orientations have different sputtering yields, they are eroded with different efficiency by the incoming ions and become visible microscopically thus causing an increase in the surface roughness (and thus an increase in the diffuse reflectivity).

The depth of the sputtered layer (about 150 nm) during the exposure was evaluated from the ion fluence measured during the experiment and the sputtering yield of the different materials found in the literature [116]. It was found that the sputtering was mainly due to C^{4+} ions present as impurities in the SOL plasma with typical concentrations of 2-4%.

7.3 Changes in the surface composition

XPS measurements were carried out on the mirrors before and after exposure to investigate both the changes in the surface composition and chemical structure induced by the exposure in the SOL of TEXTOR. Fig. 7.5 shows the Mo 3d and C 1s lines measured on the single crystal molybdenum mirror before and after exposure. Spectra before exposure were measured right after cleaning of the mirror by a hydrogen glow discharge.

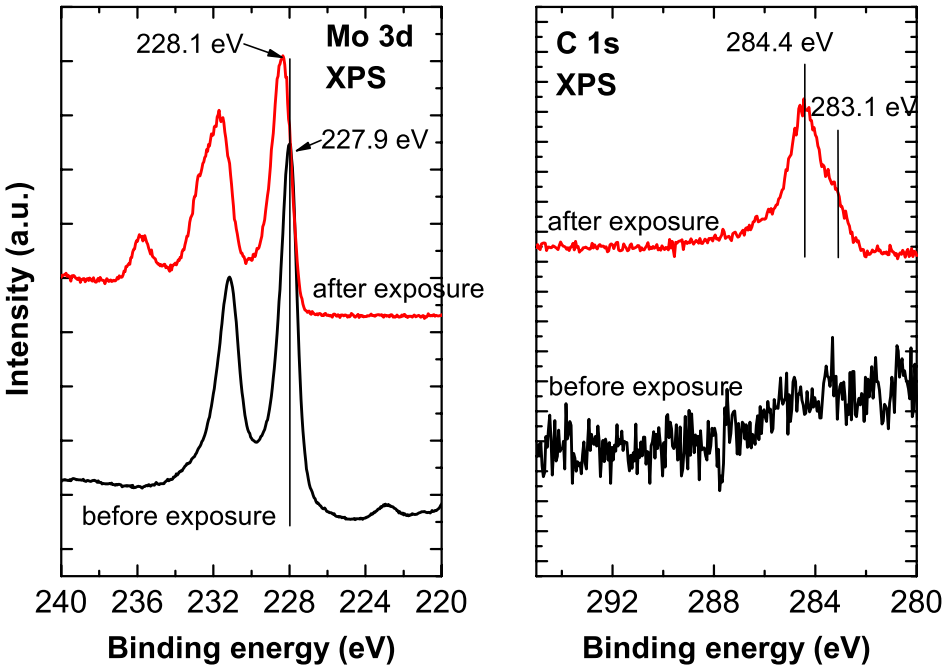

Figure 7.5: Mo $3d_{3/2;5/2}$ doublet and C 1s core level spectra measured by XPS on the single crystal molybdenum mirror before and after exposure in TEXTOR.

Before exposure, no traces of carbon can be found on the surface. The Mo 3d line is made of

one doublet with the Mo $3d_{3/2}$ peak at 227.9 eV, corresponding to metallic molybdenum. This indicates a clean mirror surface. After exposure the Mo 3d line is composed of 2 doublets. The position of the most intense is slightly shifted (about 0.2 eV) towards higher energy compared to the signal measured before exposure. The position of the Mo $3d_{3/2}$ peak (228.1 eV) indicates that molybdenum atoms are bond to carbon forming molybdenum carbide [117, 118]. Formation of the carbide has been reported by other authors [119] for the case of a carbide forming material (like Mo) bombarded by energetic carbon ions. The formation of the carbide is confirmed here by the presence of two components in the C 1s line at 284.3 eV and 283.2 eV respectively. The former is associated to an amorphous carbon phase while the latter reveals the typical chemical shift of molybdenum carbide. The second doublet of the Mo 3d line (shifted towards higher binding energies) reveals the presence of molybdenum oxide (MoO_3) which is likely to be due to the O^{x+} ions present as impurities in the SOL plasma of TEXTOR.

7.4 Conclusions

The direct comparative test of single crystal and polycrystalline mirrors under erosion conditions in TEXTOR confirmed that mirrors made from a high-Z material in the form of a single crystal can better withstand the deterioration of the specular reflectivity expected by erosion due to charge-exchange neutrals in ITER. After exposure in TEXTOR to an ion fluence equivalent to about 1000 ITER discharges, a significant decrease in the specular reflectivity was observed for the polycrystalline molybdenum mirror for an eroded depth of about 150 nm. On the other hand the specular reflectivity of the single crystal mirror is almost unaffected by the plasma exposure.

The degradation of the reflectance of the polycrystalline mirror is due to the appearance of the crystallographic structure of the material. The grain size observed here is in the micrometer range i.e. of the order of magnitude of the wavelength of the light used for optical measurements. As for the single crystal mirrors, their intrinsic structural homogeneity implies that they are also homogeneoulsy sputtered by the impinging plasma ions. To ensure the longest possible lifetime for mirrors under erosion, single crystal mirrors thus appear as a very attractive solution. However, from a technological point of view it remains very challenging to manufacture single crystal mirrors of ITER-relevant sizes (i.e. with diameter in the range of tens of cm).

Another attractive approach would be to use materials with crystallite size much smaller than the wavelength of the light, which means with a grain size in the nanometer range. Indeed even if polycrystalline such a material may maintain its reflectivity under erosion conditions because the crystallographic structure would remain "invisible" for the light preventing reflectivity losses due to an increase of the diffuse scattering. Such an approach is being pursued at the University of Basel [120] where nanocrystalline Rh films (2 μm thick) have been produced on different substrates by magnetron sputtering. The grains size ranges from 20 to 40 nm depending on the deposition parameters (substrate temperature, gas pressure,...). However despite the relative reliability and robustness of this technique, the resistance of such layer under erosion conditions in a tokamak is yet to be assessed as well as the adhesion of the layer on the substrate in the case of temperature excursions due to power loads.

Chapter 8

Influence of the mirror temperature

8.1 Carbon deposition mitigation on mirrors exposed in DIII-D

8.1.1 Experiment with non-heated mirrors: estimation of the deposition rate

As described in chapter 4.2, two sets of molybdenum mirrors were exposed on 2 consecutive days in the DIII-D divertor to series of identical ELMy H-mode discharges. The first set of two mirrors was exposed to 6 plasma discharges for a total plasma duration of about 25 s. The mirrors were at room temperature at the beginning of the experiment and no temperature control was used during the plasma discharges. The aim of the experiment was to evaluate the deposition rate of carbon to be expected in the private flux region of the divertor.

After removal from the vacuum chamber, visible deposits were found on both mirrors (fig. 8.1). A strong asymmetry in the deposition patterns on both mirrors is observed. The deposition on the upstream mirrors is rather uniform with a brownish colour, while on the dowstream mirror a clear gradient was observed with the thickest deposit near the top of the mirror.

Estimation of the deposited thickness was made by ellipsometry. Similarly to what was described in chapter 3.3, the optical constants of the deposited layer were described by a Cauchy dispersion relation. Two measurements were made on each mirror (indicated by the blue and red spots in fig. 8.1), both the film thickness and its optical properties have been determined. Results are listed in table 8.1. A film thickness of about 50 nm is found on the upstream mirror, the values determined for the two measurement spots are in good agreement and are consistent with the visual homogeneity of the film. The refractive index of the film (n=1.43 at 632 nm) indicates a soft amorphous hydrogenated carbon (a:C-D) film [71], which is confirmed by the Nuclear Reaction Analysis (NRA) measurements indicating a deuterium to carbon (D/C) ratio of about 0.55 [103].
In the center of the downstream mirror (spot 2) the estimated thickness is relatively close to the values determined on the upstream mirror (56 nm). A much larger thickness is found however on the spot 1 which was the closest to the floor surface, with a value (93 nm) almost twice as large as the one found in the middle of the exposed surface. The refractive index of the film

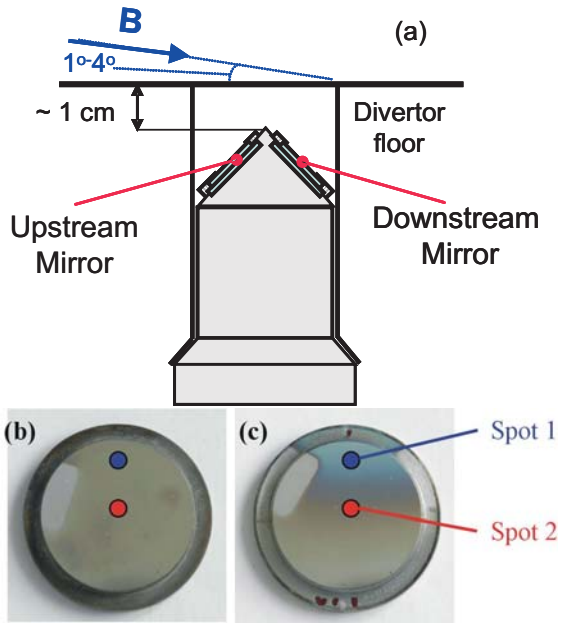

Figure 8.1: (a) Definition of the designation upstream and downstream mirrors with respect to the plasma flow. Pictures of the (b) upstream and (c) downstream mirrors exposed at ambient temperature in DIII-D. The red and blue spots indicate the locations of the ellipsometry measurements.

(1.53 at 632 nm) is slightly higher than that found on the upstream mirror. The D/C ratio determined by NRA measurements (0.58) is hardly higher than the ratio found for the upstream mirror. It should be noted that the fitting coefficients (n_i and n_i) used for the measurements on the two spots of the downstream mirror are slightly different. This is consistent with a slight variation of the D/C ratio measured at both locations (0.58 and 0.54 for the spots 1 and 2 respectively). From the knowledge of the deposited film thickness and the plasma exposure time, one can infer the average hydrocarbon deposition rate on the mirror during the exposure. The film thickness determined on the upstream mirror corresponds to a net deposition rate of 2 nm.s^{-1}, while the thickness measured on the thickest deposit of the dowstream mirror yields a value of 3.7 nm.s^{-1}. The higher deposition rate found on the downstream mirror is probably due to the enhanced re-deposition of the carbon sputtered locally from the leading edge of the

Mirror	Spot	d (nm)	n_0	n_1	n_2	k_0	k_1	k_2	n (632 nm)
upstream	1	**46.43**	1.361	294	-150.4	0	112.776	-34.102	**1.43**
upstream	2	**52.17**	1.361	294	-150.4	0	112.776	-34.102	**1.43**
downstream	1	**92.75**	1.492	309.8	-270.4	0.001	5.087	104.109	**1.53**
downstream	2	**56.05**	1.49	126.1	-12.5	0	0	73.403	**1.52**

Table 8.1: Thickness and optical properties of the layer deposited on mirrors exposed at ambiant temperature in DIII-D, as determined by ellipsometry. Optical constants are assumed to follow a Cauchy dispersion relation ($n(\lambda) = n_0 + 10^2 \frac{n_1}{\lambda^2} + 10^7 \frac{n_2}{\lambda^4}$).

downstream graphite tile (fig. 4.5) and thus predominantly re-deposited onto the surface of the downstream mirror. Therefore it is reasonable to consider the deposition rate measured on the upstream mirror as the relevant extrapolation to ITER conditions because there the geometry of the diagnostic duct will have to prevent enhanced re-deposition effect.

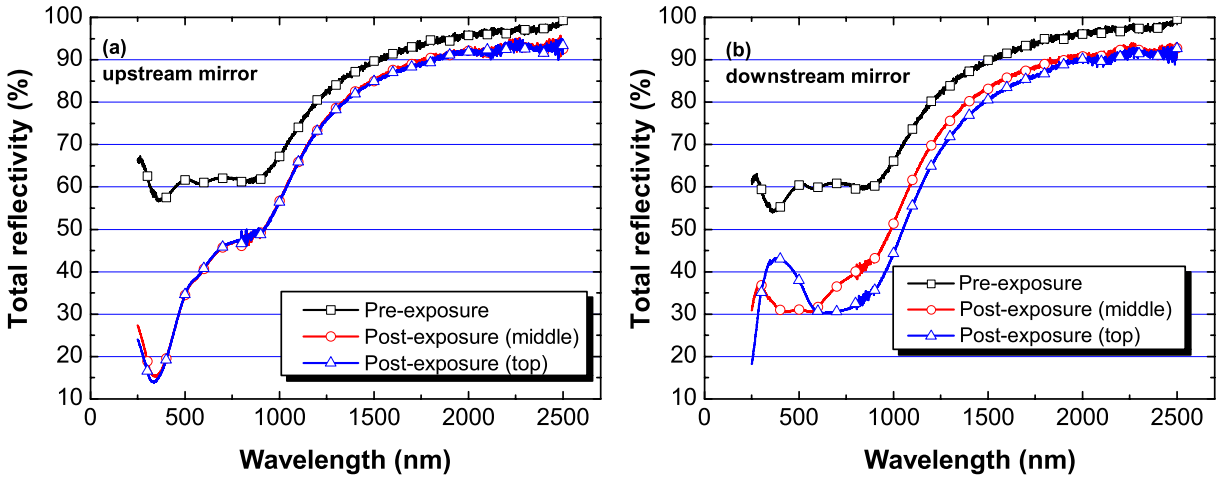

Figure 8.2: Total reflectivity of the (a)upstream and (b) downstream mirrors before and after exposure in DIII-D.

The total reflectivity of both mirrors was measured before and after exposure at the same locations as the ellipsometry measurements (fig. 8.2). As already observed in the simulations presented in chapter 3.3, the reflectivity of both upstream and downstream mirrors is only slightly affected in the near infrared (for wavelengths higher than 1500 nm). However, strong modifications of the initial reflectance are observed in the UV-Vis region. The differences in film thickness and optical properties described above result in differences in the reflectivity of both mirrors. For the downstream mirror, the higher refractive index and film thickness are sufficient to observe interference effects featured by the local maximum of the reflectivity at 500 nm. These interference effects are really problematic for ITER spectroscopic systems because they distort completely the reflectivity spectrum and depend on the film thickness. A significant decrease in the reflectivity of the upstream mirror (with a minimum value of 15 % at 300 nm) is also observed.

Changes in the polarization state of the light, induced by the presence of a deposited film on the mirror surface, are of particular importance for diagnostic systems like the Motional Stark Effect (MSE) system [121]. To evaluate this effect here the reflectivity of the mirrors was measured for a linearly polarized incident light (with either a s or a p polarization) using the spectroscopic ellipsometer in the wavelength range 300-800 nm and for an incidence angle of 45°. Results are shown in fig. 8.3. As seen both the s and p components are modified by the presence of the a:C-D layer on the mirror surface. However, one can observe that R_p

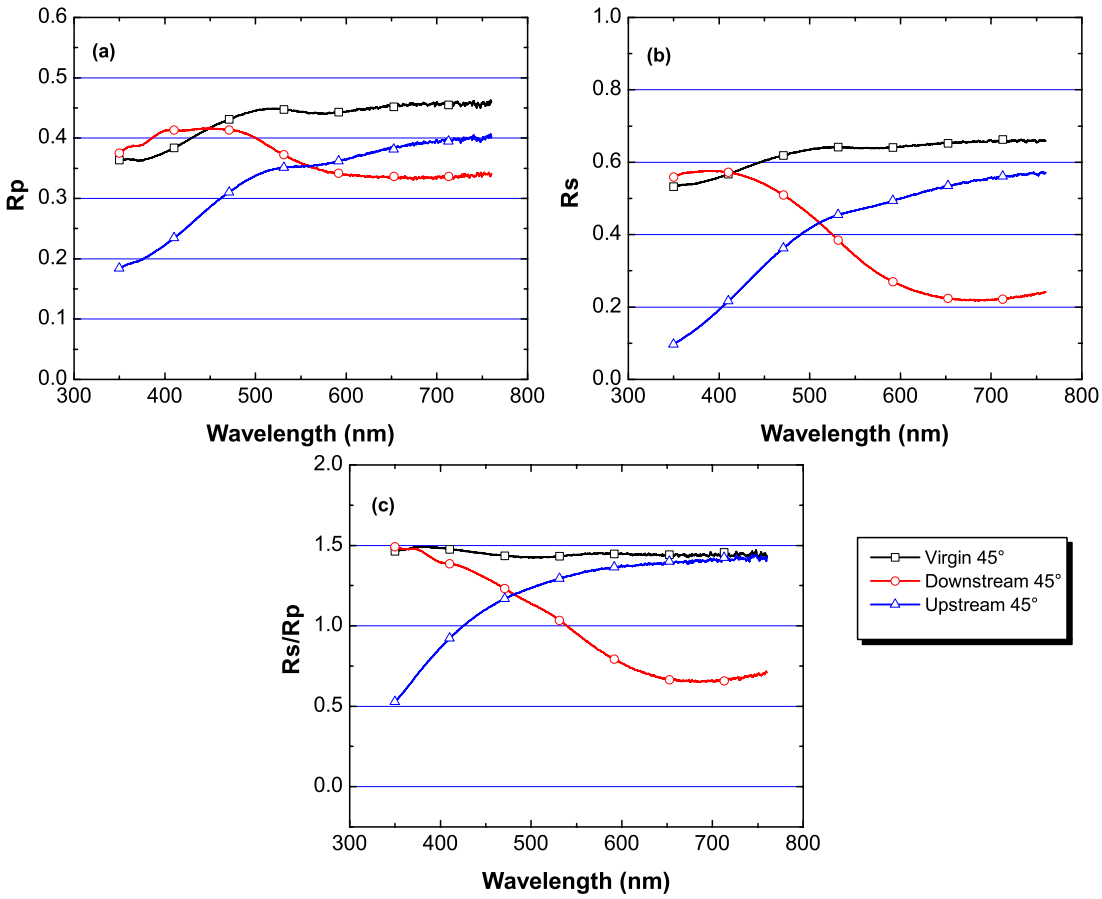

Figure 8.3: (a) and (b): Reflectivity measurements on the mirrors exposed at ambient temperature in DIII-D for linearly polarized light (p and s polarization respectively) for an angle of incidence of 45°.(c) Ratio R_s/R_p as a function of the wavelength for the two exposed mirrors.

is not as affected as R_s. Fig. 8.3c shows the ratio between the two components R_s and R_p, which indicates the rotation of the polarization direction. This effect obviously depends on the wavelength of the light and is very pronounced in the UV-Vis region where measurements were carried out. From the measurements of the total reflectivity (fig. 8.2) one can extrapolate that the effect of the deposited layer on the polarization of the light will be significantly reduced in the NIR range.

These results underline the magnitude of the problem generated by deposition of impurities on diagnostic first mirrors, especially if one thinks that the strong variations of the mirrors' reflectivity shown in fig. 8.2 are only the results of 25 s of plasma exposure in DIII-D. Even though the mirrors in the ITER divertor will not be as open to the plasma and will be partly protected from deposition by baffle structures, it is reasonable to think that deposition of similarly thick films in ITER will occur in just a few shots. According to the estimates presented

in table 3.1, the deposition rate of carbon on the mirrors below the dome may be as high as the deposition rate observed on the upstream mirror in DIII-D. This means that a significant deposit may be formed even after the first ITER shot. Therefore it is of the highest importance to find possible deposition mitigation methods and assess their efficiency and relevance for ITER conditions. This was the aim of the following experiment carried out with mirrors heated during the plasma exposure.

8.1.2 Experiment with heated mirrors: mitigation of carbon deposition

A second set of two molybdenum mirrors was exposed to 17 plasma discharges (similar to those used during the exposure of the first set), for a total exposure time of 70 s. The aim of the experiment was to expose the mirrors at a controlled temperature of 400°C. However due to a failure in the heating system, the holder temperature at the beginning of the experiment was about 140°C. According to heat transfer modelling [103, 104] and taking into account the heating of the mirrors by radiation during the plasma discharge (about 3-7°C), the mirror temperature is estimated to have been around 176-199°C during the experiment. As can be seen in fig. 8.4, and contrary to what was observed on the non-heated mirrors, no deposit is observed on the surface. The mirrors exhibit a uniform shiny grey surface.

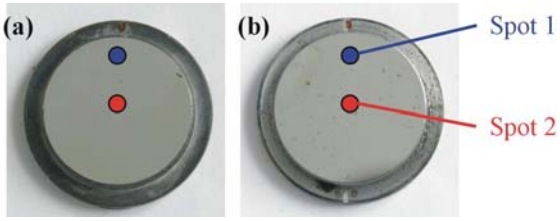

Figure 8.4: Pictures of the (a) upstream and (b) downstream mirrors exposed at about 180° in DIII-D. The red and blue spots indicate the locations of the ellipsometry measurements.

The absence of carbon deposit on the surface was confirmed by SIMS and NRA measurements carried out on the mirrors after exposure [105]. XPS measurements revealed the presence at the surface of molybdenum trioxide (MoO_3). The thickness of this oxide layer was calculated from the fit of the ellipsometric measurements. Results are listed in table 8.2. The oxide thickness was found to be in the range 9-13 nm, the oxide on the upstream mirror being slightly thicker than on the dowstream mirror. The optical properties of the molybdenum oxide film present on the mirror surface (n$\sim$ 1.9-2 at 632 nm) are consistent with the values reported for MoO_3 by other authors [122].

As expected, due to the surface oxidation the total reflectivity of both mirrors was degraded after exposure. Similarly to what was observed for the mirrors exposed at ambient temperature and coated with a carbon layer, the decrease of the reflectivity is most pronounced in the UV-Vis range. A drop of about 25 % and 40 % is noticed for the upstream and downstream mirrors respectively at 250 nm.

Mirror	Location	d (nm)	N0	N1	N2	K0	K1	K2	n (632 nm)
upstream	1	**12.2**	2.012	-110	85.4	0.38	-272	441.793	**1.98**
upstream	2	**13.11**	2.001	-84.6	41.5	0.335	-437.8	582.3	**1.98**
downstream	1	**9.62**	1.898	16	-52	0.267	158.3	97.1	**1.91**
downstream	2	**9.62**	1.994	-35	246.2	0.292	-151.9	430.9	**2.01**

Table 8.2: Thickness and optical properties of the oxide layer formed on the mirrors exposed at about 180°C in DIII-D, as determined by ellipsometry. Optical constants are assumed to follow a Cauchy dispersion relation ($n(\lambda) = n_0 + 10^2 \frac{n_1}{\lambda^2} + 10^7 \frac{n_2}{\lambda^4}$).

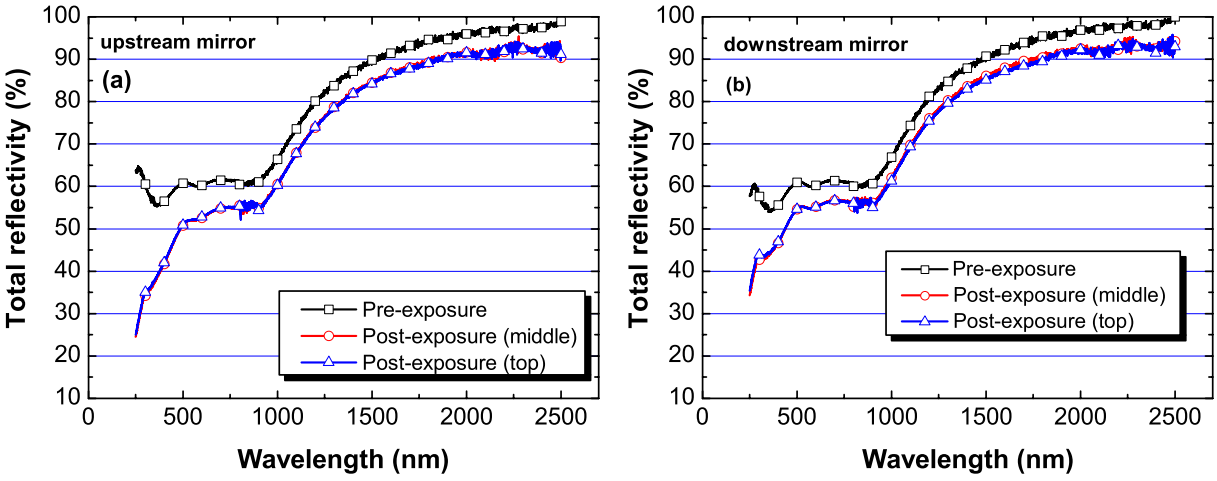

Figure 8.5: Total reflectivity of the (a)upstream and (b) downstream heated mirrors before and after exposure in DIII-D.

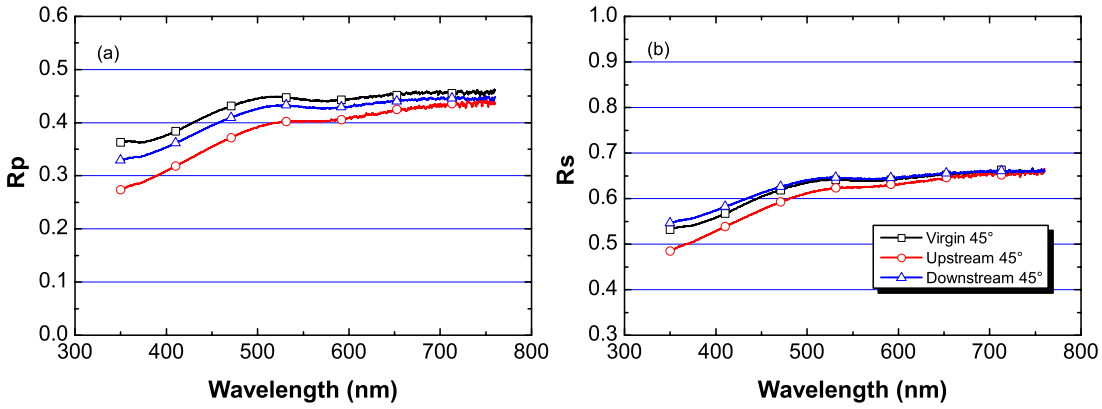

Figure 8.6: (a) and (b): Reflectivity measurements on the mirrors exposed at about 180°C in DIII-D for linearly polarized light (for p and s polarization respectively) for an angle of incidence 45°.

The reflectivity measured for linearly polarized light (fig. 8.6) on the heated mirror is much less affected than seen on the non-heated mirrors. This is of course due to the oxide thickness being much lower than the carbon layer thickness formed with mirrors at ambiant temperature.

The origin of such a surface oxidation still remains unclear. In particular, it is not clear whether the oxide was formed during storage of the mirrors in air (which occured between their cleaning and pre-characterization in the University of Basel and the actual experiment) or during exposure in the tokamak. Usually, a clean molybdenum surface stored in air is covered by a very thin native oxide layer (1-2 nm) of MoO_3. To check the effect of a long term storage in air, an experiment was carried out [123] in which a molybdenum mirror was cleaned by a hydrogen plasma and then stored in air. Reflectivity of the mirror was measured regularly, and no reflectivity changes were found after 2 months of storage in air. This indicates that the native oxide film was formed right after the exposure of the mirror to air and was stable afterwards. Therefore it appears unlikely that a 10 nm thick oxide film could be formed only by storage of the mirrors in air.

Another possibility would be that the oxidation took place during the plasma exposure in DIII-D due both to the residual oxygen impurities present in the machine (in the form of atoms or neutrals in the PFR) and the temperature of the mirrors. Other authors have reported a significant increase of the reactivity of molybdenum towards oxygen in case of low temperature oxygen plasma treatment of molybdenum, with substrate temperatures in the range 300-600°C [124]. Moreover, the fact that the oxide film formed (10-13 nm) is about ten times thicker than the usual native oxide may indicate an energetic impact of oxygen ions/atoms. One may therefore favour the hypothesis that the oxide was formed during plasma exposure.

The fact the oxide thickness is found to be higher on the upstream mirror (fig. 8.2) even strengthens this assumption. As described in chapter 8.1.1, the arrival rate of carbon on the mirror surface is higher on the downstream mirror because of the enhanced re-deposition

of carbon sputtered from the leading edge of the above graphite tile. Oxygen is known to be chemically reactive with carbon, forming CO_x compounds, and oxidative treatments of graphite tiles have been tested as fuel removal techniques [125, 126]. Therefore, if carbon and oxygen arrive simultaneously on the mirror surface (which is the case during a tokamak discharge), part of the arriving carbon will react with part of the arriving oxygen preventing both this fraction of carbon from being deposited and the oxygen from oxidizing the surface. Assuming the arrival rate of oxygen neutrals/atoms is the same for the upstream and downstream mirrors (there is a priori no reason to expect differences), the ratio of carbon to oxygen arriving at the mirror surface is higher on the downstream mirror due to the effect of the extra sputtering of the above graphite tile. If less oxygen can reach the surface, one may expect the surface to be less oxidized, which is the case if one looks at the oxide thickness determined by ellipsometry.

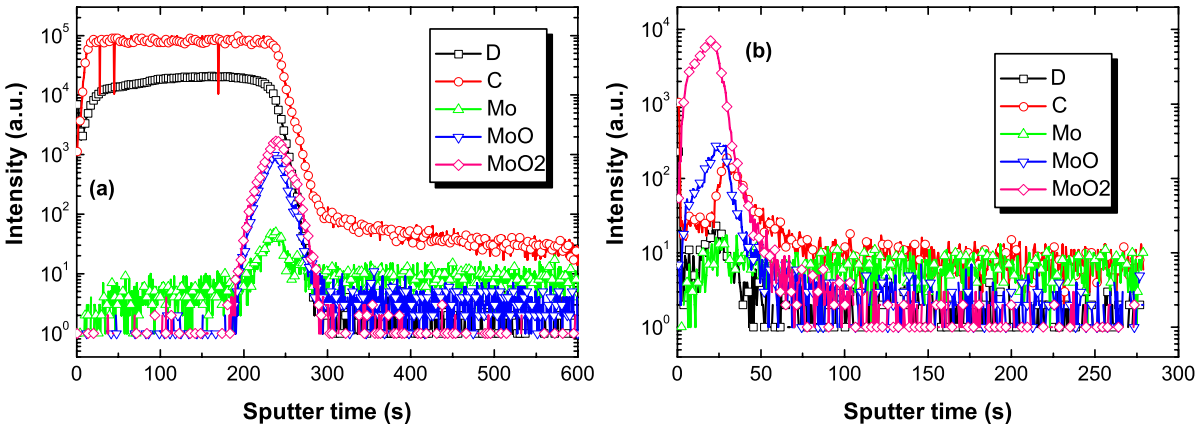

Figure 8.7: SIMS depth profiles of (a) non-heated and (b) heated mirrors after exposure in DIII-D.

However, the observations made with SIMS depth profile of heated and non-heated mirrors give contradictory results. As seen in fig. 8.7a, the presence of molybdenum oxide is detected at the interface between the molybdenum substrate and the a-C:D layer. Estimations of the thickness of this oxide yield a value of about 6-7 nm, which is very close to the resolution of the equipment and make it difficult to draw a firm conclusion on the actual thickness. Yet the signal obtained for the oxide on the heated mirror (fig. 8.7b) is very close to that observed for the non-heated mirror and estimations of the oxide thickness yield the same value. These observation may indicate that the oxide was actually formed before the mirror exposure in DIII-D, between their cleaning in the University of Basel and their installation in DIII-D, which would explain the presence of an oxide on the non-heated mirrors. However as already mentioned, the technique used here has a poor accuracy for precise determination of very low film thickness, therefore it is difficult to conclude on the relative thickness of the oxides found on both mirrors. Both hypotheses (*in-situ* and *ex-situ* oxidation) are likely but the analysis made here do not allow to strictly conclude on the actual scenario.

The results from this experiment are actually quite informative. Indeed, heating the mirrors during the exposure to a temperature of about 176-199°C was enough to mitigate the deposition of a hydrocarbon film on the mirror surface. Assuming the deposition rate determined in chapter 8.1.1, this means that in such a temperature range the chemical erosion yield is sufficient to compensate a deposition rate of 2-3 nm·s^{-1}. Since the mirror temperature (with the uncertainty linked with the experimental problems and the modeling assumptions) was lower than the temperature at which the chemical erosion yield peaks [29], one may assume that deposition of carbon with a higher deposition rate may be further mitigated for higher mirror temperature. Of course, on the other hand, increasing the mirror temperature increases the reactivity of molybdenum with oxygen which may be problematic if the oxidation occurs in the reactor (accidental vent, leak).

8.1.3 Conclusions

The exposure of mirrors in the Private Flux Region of the DIII-D divertor lead to some important results. These experiments have confirmed that mirrors placed in the PFR are likely to suffer from carbon deposition leading to strong modification of their reflectivity and strong modifications of the polarization state of the reflected light. The higher deposition rate measured on the downstream mirror caused by the erosion of the leading edge of the graphite tile above emphasizes the necessity to optimize the geometry of the diagnostic ducts to avoid artificial increase of the deposition rate of impurities. The determination of the deposition rate on the upstream mirror, which was not influenced by geometrical effects, yields a value of 2 nm.s^{-1}. As shown in fig. 3.1, the flux of carbon arriving at the mirror location under the divertor dome may lead to a deposition rate as high as that measured on the DIII-D mirrors. Even if a partial protection of the mirrors located in the ITER divertor will be achieved by the use of baffle structure, thus reducing the deposition rate of impurities on the mirror surface, the present data indicate that a significant layer will be deposited during each ITER shot.

One possible deposition mitigation method was tested in DIII-D, by heating the mirrors at a moderate temperature, which was enough to prevent the formation of a carbon layer on the mirror surface both on the upstream and downstream mirrors by thermally enhancing the carbon chemical erosion. Further experiments are envisaged with a more controlled monitoring of the mirror temperature which was not possible in the experiment described here (at the time of writing this text, the experiment was just made and confirms the results described here). Although no carbon was detected on the mirror surface after exposure, the degradation of their reflectivity due to the surface oxidation represents a serious concern. Indeed if the surface oxidation occured during the plasma exposure due to the combined action of the surface temperature and oxygen from the residual impurities in the tokamak, it will be necessary to develop *in-situ* cleaning techniques to the mirrors in ITER even if mitigation methods are applied.

8.2 Effect of the mirror temperature on the deposition of Be/C layers and its impact on mirror reflectivity

As just described, a possible mitigation method for the deposition of carbon impurities on the mirror surface consists in increasing the mirror temperature to enhance the chemical erosion yield of the deposited a-C:D layer. However as mentioned in chapter 5.2, the plasma flow arriving at the ITER divertor targets (made from graphite) will contain between 1 and 10 % of Be arising from the erosion of the main chamber wall. Recent experiments made in PISCES-B have shown that the presence of Be ions in a deuterium plasma tends to mitigate the erosion of carbon, both physical sputtering and chemical erosion. Indeed, Be ions incident on the graphite target are implanted into the carbon surface and, due to their energy, tend to bond with carbon atoms to form beryllium carbide. The formation of the carbide acts to inhibit the reaction chain responsible for chemical erosion of carbon and also reduces physical sputtering of carbon atoms from the surface. Once a protective carbide layer forms on the surface, subsequent beryllium ion bombardment will produce an enrichment of the surface with beryllium that will be easier to erode (compared to beryllium bonded as the carbide). In turn, Be re-erodes and leads to Be-rich deposited layers in line-of-sight locations from the target [93]. Under such conditions, beryllium and not carbon may be the main deposited impurity in the divertor region. Such observations were already made in JET during the Be limiter phase [42, 127]. If this situation occurs in ITER it could be expected that deposition of Be films occurs on these mirrors in direct line-of-sight from the plasma. Up to now no detailed investigations on the effects of a Be containing film on the reflectivity of a metallic mirror have been carried out. In [54], it was assumed that if deposition of Be occurs then the reflectivity of the initially pure mirror surface will tend to the reflectivity of a pure Be surface. This would be true if the deposited layer was made of pure Be which is very unlikely given the high reactivity of Be towards oxygen and the probable presence of carbon in the layer. Moreover this assumption neglects any evolution of the surface roughness during the deposition process.

Removing some of the uncertainties related to this issue was the aim of the experiments carried out in PISCES-B (see chapter 5.2). Both the effect of a Be/C layer on the reflectivity of a metallic mirror and the effect of the mirror temperature on the formation of the layer were investigated. Although increasing the mirror temperature is an effective deposition mitigation method for carbon, its effect on a mixed Be/C layer is yet unknown.

The following experiments represent the first ever dedicated investigations of the effects of Be/C layers on the reflectivity of a metallic mirror. They were made during June/July 2006. After their exposure in PISCES-B the samples were sent to the Institüt für PlasmaPhysik in Garching (Germany) for surface analysis (their equipment being fully compatible with Be handling). However at the time of writing this text only the results from the NRA and RBS measurements are available. Therefore the next sections will describe the results from this analysis as well as from the reflectivity measurements (made in UCSD using the system described in chapter 5.2). A detailed analysis of all the results,when available, will be the subject of a dedicated publication.

8.2.1 Experiments with molybdenum mirrors

Polycrystalline molybdenum mirrors have been used as deposition probes (see fig. 5.3) to collect the material eroded by the intense ion bombardment of a graphite target by a Be-containing deuterium plasma. During the exposure, even if the mirrors are protected from direct plasma impact, heating of the mirror surface occurs due to the radiation from the plasma. A temperature increase of up to 100°C (for one hour exposure time) is observed for a mirror initially at room temperature. Therefore experiments were made with two different initial temperatures: room temperature and 240°C. Evolution of the temperature is followed by a

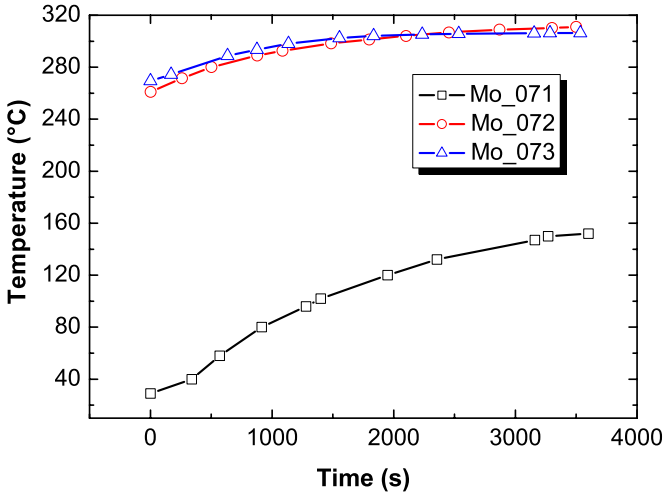

Figure 8.8: Evolution of the mirror temperature during exposure at the witness plate location in PISCES-B, for the case of initially heated and non-heated mirrors. The increase in the mirror temperature with exposure time corresponds to the surace heating by the plasma radiation.

thermocouple installed at the backside of the mirror. Fig. 8.8 shows the evolution of the mirror temperature during a typical exposure. For a non-heated mirror the temperature varies between 25 and 150°C, whilst it varies between 260 and 310°C for a heated mirror.

The plasma parameters (as measured by means of the reciprocating Langmuir probe) used were $n_e \sim 2.5\text{-}3.5 \cdot 10^{12}$ cm^{-3}, $T_e \sim$ 6-8 eV, the ion flux to the target was 2.5-3.5·10^{18} ions·cm^{-2}·s^{-1}. Additionally a negative bias of -50 V is applied to the graphite target in order to control the energy of the impinging ions. The temperature of the graphite target was about 700°C to suppress chemical erosion of the target and favour its physical sputtering by the incoming plasma ions. The plasma was first started without Be and allowed to stabilize. Then Be was introduced in the plasma through the evaporator and finally the sample holder with the mirror was introduced in the plasma chamber. The exposure time was fixed to one hour.

One mirror was exposed at low temperature with a Be fraction in the plasma of 0.1 % in order to obtain a reference sample. Three mirrors were exposed at elevated temperature

with different Be fraction in the plasma (0.04 and 0.05%) and different times between the moment the Be injection was started (the Be evaporator is switched on) and the moment they were introduced in the plasma chamber. Fig. 8.9 shows the results from the reflectivity measurements made after exposure whilst table 8.3 summarizes the values of the deposited film thickness determined by NRA measurements.

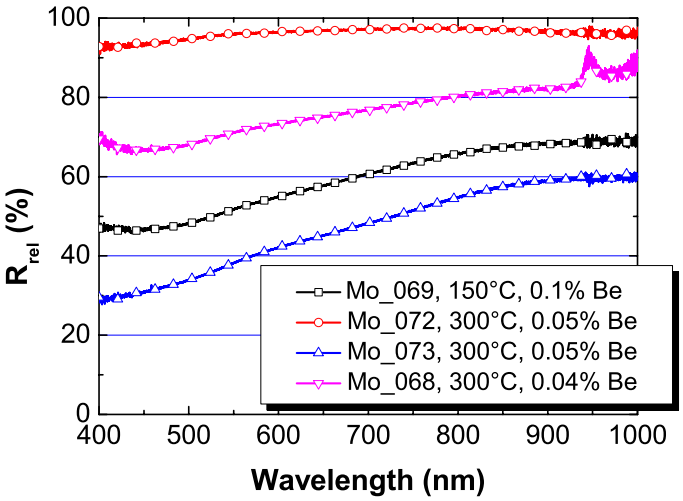

Figure 8.9: Relative reflectivity of the molybdenum mirrors exposed in PISCES-B.

Sample	Temperature (°C)	Be (at·cm^2)	Thickness (nm)
Mo-069	25-150	$3.40{\cdot}10^{17}$	31
Mo-068	250-310	$6.10{\cdot}10^{16}$	5.4
Mo-072	250-310	$4.15{\cdot}10^{16}$	3.8
Mo-073	250-310	$6.60{\cdot}10^{17}$	60

Table 8.3: Deposit thickness on the exposed mirrors determined from NRA and RBS measurements.

According to analysis made by NRA and RBS, the deposited films mainly consists of Be, the concentation of carbon being lower than 10 %. This is consistent with the observations made in [92] and [93] where the deposited layers were formed in similar conditions. The 31 nm thick film obtained for the exposure at 25-150°C has a drastic effect on the mirror reflectivity with a decrease of the reflectivity of 40-60% over the whole wavelength range. The deposited film is quite dark and can clearly be seen by the naked eye. For the mirrors heated during the exposure, one can see in table 8.3 that there are two different cases. The thickness deposited on the sample Mo-073 is 60 nm while hardly a 5 nm thick film is obtained on the mirrors Mo-068 and Mo-072. The evolution of the relative reflectivity of the mirrors after exposure is in good agreement with these observations. Reflectivity of Mo-073 has dropped to values lower than those measured on the non-heated mirror, while reflectivity of Mo-068 and Mo-072 is only

weakly affected by the exposure. It should be noted that on these two mirrors no deposit was visible by eye, only on Mo-068 a dark deposit could be seen at the edge of the exposed area which could have been seen by the light during reflectivity measurements. This would explain the lower reflectivity measured on Mo-068.

To understand these results we need to take into account the time ellapsed between the start of the Be injection and the moment when the sample is introduced in the plasma chamber. Indeed as shown in [128], the suppression of carbon erosion is due to the progressive coverage of the graphite target with a Be film. The rate of the erosion suppression may be followed spectroscopically by measuring the temporal evolution of the CD or C I band emission, indicating the chemical and physical erosion yields of the target respectively. In the experiments described here the target temperature is sufficiently high to reduce significantly the rate of chemical erosion of the target which is thus only physically sputtered. Let I_{CD} be the intensity of the CD line. The temporal evolution of I_{CD} can be described by a simple exponential relation [128]:

$$I_{CD} = exp(-t_{exp}/\tau_{Be/C}) \tag{8.1}$$

where t_{exp} is the target exposure time and $1/\tau_{Be/C}$ the erosion decay. A parametric study of the dependence of $\tau_{Be/C}$ on the graphite target temperature (T_s), ion energy (E_i), ion flux (Γ_i), and beryllium ion concentration (c_{Be}) in the deuterium plasma, was performed in [129]. The erosion decay time corresponds to the characteristic formation time of a protective Be layer on the graphite target. The following law was determined experimentally [129]:

$$\tau_{Be/C}[s] = 1.0 \times 10^{-7}\ c_{Be}^{-1.9\pm0.1}\ E_i^{0.9\pm0.3}\ \Gamma_i^{-0.6\pm0.3}\ e^{\frac{(4.8\pm0.5)\times10^3}{T_s}} \tag{8.2}$$

As can be inferred from eq. 8.2, the higher the Be fraction in the plasma the lower $\tau_{Be/C}$. Combining eq. 8.2 and eq. 8.1, one can calculate the decay of the CI band as a function of the exposure time (fig. 8.10) for the conditions of interest here. In fig. 8.10, the time t=0 corresponds to the moment when the injection of Be is turned on. The instant corresponding to the introduction of the mirrors in the plasma chamber and their retrievals are also indicated. Both Mo-068 and Mo-072 were introduced simultaneously to the start of Be injection, while the mirror Mo-073 was introduced about 1000 s after the beginning of Be injection. Since the suppression of carbon erosion in a Be-seeded deuterium plasma is related to the progressive coverage of the graphite target by a Be layer, the following conclusions may explain the experimental observations. Since the Be fraction in the plasma for the heated mirrors was two times lower than during the experiment with the non-heated mirror, the characteristic time for the formation of the protective layer is much longer for the low Be fraction case. Therefore the erosion of carbon from the target needs more time to be suppressed. For samples 068 and 072, which were introduced right after the Be injection begins, erosion of carbon was still not mitigated. Thus carbon was arriving at the mirror surface but prevented from being deposited by chemical sputtering from deuterium neutrals enhanced by the mirror temperature. Only a very thin layer of Be started to be deposited at the end of the exposure. For Mo-073 however, the Be layer was built continuously. These results would indicate that carbon deposition on the mirror surface may be suppressed by heating the mirror to 250-300°C (which is consistent with the observations made in DIII-D) even in the presence of Be. However increasing the mirror

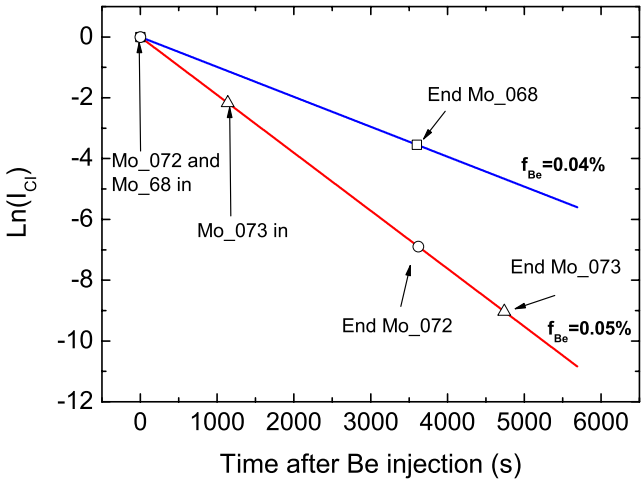

Figure 8.10: Temporal decay of the graphite target erosion as a function of the Be injection time.

temperature seems to have no effect on the deposition of Be. Of course these observations need to be confirmed by further surface analysis with XPS and depth-sputter XPS.

8.2.2 Experiments with copper mirrors

There are at least to reasons to perform experiments with copper. As will be described in chapter 9, copper has the property of not forming stable carbides. Moreover, diffusion of beryllium into copper (and possible alloying) has been reported by other authors [130] for temperatures higher than 300°C. Diffusion or alloying may complicate the possible mirror cleaning because of the formation of a Cu/Be mixed layer. On the other hand, if the diffusion of Be into Cu was fast enough, we may imagine that the top layer would remain clean while Be would diffuse into the bulk material.

Two copper mirrors were exposed to a Be containing deuterium plasma at a very low beryllium fraction (0.03%). As described above, under such conditions carbon erosion needs a longer time to be mitigated by the deposition of Be. Therefore we expect to form a carbon rich film on the mirror surface. The aim was to try to mitigate the carbon deposition and to reproduce previous results. Therefore one mirror was exposed without any active heating while a second one was initially heated at 250°C. Evolution of the mirror temperatures during the exposure is plotted in fig. 8.11a.

After exposure in conditions similar to those described for the Mo mirrors, the non-heated mirror (Cu-082) came out from the chamber with a visible deposit whose colour seemed quite different from the layers observed on Mo mirrors exposed to D_2 plasma containing higher Be fraction (Mo-069 for example). The reflectivity is most affected in the range 400-700 nm with a drop of the reflectivity of about 50-60% (fig. 8.11b). The higher the wavelength the less affected the reflectivity, this trend is commonly observed in the case of carbon-based deposits

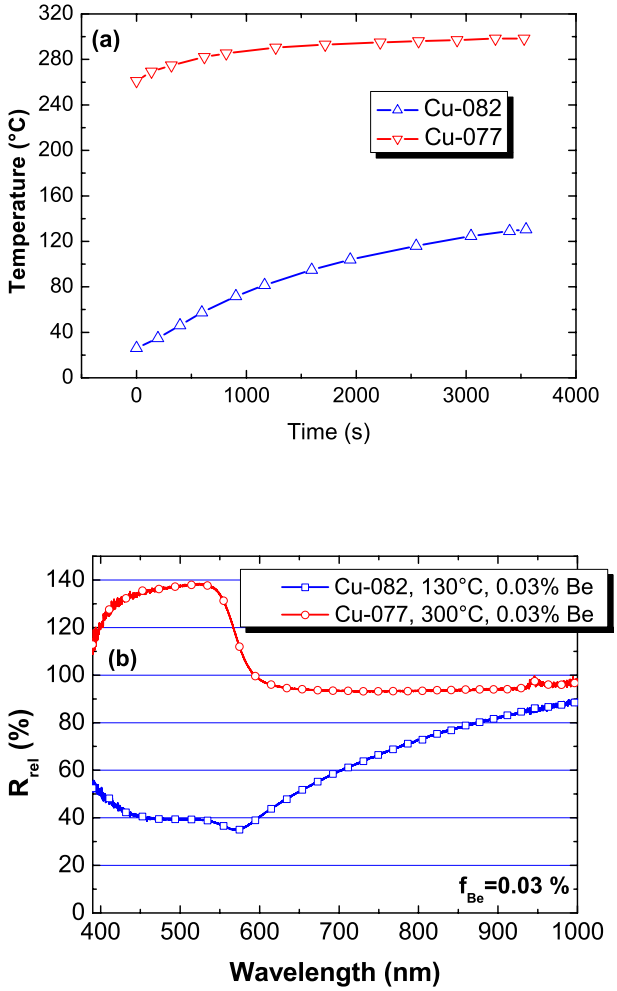

Figure 8.11: (a) Evolution of the copper mirror temperature during exposure in PISCES-B and (b) relative reflectivity of the mirrors after exposure.

(which are transparent in the near-infrared range). On the contrary, the heated mirror came out of the chamber with a very shiny surface which looked like pure copper, albeit a little more grey. The reflectivity spectrum measured after exposure is quite surprising (fig. 8.11b). A clear enhancement of the reflectivity is noticed in the range 400-600 nm whereas no changes are found for higher wavelengths. XPS measurements on the samples will provide more information on the composition of the surface in both cases. However according to NRA measurements, both samples are coated with a Be-containing layer. NRA is not sensitive to carbon therefore it is difficult to make assumptions about the carbon content of the films. However, from the colour of the samples one may infer that the non-heated mirror was coated with a carbon-rich film while for the heated mirror deposition of carbon was mitigated and only a thin pure Be layer was formed.

To study the possible diffusion of Be into Cu, two copper mirrors were exposed to a deu-

terium plasma with f_{Be}=0.5%, for two different temperatures. Cu-081 was initially at room temperature while Cu-079 was at 250°C at the beginning of the exposure. Fig. 8.12 shows the RBS spectra measured on both samples after exposure in comparison with the spectrum obtained for a reference sample. Cu-081 shows an edge shift due to the Be layer on the surface (51 nm thick according to NRA) whilst the shape of the spectrum obtained for Cu-079 indicates both the existance of a Be layer on the surface and diffusion of Be into Cu at the interface.

According to kinetic studies on beryllium diffusion into copper published in [130] and [131],

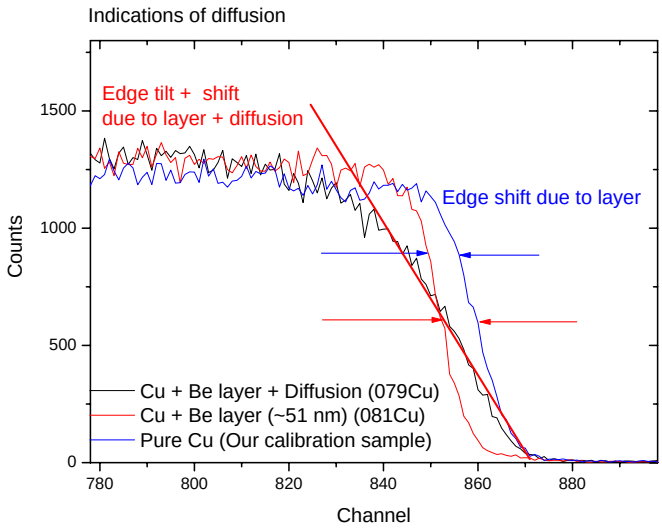

Figure 8.12: RBS spectra of the copper mirrors after exposure in PISCES-B to a beryllium containing deuterium plasma (f_{Be}=0.05%).

the diffusion rate of Be into Cu can be described by the following expression:

$$X = \left(0.588 \cdot e^{\frac{-66300}{RT}} \right) \cdot t^{1/2} \tag{8.3}$$

where X is the thickness of the BeCu phasse formed (in mm), R is the constant 8.314 (in J·mol^{-1}K^{-1}), T is the temperature in K, and t is the time (in s). This expression was established for the case of a Cu coated Be disk annealed at a certain temperature which is a situation slightly different to what happens in PISCES-B. However this formula allows the magnitude of the expected diffusion process to be determined. At 300°C, and for a duration of one hour, eq. 8.3 yields a 31 nm thick diffusion zone.

8.2.3 Preliminary conclusions from experiments in PISCES-B

More information will be obtained by XPS depth-profile measurements of the samples exposed in PISCES-B, and the results presented here do not allow firm conclusions on the effect of the mirror temperature on the formation of a Be/C mixed layer to be established. However it is

already clear that if deposition of carbon can be mitigated by heating the mirrors, this method is inefficient in the case of Be deposition. Results presented here seem to indicate that carbon deposition can be mitigated even in the case of the simultaneous deposition of Be and C. But the mirrors are still covered with a Be layer, affecting drastically their reflectivity.
For copper mirrors exposed to a Be-containing plasma at about 300°C, diffusion of beryllium into copper has been observed by RBS. XPS measurements will give more information about the alloy formed, but in any case the presence of the diffusion layer would complicate the possible mirror cleaning, because the alloy formed will have to be removed without damaging the copper surface.

Chapter 9

Influence of the mirror material choice on the erosion/deposition effects

In the previous chapters, we have studied the effect of erosion and deposition on the mirror reflectivity as separate phenomena. Erosion and deposition were considered to be independent of the mirror material neglecting any role that may be played by the substrate. In the following chapter, results from experiments made in Tore Supra, TCV and in a laboratory discharges will be described. They show that the erosion/deposition patterns observed for different substrate materials under similar exposure conditions can be quite different.

9.1 Erosion of mirrors exposed in Tore Supra

9.1.1 Reflectivity of the mirrors after exposure

Metallic mirrors made from different candidate materials (single crystal molybdenum, copper, stainless steel) were installed for long term exposure on the first wall of Tore Supra (see chapter 4.3.1). Specular and diffuse reflectivity of both the reference and the mirrors exposed for one year in Tore Supra were measured in the wavelengtt range 250-2500 nm. As shown in fig. 9.1, the reflectivity of the three exposed mirrors was affected in quite different ways.

For all mirrors, a decrease of the specular reflectivity is noticed after exposure. For the single crystal molybdenum mirror, this effect is the most pronounced in the UV and visible regions with a drop of about 18 % at 250 nm. The diffuse reflectivity remains very low (≤ 2 %) and no increase is noticed compared to the values measured on the reference mirror. For the stainless steel mirror, both a decrease of the specular reflectivity and an increase of the diffuse scattering are observed. Reflectivity of the copper mirror after exposure exhibits the most drastic changes. First of all, it should be noted that due to problems during the transportation of the mirrors and long-term storage in air (one year), the surface of the virgin mirror was deteriorated (which could be observed visually). Therefore the values of the reflectivity measured for this sample are not representative of what a perfect non-exposed sample could be. This explains why the specular reflectivity of the exposed copper mirror is slightly higher than the reflectivity of the reference mirror for wavelengths lower than 400 nm. For higher wavelenghts, a fall of the

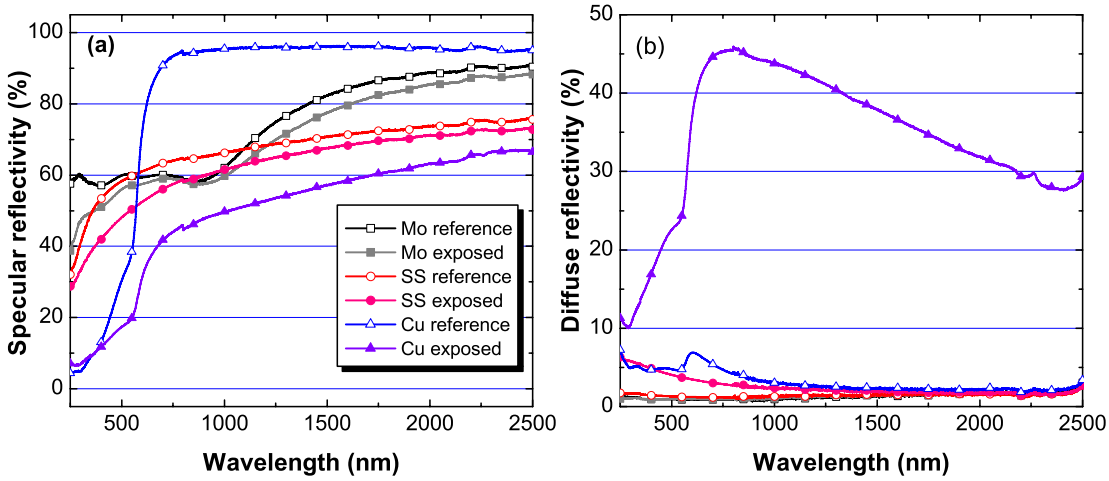

Figure 9.1: (a) Specular and (b) diffuse reflectivity of virgin reference mirrors and mirrors after one-year exposure in Tore Supra.

specular reflectivity is found over the range 500-2500 nm. Correspondingly a strong increase of the diffuse reflectivity, showing extreme values of about 50 % at 800 nm is measured (fig. 9.1).

Values of the RMS roughness of the different samples were inferred from the reflectivity measurements using the methodology described in chapter 7.2. Results are listed in table 9.1. The unchanged roughness of the molybdenum mirror after exposure indicates that the changes in the specular reflectivity are due to absorption of the light in a thin deposited carbon-based layer whose presence was confirmed by SIMS measurements [107]. A film thickness of about 5 nm was calculated by ellipsometry. Other impurities like boron, silicon and oxygen were found by XPS measurements. For copper and stainless steel however, even if the presence of similar impurities was evidenced by XPS and SIMS, assumptions about the layer thickness were not possible. In the case of copper, the increase of the diffuse reflectivity fits very well with the decrease of the specular reflectivity pointing out the increase of the surface roughness as the main contributor to the degradation of the reflectivity.

9.1.2 Erosion of the samples

Measurements of the thickness eroded after exposure in Tore Supra were made using confocal microscopy, results are listed in table 9.1 both in terms of eroded depth and in terms of number of eroded atoms per area unit. According to numerical simulations (with the Eirene and BBQ codes [132]), most of the erosion arises due to the helium and deuterium conditioning glow discharges performed regularly during the experimental campaign. Indeed locations of the mirrors inside the vacuum vessel were such that the flux of CXN was minimum, thus minimizing erosion and deposition during tokamak plasma operations [132]. This was confirmed during ex-

Mirror	R_{RMS} (nm)	Net eroded depth (μm)	Erosion (atoms/cm^2)	Y(He 150 eV)	Y(D_2 200 eV)
Mo reference	1.6	/	/	/	/
Mo exposed	1.9	0.12	$7.32{\cdot}10^{15}$	$7{\cdot}10^{-3}$	10^{-3}
SS reference	3.3	/	/	/	/
SS exposed	9.2	0.22	$2.98{\cdot}10^{16}$	$5{\cdot}10^{-2}$	$1.7{\cdot}10^{-2}$
Cu reference	7.3	/	/	/	/
Cu exposed	54.5	2.68	$2.85{\cdot}10^{17}$	$11{\cdot}10^{-2}$	$4{\cdot}10^{-2}$

Table 9.1: RMS roughness of virgin and exposed mirrors. Values of the eroded depth (determined by confocal microscopy), number of eroded atoms (normalized to a 1 cm^2 area), and sputtering yields of the different mirror material by He and D ions at the indicated ion energies, are also shown.

vessel experiments in which another set of mirrors was exposed to He and D_2 glow discharges with the same parameters as those performed in Tore Supra [107]. Values of the eroded depths measured after ex-vessel glow discharges were extremely close to the values measured on the mirrors exposed in Tore Supra.

Values of the sputtering yields of the different mirror materials by helium and deuterium ions for ion energies measured during the glow discharges are shown in table 9.1.

	Y(Mo)/Y(SS)	n(Mo)/n(SS)	Y(Cu)/Y(SS)	n(Cu)/n(SS)
He (150 eV)	0.14	0.4	2.2	11.8
D (200 eV)	0.06		2.35	

Table 9.2: Ratio of the sputtering yields of the different materials for the corresponding ions and energies, and ratio of the number of eroded atoms (n) determined from erosion measurements.

The most striking results from the mirror exposure in Tore Supra, taking into account erosion during glow discharges as the main degradation effect for the mirror, is found when looking at the data shown in table 9.2. It is seen that the ratio $\frac{n(Mo)}{n(SS)}$ of the number of eroded atoms on Mo and SS mirrors respectively is higher than the ratio of the sputtering yields of these materials by He and D ions found in the literature [116]. This means that the stainless steel mirror was eroded less than expected when looking at the relative sputtering yields. The same remark is also true when comparing the erosion and sputtering yiels of copper and stainless steel mirrors. The number of eroded copper atoms is 11 times higher than the number of atoms removed from the stainless steel mirror despite the ratio of 2 normally observed for their sputtering yields. Again the surface of the stainless steel mirror was eroded much slowly and/or the copper mirror was eroded more efficiently than would have been expected when comparing the sputtering yields of the two materials.

The experiment in Tore Supra demonstrates the differences in the erosion patterns of mirror

from different materials exposed in similar conditions. Given the use of carbon for the limiters in Tore Supra [133], carbon is expected to be the main impurity in the plasma during the glow discharges during which the major part of the erosion occured. The mirror surface is therefore simultaneously bombarded by deuterium and carbon ions during the conditioning discharges. In similar conditions, experiments in PISCES-B have shown that after exposure of different materials to hydrogen plasma contaminated by carbon (coming from the background vacuum), formation of a carbon layer was observed on a Be substrate and not on a W substrate [134]. The difference was explained by a different chemical activity of these metals towards carbon. In the case of the Tore Supra mirrors, it is difficult to draw firm conclusions about the role of carbon (if any) on the differences observed because of the very long exposure time which limits precise knowledge of the exposure conditions. Both experiments indicate that under similar conditions different substrates do not exhibit the same behaviour with respect to erosion/deposition.
To clarify the differences observed in the effective sputtering yields of the different materials, a dedicated laboratory experiment, whose results will be detailed in the next sections, was performed in Basel (chapter 5.1).

9.2 Erosion/deposition of mirrors in laboratory discharges

9.2.1 In-situ evolution of the reflectivity during plasma exposure

Copper and stainless steel mirrors have been exposed to a deuterium glow discharge with controlled partial pressure of methane in the gas mixture. Copper and stainless steel were chosen as substrate material for this experiment because mirrors made from these materials showed the most different behaviours after exposure in Tore Supra. The sample bias was chosen to ensure that the energy of the impinging ions was above the sputtering threshold of the two materials and close to the energy of the impinging ions during glow discharges in Tore Supra. Methane was used as a carbon source to account for the hydrocarbons created in a tokamak by the chemical sputtering and transported to the various areas of the machine. Three different deuterium/methane mixtures were used with the following fractions of methane in the gas mixture: $f_{CH_4} = 0$, $f_{CH_4} = 1.8$, and $f_{CH_4} = 3.5$ %.

Fig. 9.2 shows the evolution of the specular reflectivity (R) of the mirrors as a function of the ion fluence during plasma exposure; the values have been normalized to the initial value for ease of comparison. Results obtained by *in-situ* reflectometry (λ=532 nm) for the two materials are quite different. In the case of stainless steel (fig. 9.2a), for $f_{CH_4} = 0$ and 1.8 %, the evolution of the reflectivity with the ion fluence is linear, showing a final value of 0.96 after a fluence of $8 \cdot 10^{19}$ ions.cm^{-2}. For higher fraction of methane in the gas mixture, constructive and destructive interferences associated with the growth of an amorphous hydrogenated carbon film are observed. For copper the degradation rate of the reflectivity is directly related to the fraction of methane in the gas mixture: the higher the methane content the faster the reflectivity decreases. For a pure deuterium plasma, and similarly to what is observed for the stainless steel mirrors, the reflectivity seems to be a linear function of the ion fluence. At $f_{CH_4} = 3.5$ %,

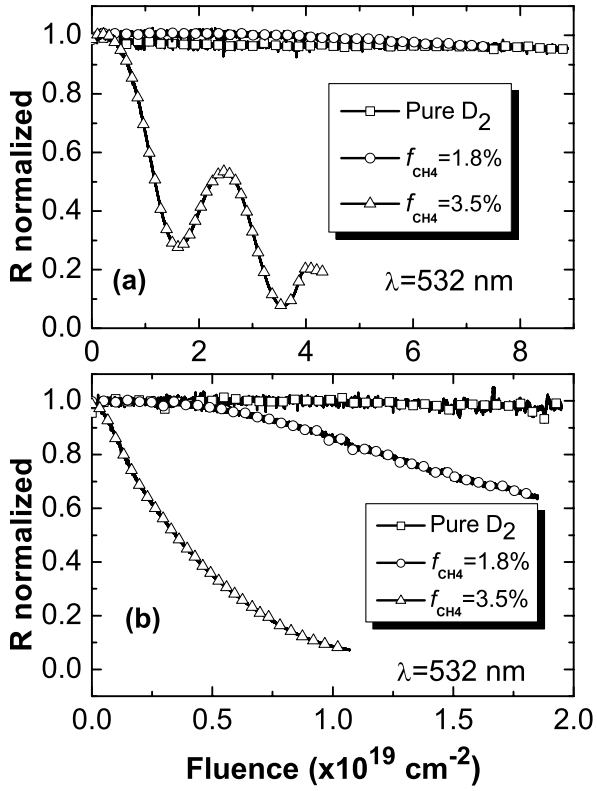

Figure 9.2: Real-time evolution of the specular reflectivity R (normalized to unity) of (a) stainless steel and (b) copper mirrors during laboratory plasma exposure. Typical exposure time of samples is about 10 hrs. Note the lower ion fluence to which the copper mirrors were exposed.

the reflectivity falls essentially to zero for a fluence of $1 \cdot 10^{19}$ ions.cm^{-2}.

9.2.2 Reflectivity of the mirrors after exposure

Specular reflectivity of the mirrors was measured before and after plasma exposure in the wavelength range 250-2500 nm. These measurements are consistent with the data measured by laser-reflectometry during the plasma exposure. For stainless steel (fig. 9.3a), only slight changes of the reflectivity are measured for mirrors exposed with methane fraction of $f_{CH_4} = 0$ and $f_{CH_4} = 1.8$ %. In the range 250-500 nm, reflectivity measured on the mirror with $f_{CH_4} =$ 1.8 % is hardly higher than the reflectivity of the mirror exposed to a pure deuterium plasma. These observations (added to the fact the surface roughness is almost unaffected by the plasma exposure) also rule out the presence of carbon on the surface, since even thin carbon layers can be easily detected in the visible region of the spectrum. A strong decrease of the specular reflectivity is found for the mirror coated with a hydrocarbon film ($f_{CH_4} = 3.5$ %), due to both absorption of the light in the deposited layer and to interferences. However, the fact the reflectivity is close to zero in the range 250-500 nm is most probably due to the rough structure

of the film shown in fig. 9.5b.

For copper (fig. 9.3b), the higher the methane fraction the more affected the reflectivity. This is consistent with the SEM pictures described later and the evolution of the surface roughness. Given the absence of a detectable amount of carbon on the surface by EDX, the evolution of the specular reflectivity should be only caused by the surface roughening and the development of a microrelief on the surface.

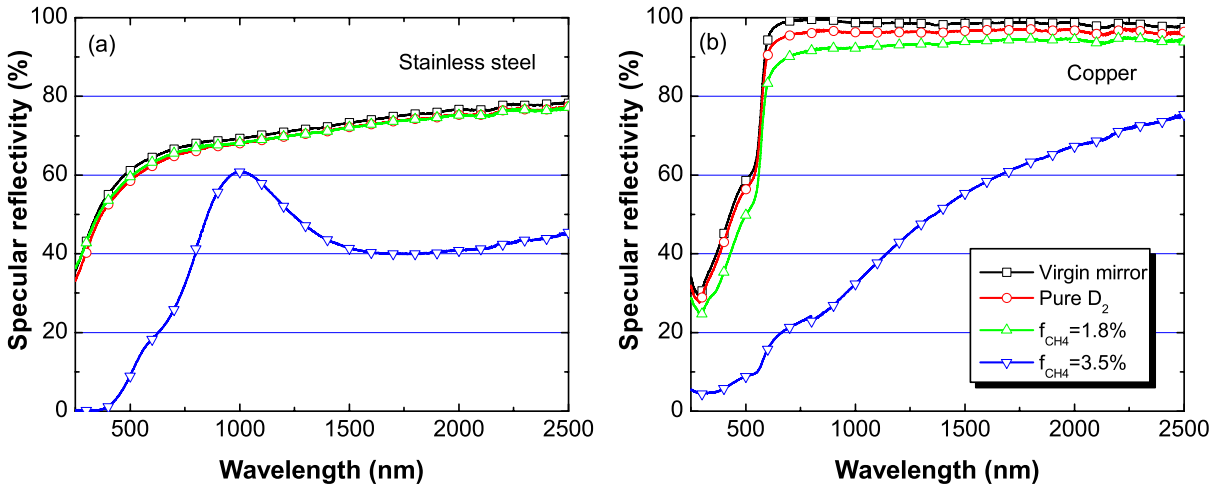

Figure 9.3: Specular reflectivity of (a) stainless steel and (b) copper mirrors before and after laboratory plasma exposure as a function of the wavelength.

Measurements of the reflectivity of linearly polarized light were made using the spectroscopic ellipsometer for different angles of incidence in the range 40-80°. To represent the changes in the polarization of the light induced by the plasma exposure, the ratio R_s/R_p is plotted in fig. 9.4, as a function of the angle of incidence of the light, for a wavelength of 630 nm. For stainless steel no significant changes in the polarization of the light are found for methane fraction of 0 and 1.8 % and for angle of incidence lower than 75°. Strong changes are however found for the carbon coated mirror. From measurements made on copper mirrors (fig. 9.4), it is found that a drastic increase of the surface roughness has less effect on the polarization of the light than the deposition of a carbon layer. Indeed the relative variations of the ratio R_s/R_p caused by the surface roughening are lower than the changes induced by the presence of the carbon layer on the stainless steel mirror. *We could therefore conclude that deposition of impurities on the mirror surface is a more serious problem than increase of the roughness due to sputtering for diagnostic systems using polarized light (like the ITER LIDAR system).*

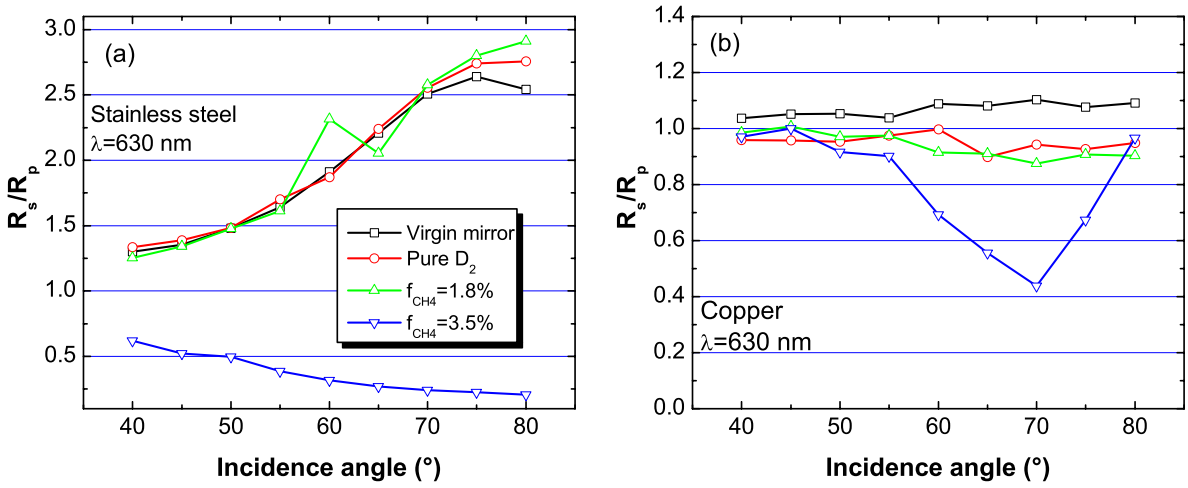

Figure 9.4: Ratio R_s/R_p measured at $\lambda = 630$ nm on (a) stainless steel and (b) copper mirrors for different angles of incidence.

9.2.3 Surface morphology of the mirrors after exposure

Investigations of the surface morphology by SEM provides some clues regarding the damaging effects of the plasma exposure for the two materials. For $f_{CH_4} = 0$ and 1.8 %, the stainless steel mirror surface surface remains undamaged (fig. 9.5a), with no sign of the stepped-structure found, for example, in [69] for polycrystalline samples exposed to similar deuterium ion fluence (but with higher ion energies). The roughness remains very low (R_a=6 nm compared to an initial value of 5 nm) for both cases, consistent with the slight change observed for the specular reflectivity in fig. 9.2. It should be noted that EDX analysis finds no trace of carbon on samples exposed to $f_{CH_4} = 0$ and 1.8 %, although given the information depth of EDX (about 1 μm) one could not exclude the presence of carbon as impurity on the surface. The surface of the mirror exposed to $f_{CH_4} = 3.5$ % is coated with a 250 nm thick a-C:H film. As seen in fig. 9.5b, the film is quite rough. It has a very poor adhesion to the substrate and can be peeled away very easily.

For copper, the evolution of the surface morphology with the methane fraction in the plasma is very different to that observed for stainless steel. For $f_{CH_4} = 0$ %, neither visible damage of the surface nor any increase in the surface roughness is found (R_a =7 nm compared to an initial value of 6 nm). However, when the methane fraction in the plasma is increased, the crystallographic structure becomes visible. In fig. 9.6, on can clearly see the grain-to grain relief, and the sharp grain boundaries. The resulting increase in the surface roughness (R_a =26 nm after exposure) explains the degradation of the specular reflectivity described above.

The effect is even more pronounced for $f_{CH_4} = 3.5$ % as seen in fig. 9.7. Besides the more distinct appearance of the different crystallographic grains (fig. 9.7a and b), many micrometer-

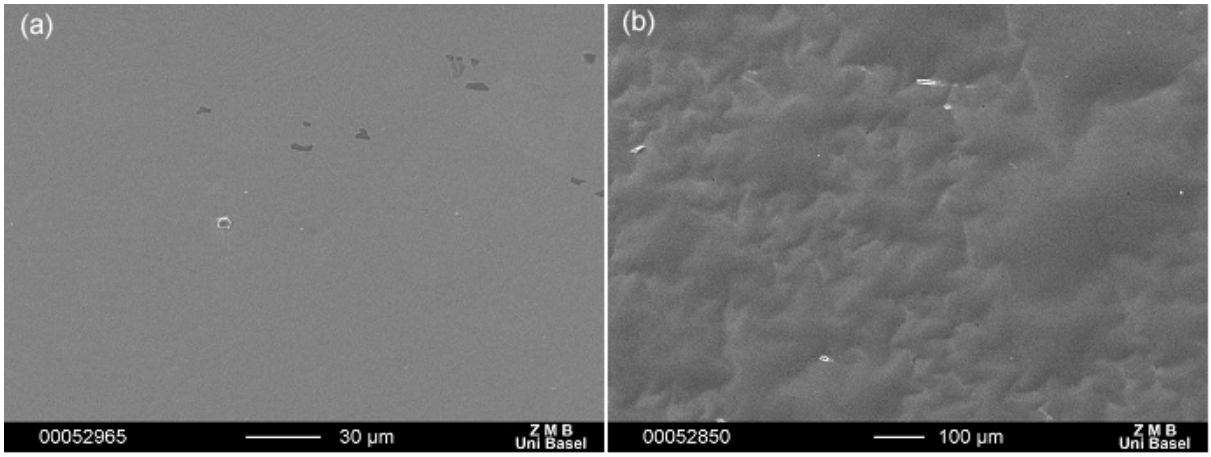

Figure 9.5: SEM picture of the surface morphology of the stainless steel mirror exposed to (a) $f_{CH_4} = 1.8$ and (b) $f_{CH_4} = 3.5$ %.

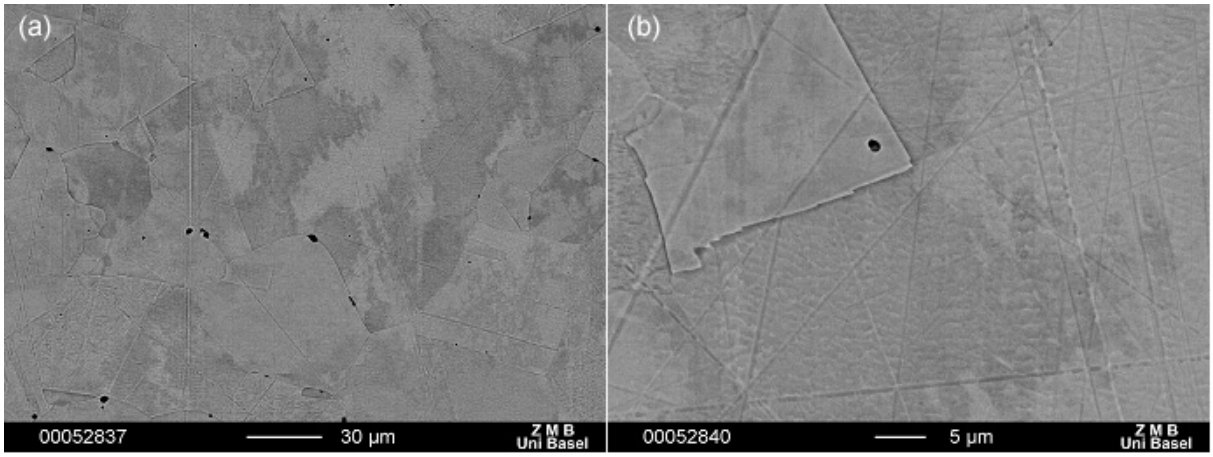

Figure 9.6: SEM picture of the surface morphology of the copper mirror exposed to $f_{CH_4} = 1.8$ % for two different magnifications ((a) $\times$ 500 and (b) $\times$ 2000.

sized particles can be seen all over the surface (fig. 9.7c and d) as well as conical structures on top of some grains (fig. 9.7c). Observations of conical micrometer structures have been reported by other authors for copper (and also for other materials) under ion bombardment [135, 136]. The combination of these morphological changes results in a strong increase of the surface roughness (R_a =70 nm after exposure) and to a complete loss of the specular reflectivity in the visible region.

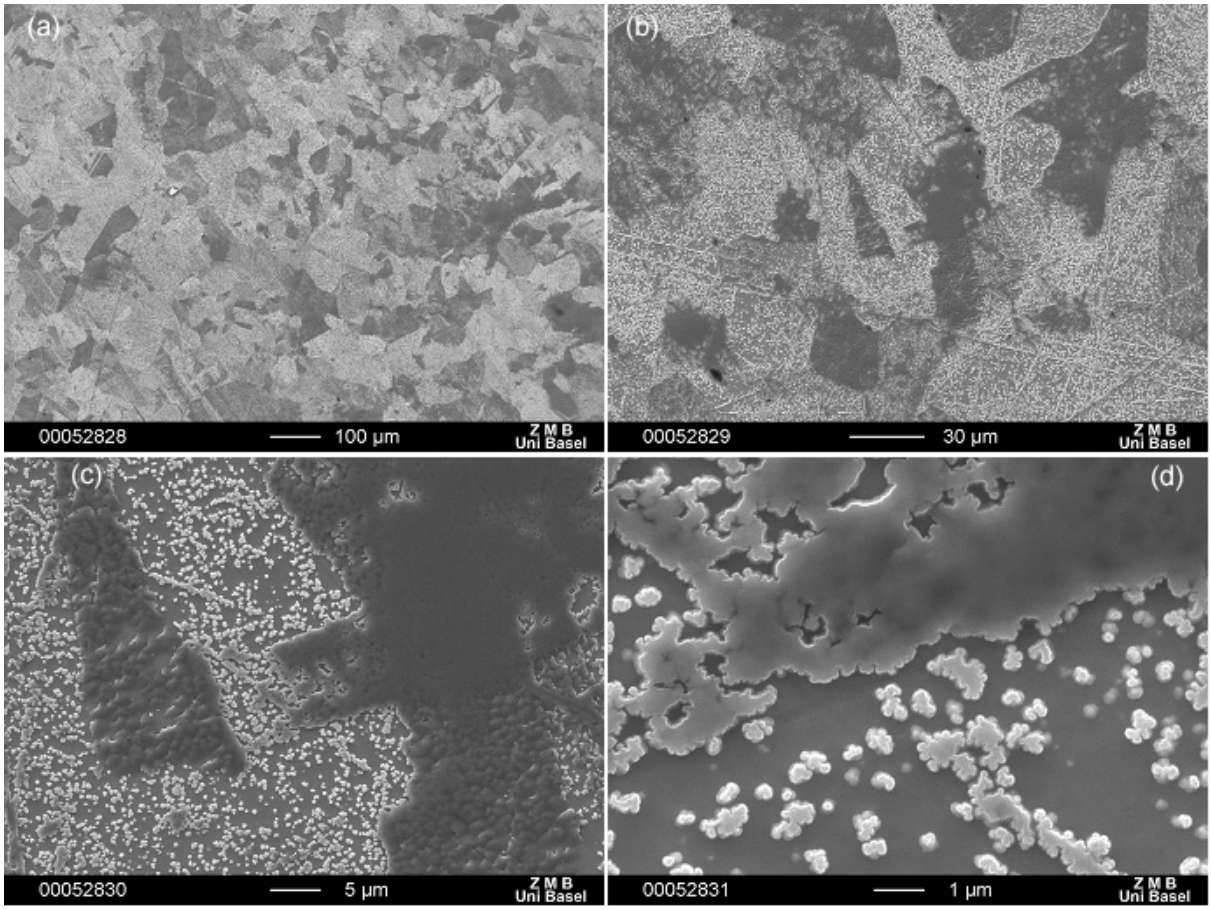

Figure 9.7: SEM picture of the surface morphology of the copper mirror exposed to $f_{CH_4} = 3.5$ % for four different magnifications ((a) × 100, (b) × 500, (c) × 5000 and (d) × 10000.

9.2.4 Erosion/deposition mechanisms

Fig. 9.8 summarises the eroded/deposited depth measured for the different mirrors from the weight measurements, showing very different behaviours of the two substrates under similar conditions. From $f_{CH_4} = 0$ to $f_{CH_4} = 1.8$ %, a reduced erosion of the stainless steel mirror

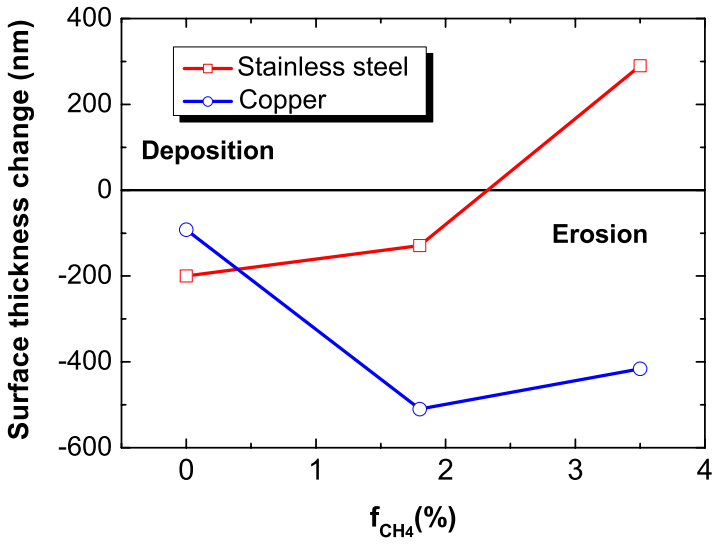

Figure 9.8: Surface thickness change of the different mirrors exposed in laboratory plasma experiments as determined from weight measurements and profilometry as a function of the methane fraction in the gas mixture. Note the higher ion fluence to which the stainless steel mirrors were submitted to.

is noticed. Deposition of an a-C:H layer is then found for higher methane content. In the case of copper, there is a strong increase in the eroded depth from $f_{CH_4} = 0$ % to $f_{CH_4} = 1.8$ %, with only a slight reduction of the sputtered depth at the highest methane content. From these measurements we infer that under simultaneous bombardment with carbon and deuterium ions (with $f_{CH_4} = 3.5$ %), the reflectivity of a copper mirror is damaged by physical sputtering from the plasma ions whilst a stainless steel mirror becomes coated with an a-C:H film. These observations seem to indicate different evolutions of the effective sputtering yields of the respective material with the fraction of carbon.

The effective sputtering yield of a given material can be defined as the ratio:

$$Y_{eff} = \frac{n_{eroded}}{\Gamma \cdot \Delta t} \tag{9.1}$$

where n_{eroded} is the number of atoms sputtered from the surface (calculated from the measured eroded depth and the atomic density of a given material), Γ is the ion flux and Δt is the exposure time. It thus corresponds to the experimentally observed sputtering yield. Table 9.3 shows the values of the effective sputtering yields for the different mirrors. According to what was observed in fig. 9.8, a decrease of Y_{eff} is noticed for stainless steel from $f_{CH_4} = 0$ to 1.8 %

with a factor 2 between both values. In contrast, for copper, a strong increase of Y_{eff} (about $\times 5$) is found between mirrors exposed to a carbon containing plasma and mirrors exposed to a pure deuterium plasma. From table 9.3 it is seen that for $f_{CH_4} = 1.8$ % the ratio $\frac{Y_{eff}(Cu)}{Y_{eff}(SS)}$ amounts to about 18, which is in the same order of magnitude than the value found for mirrors exposed in Tore Supra. For mirrors exposed to pure deuterium plasma, the ratio of the effective sputtering yields fits well with the theoretical values. It is therefore only in the presence of carbon impurities in the plasma that differences are found between the two materials.

Material	f_{CH4} (%)	Y_{eff}
Stainless steel	0	0.02
	1.8	0.012
	3.5	/
Copper	0	0.039
	1.8	0.22
	3.5	0.16

Table 9.3: Effective sputtering yields of the different mirrors exposed in laboratory plasma experiments calculated from the measured eroded depth and the total ion fluence.

In the case of simultaneous bombardment of a surface by deuterium and carbon ions the effective sputtering yield of a material M can be expressed by [137]:

$$Y_{eff} = (Y^{D\to M} \cdot f_D + Y^{C\to M} \cdot f_C) \cdot \left(1 - \frac{f_C \cdot (1 - R^{C\to M})}{Y^{D\to C} \cdot f_D + Y^{C\to C} \cdot f_C}\right) \tag{9.2}$$

where f_I is the concentration of the element I in the plasma with respect to the electron density, and q_I the ionization stage of the element I ($\sum_i f_i \cdot q_i = 1$), and $\mathrm{Y}^{C\to M}$ is the sputtering yield of the material M by carbon ions. The term in the second brackets of eq. 9.2 takes into account that a flux

$$\Gamma \cdot \left(\frac{f_C(1 - R^{C\to I})}{Y^{D\to C} \cdot f_D + Y^{C\to C} \cdot f_C}\right) \tag{9.3}$$

is necessary to sputter the carbon ions coming from the plasma and sticking with a probability $S^{C\to I} = 1 - R^{C\to I}$ ($R^{C\to I}$ is the particle reflection coefficient of carbon ions scattered from the surface of element I) on the surface before the plasma ions can further sputter the material. That is to say, since carbon can be deposited on the surface part of the incoming ions sputter the deposited carbon atoms and do not contribute to the further sputtering of the surface. If the expression (9.3) is larger than the total ion flux Γ, carbon will be deposited on the surface. In the other case, the material will be sputtered by the reduced flux of plasma ions.

To confirm the results obtained with copper, the experiment described above was repeated with a higher ion fluence. Similar procedure as that described in chapter 5.1, was applied for the experiment. This time in addition to the weight measurements, a mask was placed at the sample edge to allow measurements of the sputtered depth by profilometry. Fig. 9.9 shows the

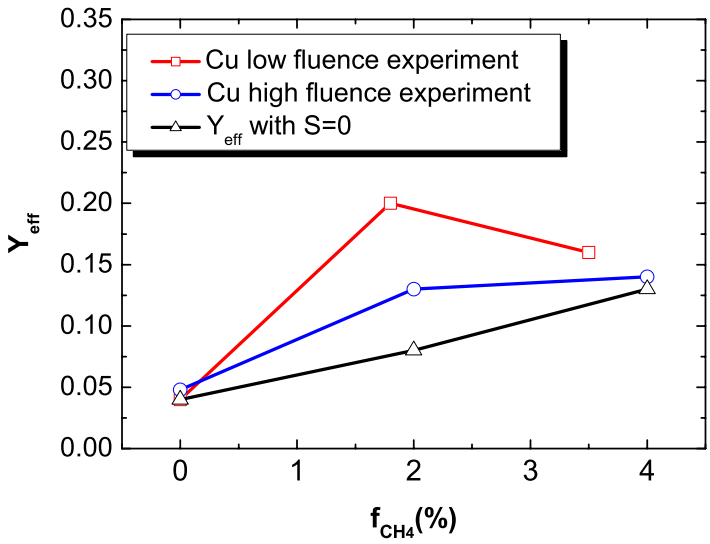

Figure 9.9: Values Y_{eff} calculated for the two series of copper mirrors exposed to methane containing deuterium plasma. Also plotted are the values of Y_{eff} calculated from eq. 9.3 assuming the sticking coefficient is 0.

values of Y_{eff} inferred from both experiments. There is evidently a good agreement for the values calculated for a pure deuterium plasma and for the highest methane fraction. However there is quite a large discrepancy for the case when $f_{CH_4} = 1.8$ %. We do not have yet a clear explanation for this discrepancy. An overestimate of the eroded thickness from the mass loss measurements in case of the low fluence experiment cannot be excluded.

The second experiment confirms the increased erosion observed when carbon impurities are introduced in the gas mixture. As seen from eq. 9.3, assuming the sticking coefficient of carbon on the surface is not zero (i.e. assuming carbon can be deposited on the surface), the effective sputtering yield of the material should be lowered when the carbon content in the plasma is increased, compared to the case of a pure deuterium plasma. This is what is observed for the stainless steel mirrors. We may even say that the surface of the stainless steel mirror is partially protected from being sputtered when carbon is present in the plasma. For copper however, the experimental findings indicate that the carbon ions are not deposited and contribute only to the further sputtering of the mirror surface thus increasing the effective sputtering. To check this assumption, the effective sputtering yield of copper was calculated using eq. 9.3 but with the rather extreme hypothesis $S^{C \to I} = 0$, the sputtering yields used in the calculation are taken from the Monte Carlo code SRIM [138]. The calculated values are plotted in fig. 9.9. A rather good agreement is found between the calculated and experimental values, confirming the enhanced erosion of the surface due to carbon ions.

The results described in this section confirmed the very different behaviour observed for copper and stainless steel mirrors exposed in Tore Supra. The addition of methane in the deuterium plasma has opposite consequences for copper and stainless steel. While a decrease

of the effective sputtering yield is found for stainless steel (and then carbon deposition for a sufficient methane fraction), an increase of Y_{eff} is found for copper with increasing carbon fraction.

Experiments in Tore Supra and in Basel, were made with ion energies above the sputtering threshold for the respective materials i.e. under erosion dominated conditions. The next section will described the different deposition rate observed on different types of substrates with particle energies below the sputtering threshold of the given materials.

9.3 Substrate-dependent carbon deposition efficiency on samples exposed in the TCV divertor

9.3.1 Surface analysis of the deposited material

As described in chapter 4.4, mirror samples from a variety of different materials of interest to ITER mirrors were exposed in pairs on a specially designed sample manipulator allowing sample insertion in the divertor floor region of the TCV tokamak. Table 9.4 summarises the different materials tested, the experimental conditions (recessment distance, number of tokamak shots, glow discharge conditioning time etc.) and estimation of the deposited thickness. Evidently,

Experiment number	Material	d (mm)	Number of shots	Glow discharge (hrs)	Deposited thickness (nm)
1	Mo	15	323	33.44	4.7
2	Mo W	10	19	1.47	≈1
3	Mo W	50	214	21.54	≈0.85
4	**Mo** **Si**	50	223	24.5	**1.3** **15.89**
5	**Mo** **Si**	50	820	90.5	**4** **24**

Table 9.4: Experimental conditions of the mirror exposures in the TCV tokamak. d is the distance between the sample surface and the front surface of the graphite divertor tiles. The experiment numbers in the left column are only indicative.

only very thin layers have been found on the different samples, especially when high-Z materials (Mo, W) have been exposed. No difference in the carbon layer thickness was found when Mo and W were exposed simultaneously. The thickness values were determined from ellipsometric measurement, although, given the very low values obtained, one should keep in mind the large relative uncertainties in these values. In addition, the presence of low amounts of deposited carbon on the sample surfaces was established by XPS measurements.

As seen from the table, there seems to be no correlation between the deposited thickness and the recess distance below the divertor target tiles, though the significance of this observation must be gauged against the large differences in terms of plasma configurations and conditions (ohmic, H-mode, high power, low density electron cyclotron heated discharges, limiter, divertor etc.) characterising the different sample exposure periods. The most striking results in terms of deposited thickness are obtained when molybdenum and silicon samples are simultaneously exposed. The deposition rate on the Si sample is found to be much higher than on Mo, a phenomenon observed in two separate experiments. Since the geometry of the sample holder and the exposure in pairs ensures that the samples experience nearly identical conditions, the

only parameter which can play a role is the substrate material itself.

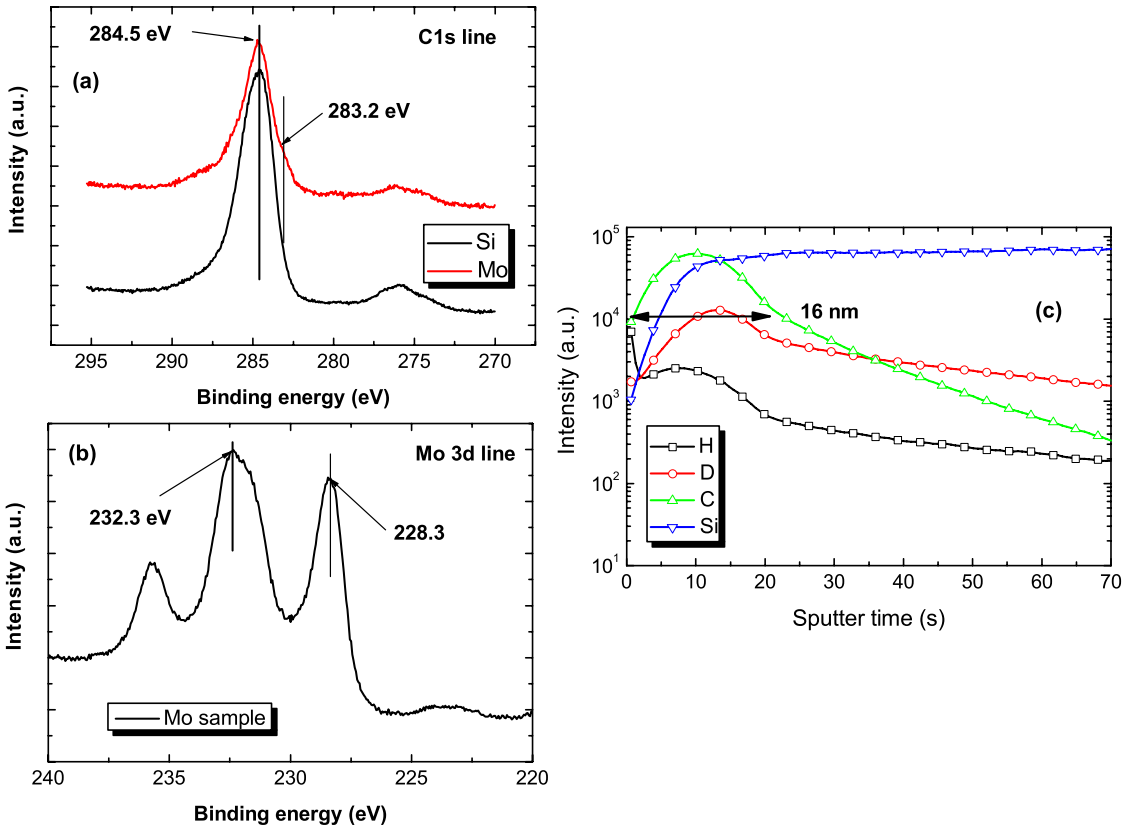

Figure 9.10: (a) C 1s core level spectra and (b) Mo $3d_{3/2,5/2}$ doublet measured by XPS on samples exposed during experiment 5 in the divertor of TCV. (c) SIMS depth profile of the Si sample exposed during experiment 4.

The composition of the deposited layer has been investigated by means of XPS and SIMS. Examples of the C 1s and Mo 3d lines measured on the samples exposed during experiment 5 are given in fig. 9.10, as well as a SIMS depth profile measured on the Si sample exposed during experiment 4. The deposited layers were found to be mainly deuterium and carbon, as expected given the use of deuterium as main plasma fuel and the extensive graphite coverage of the TCV first wall. The optical constants of the films were determined by ellipsometry. The layers have a rather low refractive index (n≈ 1.5 at 632 nm) indicating a soft hydrocarbon film, and these values are in good agreement with those measured on samples exposed in the pump ducts of the ASDEX-Upgrade divertor [162]. The differences in terms of film thickness on the Si and Mo samples exposed during experiment 5 are visible indirectly with XPS. The signal coming from the substrate can no longer be seen on the Si sample due to higher carbon film coverage whereas the Mo 3d line is still very intense for the Mo sample. Moreover as seen

in fig. 9.10a, the C 1s line measured on the Mo sample reveals two components at 284.5 and 283.2 eV respectively. The former line is associated with an amorphous hydrogenated carbon phase while the latter reveals the typical shift of molybdenum carbide. This is consistent with the mechanism proposed in [119] for the growth of an a-C:H film on a Mo substrate, starting with the formation of a carbide phase. Since the interfacial carbide is still observed in the C 1s line, it confirms the low thickness of the film on the Mo sample. The Mo 3d line shows the presence of two doublets, the most intense (with the Mo $3d_{3/2}$ peak at 228.3 eV) corresponds to molybdenum carbide, the less intense doublet shifted towards higher energy corresponds to MoO_3.

Observations of the surface morphology of the samples were done by SEM and with an interferometric microscope[1] allowing a 3D-profiling of the mirror surface. As seen in fig. 9.11a, an accumulation of carbon (according to EDX measurements) in the form of a black line can be seen in the shadowed region between the part of the sample covered by the sample holder and the part visible to the plasma. Fig. 9.11a shows an SEM picture of this deposit taken in one corner of the sample. Interferometry measurements (fig. 9.11b) demonstrate that the thickness of this deposit is not regular along the perimeter of the sample and has a mean value of about 160 nm (this value should be compared with the very low deposited thickness found at the centre of the sample) for the Mo sample exposed during experiment 2. For samples exposed during longer periods, similar observations are made, namely low deposited thickness in the centre and accumulation of carbon at the edge, but thicker deposits are found at the perimeter of the exposed area. The thickness of this deposit seems to grow with the sample exposure time.

Given that TCV is an all carbon machine, deposition of thicker layers might have been expected. SOLPS5 modelling [163] of the standard SNL discharge executed once every day and used for the dedicated exposure experiment indicates that a net carbon deposition rate of $\sim$3.5 nm.s^{-1} in the region directly above the samples might be expected (assuming the release of CD_4 only at a chemical sputtering yield of 3.5 % on the target surfaces). Due to the design of the floor tiles around the sample aperture and the sample position (recessed below the tile surface), samples are never exposed to direct ion fluxes. Layers must therefore have been formed by the deposition of hydrocarbon radicals which is consistent with the nature of the observed layers (soft hydrocarbon film) [71]. These radicals can be formed either in the divertor plasma from the dissociation of stable CD_4 or C_2D_x (x=2,4,6) molecules, produced by chemical erosion of carbon components or at the carbon divertor plates as a result of chemical erosion processes or thermal decomposition of redeposited layers [162]. Of course, since samples are recessed behind the divertor tile surfaces, the resulting lower solid angle with which the samples see the plasma naturally reduces the deposition rate, but the recessment distances investigated here are not high enough to reduce it so drastically.

Since helium glow discharges are applied routinely as a wall conditioning procedure in TCV and given that the total duration of the glow discharges during a sample exposure is much larger than the total tokamak plasma duration, one may think that erosion of the deposited layers by incoming He ions could explain the very low deposited thicknesses observed. Yet the sample

[1] OptoSurf microscope with x10 and x20 objectives; measurements realized by Eotech, Paris, France.

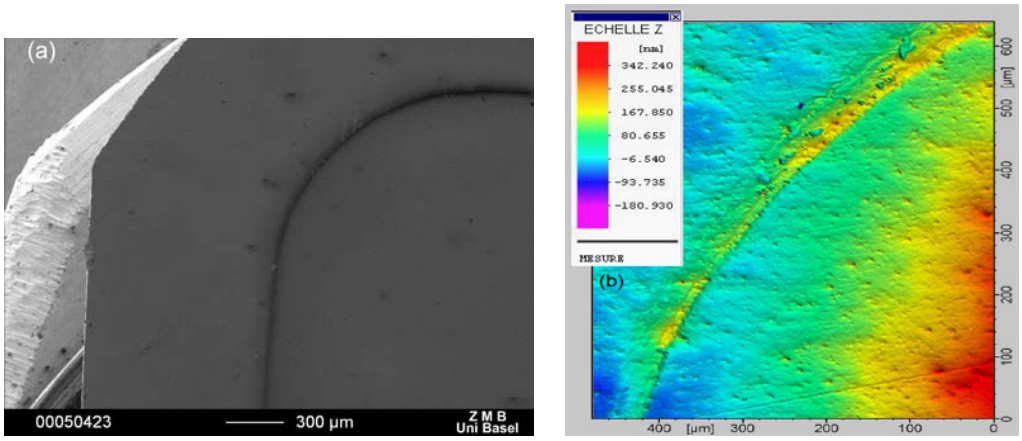

Figure 9.11: (a) SEM picture of the accumulation of carbon found on samples exposed in the TCV divertor at the border between exposed and non-exposed areas, (b) interferometry measurement of the same area of the sample.

holder is maintained at the local floating potential during the glow discharges and the energy of the impinging ions does not exceed $\approx$ 10 eV (acceleration into the sheath) and is therefore below the physical sputtering threshold for He. Moreover the fluxes during the conditioning glow discharges are much lower than the plasma fluxes during the tokamak shots. Removal of carbon deposited by the tokamak discharges by the He glow can therefore be neglected.

To assess the possible erosion due to energetic charge exchange neutrals, a special sample with an erosion marker was prepared. It consisted of an Al layer of known thickness deposited on a Si sample by magnetron sputtering in a UHV chamber. Aluminium was deposited on a spot of $\approx$ 3 mm diameter (thus covering only part of the surface) and with a thickness of 230 nm. The thickness of the Al marker was measured before and after a 3 week exposure in TCV by means of a stylus profilometer. Aluminium was chosen as a marker element because of its low-Z and because it is not present elsewhere in the machine, therefore if after exposure traces of Al are found at other parts of the sample one can be sure that it comes from the marker. Results are shown in fig. 9.12a. As seen, no noticeable decrease of the marker thickness is observed, instead an increase of the thickness of about 15 nm is found after exposure. XPS reveals that this increase is due to carbon deposited on the marker surface which is also seen on the SIMS depth profile in fig. 9.12b where the carbon layer, the Al marker and the Si substrate are clearly distinguished. No traces of aluminium are found on the rest of the Si sample. Therefore we can rule out possible erosion of the mirrors by energetic CXN.

The reason for the accumulation of carbon at the edge of the exposed area is not known. The black colour of the deposit indicates a low deuterium content. One hypothesis for the formation of this deposit may be the accumulation of dust particles. Formation of dust has been observed in several fusion devices with carbon PFCs [164, 165]. At the end of a tokamak discharge, most dust particles fall down due to gravity. The lighter ones may be reinjected into the plasma either by magnetic or by electric forces when the dust flakes are charged by plasma electrons [166]. One can speculate that the accumulation of carbon observed on TCV samples is formed by dust particles swept away from the sample surface and retained by the edges of

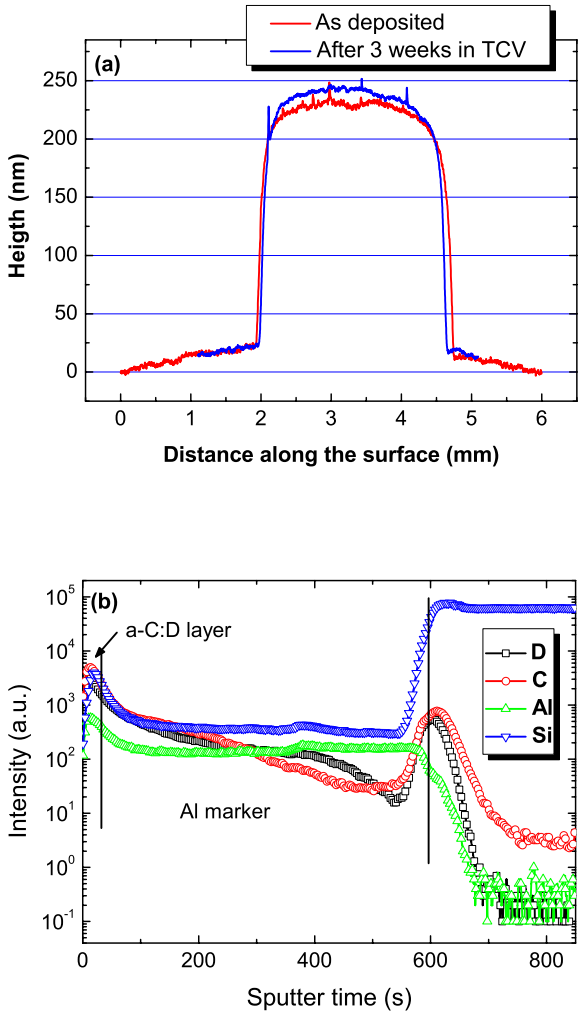

Figure 9.12: (a) Thickness of the Al marker deposited on a Si sample by magnetron sputtering before and after exposure in TCV as measured with a stylus profilometer and (b) SIMS depth profile of the Al marker after exposure in the TCV divertor.

the sample holder thus forming the black line observed.

9.3.2 Deposition efficiency on different substrates

As described in chapter 9.3.1, under identical exposure conditions the deposition rate of carbon on a silicon substrate has been found to be much higher than on molybdenum. The reason for these differences will be described in more detail in chapter 9.4.2. Firstly, the reflection coefficients of D and C on Si are much lower than on Mo. Secondly, due to the higher particle reflection coefficients, enhanced physical re-sputtering of the deposited material by the impinging deuterium neutrals may take place.

Boronisation of the vacuum vessel is used in TCV as a wall conditioning technique, and is made regularly. During such procedure a glow discharge is created in a mixture of helium and

diborane in order to coat all PFCs with a boron containing layer [49]. The ability of boron to

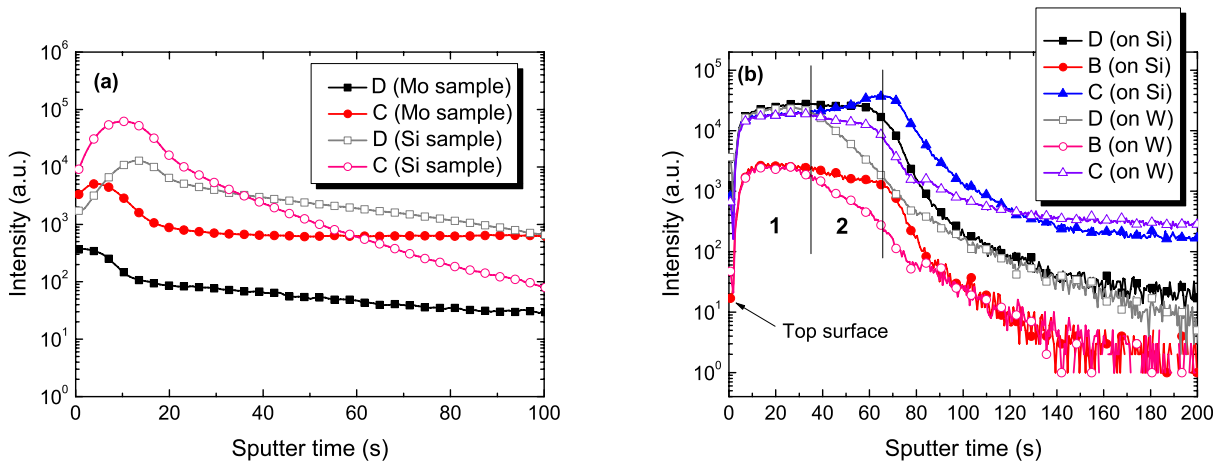

Figure 9.13: SIMS depth profile of (a) Mo and Si samples exposed during three weeks in TCV and (b) of Si and W samples exposed during a boronisation of the TCV vacuum vessel.

getter oxygen helps in reducing the oxygen content in the plasma and allows an improvement of the plasma conditions. Two samples (W and Si) were exposed during a boronisation being recessed 50 mm below the divertor tile surface (to make it comparable with other exposures). The aim was first to characterize the boron layer and also to see if differences in the film composition may be observed. During the boronisation the samples were insulated from the rest of the torus and thus maintained at the local floating potential. After boronisation the samples are coated with a ∼20 nm thick layer consisting of C, B and O. They were analyzed with Tof-SIMS in order to obtain the depth profile concentration of the different elements in the deposited layer. Results are shown in fig. 9.13. For the samples exposed during tokamak operations, for a three week period, differences in the thickness of the deposited layer are found which are seen from the differences in the depth profile of C and D in fig. 9.13a. Some differences in the concentration profiles are also noticed for the samples exposed during the boronisation. They are the most pronounced near the interface film/substrate (zone 2 in fig. 9.13b). A thinner film is found on the W sample. The composition of the homogeneous layer (zone 1) seems identical for both samples which is in agreement with surface analysis done by XPS (for which only the topmost layer is analyzed). These observations confirm that the substrate plays a significant role until a certain film thickness has been deposited, beyond this point the incoming particles will only see the deposited layer with the substrate becoming invisible, masked by the deposited layer. As reported in [167], some deposition probes (Si and C) were exposed during a boronisation in ASDEX-Upgrade. These samples were maintained at machine potential such that the energy of the impinging particles was about 270 V. The composition and thickness of the layer deposited on Si and C was found to be different.

It is now clear that the substrate material plays a role in determining the importance of the erosion/deposition mechanisms. It is possible to extract complementary information on

the physical mechanisms involved with a theoretical approach using a Monte Carlo simulation code of the sputtering processes. Numerical simulations of the simultaneous bombardment of a mirror surface by deuterium and carbon ions have been performed using the TRIDYN code. The results of these studies will be described in the following section.

9.4 Numerical simulations

9.4.1 The TRIDYN Monte Carlo code

TRIDYN (or SD-TRIMSP) [139, 140] is a Monte Carlo code for binary collision simulation of atomic collisions and dynamic composition changes in solids. It is based on the well-known TRIM code [141] which provides fast simulations of collisions in amorphous materials. Originally TRIM was developed for the calculation of the slowing down of fast particles only, disregarding any recoil of the target atoms. Later, the original code was modified to include recoil atoms (thus allowing simulations of the sputtering process) but always with a static target substance, i.e. being strictly valid only in the limit of low implantation fluences.

By comparison, TRIDYN is a dynamic code in the sense that changes in the surface composition induced by the impinging ions are accounted for at each calculation step. The program determines the thickness removed or deposited as a function of the ion fluence. In addition, sputtering yields, reflection coefficients, surface composition and depth distributions of the different species are calculated versus the incident ion fluence.

Ballistic effects such as projectile deposition and reflection, sputtering, and ion mixing are computed for a target at zero temperature. Radiation damage is not taken into account. The target and the deposited layer are assumed to be amorphous. Each simulated projectile ("pseudo-projectile") represents a physical increment of incident fluence (incident particles per unit area). TRYDYN covers only non-thermal processes so that diffusion and segregation processes are neglected.

According to the procedure described in [80], the "krypton-carbon" potential [142] is applied as an interaction potential. The electronic stopping cross section is calculated as an equipartition of the continuous Lindhard-Scharff [143] and the local Oen-Robinson [144] interactions. The binding of the surface atoms is described by a planar potential with the heat of sublimation as the value of the surface binding energy. Projectiles and target atoms are followed as long as their energy is above the surface binding energy.

In the framework of the present study, TRIDYN was used to shed some light on the different erosion/deposition patterns observed both in laboratory experiments and in Tore Supra. In order to match the experimental conditions the simulation parameters were defined as follows:

- electronic temperature of 13 eV and sheath potential of 200 V (using the Langmuir probe measured T_e and with the sheath potential corresponding to the bias applied to the mirrors during the laboratory experiment),
- D^+ and C^{3+} as impinging ions (according to an ion-recombination balance calculation C^{3+} is the majority carbon species in the plasma [145]),
- Maxwellian ion energy distribution,
- isotropic angular distribution (which is transformed to a more normal incidence by the sheath potential) [146].

9.4.2 Simultaneous bombardment of different candidate materials by deuterium and carbon ions

Results

Numerical simulations were carried out using the parameters described above for a selection of relevant materials: copper, iron, molybdenum and silicon. Silicon was chosen because of the interesting results obtained with silicon samples exposed in the divertor of TCV [113], even if it is not really a good candidate material for first mirrors in ITER. Moreover, iron was used in the simulations instead of stainless steel mainly for ease of modelling, though we implicitly assume that since iron is the main constituent of stainless steel, the results obtained here are illustrative of the real case. Fig. 9.14 shows the results of the TRIDYN calculations made for different fractions of carbon ions in the plasma.

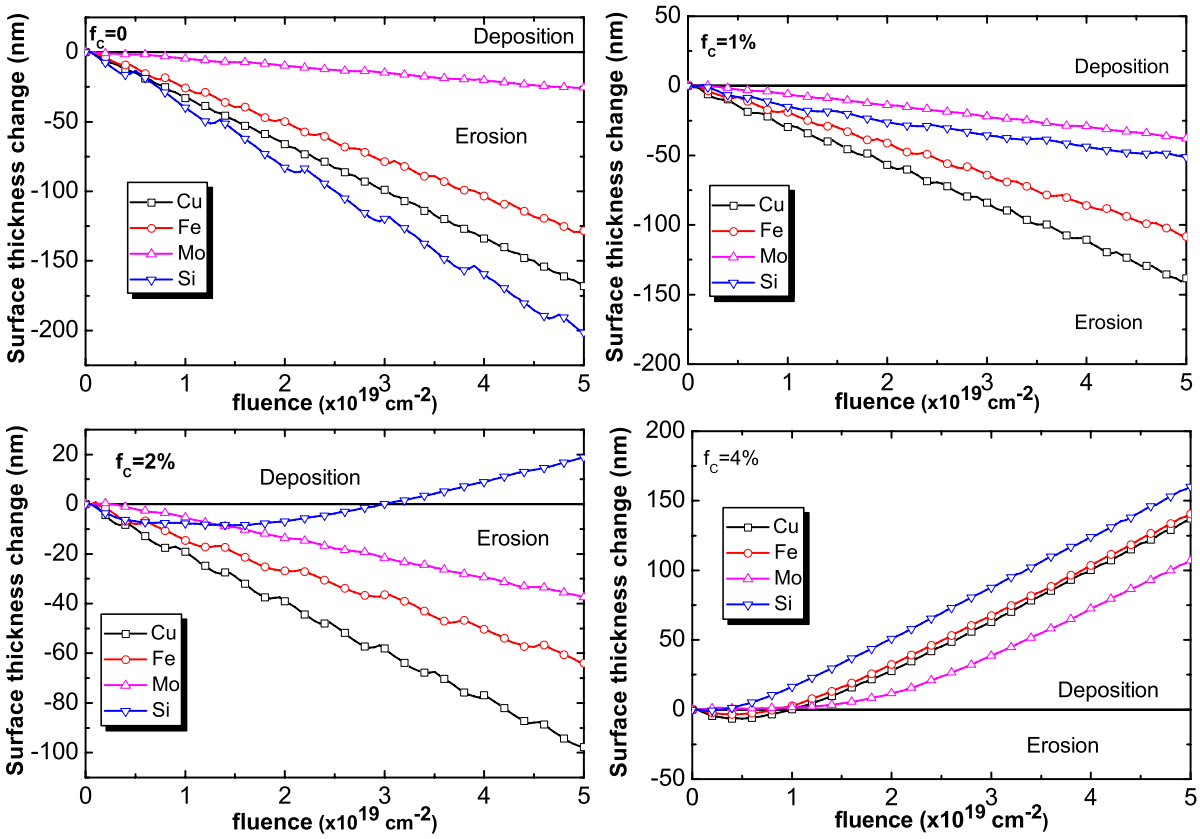

Figure 9.14: TRIDYN calculations of deposition and erosion versus ion fluence for different mirror materials bombarded simultaneously by D^+ and C^{3+} ions with T_e=13 eV and for different carbon concentrations in the plasma.

For the case of a pure deuterium plasma ($f_C = 0$), the surface of all materials is eroded

systematically with the incoming ion fluence. The erosion rates are consistent with the relative sputtering yields of the different materials. For $f_C = 1\%$, the evolution of the surface thickness of all materials is still linear with the ion fluence, but differences in the erosion rates of the different materials are observed. The erosion rate of molybdenum for $f_C = 1\%$ is larger than that calculated for a pure deuterium plasma: the final eroded depth (for a fluence of $5 \cdot 10^{19}$ ions.cm^{-2}) is 38 nm compared to 25 nm when $f_C = 0$. On the contrary, a reduction in the erosion rate of Si, Cu and Fe is found from the calculations. The most drastic evolution being found for Si for which a factor of 4 reduction of the erosion is found (50 nm instead of 200 nm). Observations are the same for $f_C = 2\%$, but deposition occurs for Si. It should be noted that in this case the surface thickness does not evolve linearly with the ion fluence. The surface is first eroded by the impinging plasma ions and, after a certain ion fluence is reached ($3 \cdot 10^{19}$ ions.cm^{-2} in the conditions here), deposition starts. For higher carbon fraction in the plasma, all surfaces become deposition dominated, and exhibit the behaviour observed for Si. The point at which deposition starts depends on the material, although after a certain film thickness is reached, the deposition rate appears to be similar on all materials. Indeed after a certain thickness, the substrate becomes invisible to the incoming ions.

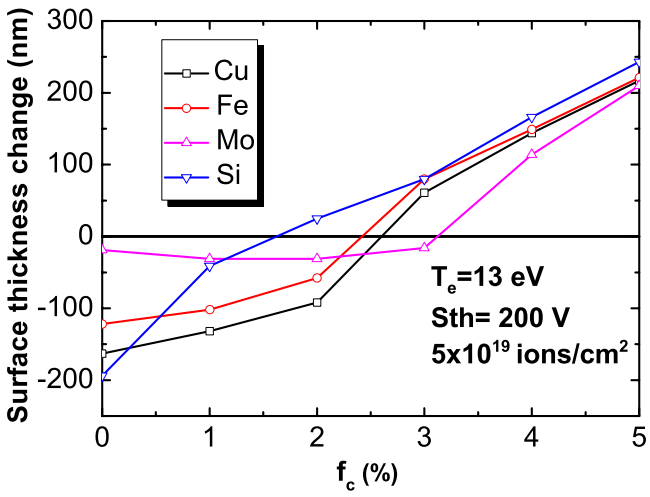

Figure 9.15: Transition between erosion and deposition for Cu, Fe, Mo and Si as a function of the fraction of carbon in the plasma for a given fluence of $5 \cdot 10^{19}$ ions.cm^{-2}.

Fig. 9.15 shows the evolution of the "surface thickness" of the materials as a function of the fraction of carbon in the plasma for a given ion fluence. This illustrates both the different behaviours exhibited by the different substrates for increasing carbon content in the plasma, and the different critical fluences at which deposition occurs. Silicon is the most sensitive substrate towards deposition, carbon deposition occurs for $f_C = 1.6\%$. In contrast, for molybdenum the transition between erosion and deposition occurs at $f_C = 3.1\%$ under the conditions of interest here.

Discussion

The problem of the simultaneous bombardment of a surface by several ion species is a very critical issue for ITER because of the combination of materials to be used as plasma-facing elements. Of particular importance in the present study are the critical impurity (carbon) to fuel (deuterium) ratio (here the C/D ratio, denoted henceforth by f_C^*) for the erosion/deposition transition, and the non-linear evolution of the surface thickness with the incoming ion fluence. We shall discuss these two points in the following paragraphs.

According to the results shown in fig. 9.15, the higher the atomic number (Z) of a given element, the higher f_C^*. This observation is consistent with the observations made by other authors [147, 148]. This can be partially explained by studying the reflection coefficients, computed with TRIDYN, of the incident carbon and deuterium ions on the different materials (table 9.5). For both types of ions, the higher the Z of the material the higher the reflection coefficient. Since a larger fraction of carbon ions is reflected from a molybdenum surface compared to reflected from a silicon sample, more carbon ions are necessary to build a layer and turn from erosion to deposition. This leads to the higher f_C^* for Mo. An alternative way of stating this is that the sticking coefficient of carbon on molybdenum is lower than that of silicon. Another possible explanation for the different transitions from erosion to deposition,

Material	**Ion**	
	D	**C**
Cu	0.36	0.16
Fe	0.32	0.13
Mo	0.4	0.22
Si	0.17	0.02

Table 9.5: Reflection coefficients of deuterium and carbon ions determined from numerical simulations with TRIDYN (at given energy of incoming species).

which is also a consequence of the higher ion reflection coefficients of high-Z materials, is the enhancement of the physical re-sputtering of carbon deposited on molybdenum. This effect has been studied in [149] for the case of boron on carbon and tungsten substrates and more recently in [150] to explain the different efficiency of hydrocarbon deposition onto carbon and tungsten. To re-sputter a deposited atom, the incident plasma ion must change its direction by a reflection from an underlying substrate atom. Since Mo atoms are much heavier than deuterium atoms, the energy transfer from an incident deuterium ion to a molybdenum substrate atom will be quite ineffective (and much less effective than the energy transfer from a D ion to a Si atom due to their smaller mass ratio). An ion will thus be reflected with a considerably higher energy than in the case of a Si substrate for example, and will therefore have a higher probability to sputter a deposited carbon atom. Fig. 9.16 illustrates this effect. A high-Z material like molybdenum is therefore much less sensitive to carbon deposition than a low-Z material.

The differences in the critical carbon fraction for the transition erosion/deposition for different materials find a natural application in the selective deposition or etching on patterned substrates e.g. for the fabrication of ultra-small microelectronic components [151, 152, 153].

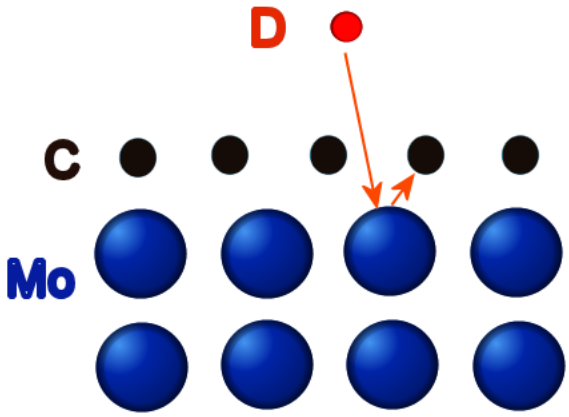

Figure 9.16: Illustration of the enhancement of the physical sputtering of carbon deposited on a Mo surface.

The non-linear evolution of the surface thickness was first investigated by Naujoks *et al* using both the TRIDYN code and an analytical model they developed [154, 80]. For a silicon substrate, at $f_C = 2\%$ (fig. 9.14), a transition from an erosion phase at the beginning of the ion bombardment to a deposition phase at higher fluences is observed. At the beginning of the bombardment, the energy of the incident plasma ions is high enough to sputter Si. But during the bombardment more and more carbon ions are deposited which cannot subsequently be removed. Consequently the sputtering of Si atoms from the surface decreases and deposition prevails for higher fluences. Similar observations were made during the bombardment of a tungsten surface with deuterium and carbon ions with energies in the keV range [155, 156].

9.4.3 Comparison with the experimental results

Fig. 9.17 shows a comparison between the results described in section 9.2.4 and the values of erosion/deposition calculated with TRIDYN. Excellent agreement is found for the case of stainless steel. The situation is very different for copper. As already noted earlier, the code predicts that copper and iron should have similar behaviour in the case of simultaneous bombardment with deuterium and carbon ions. Indeed TRIDYN deals with physical processes only: chemical processes like carbide formation, diffusion, segregation,... are neglected. Since copper and iron have atomic masses which are very close, it is not that surprising that TRIDYN predicts similar behaviour for both materials. However, as already pointed out in chapter 9.2.4, it seems that the carbon impurities in the plasma decrease the effective sputtering yield of stainless steel while enhancing that of copper. This would indicate that other effects, neglected in the code, play a fundamental role in the case of copper. From a chemical point of view, it is perhaps important to note that copper does not form stable carbides [157]; the only existing carbide phases are metastable [158]. Moreover the miscibility of carbon into copper is very low even at high temperature (C-Cu bonds are very weak) [159, 160]. Since copper cannot form carbide we may assume a very low sticking coefficient of carbon onto copper. Carbon would therefore

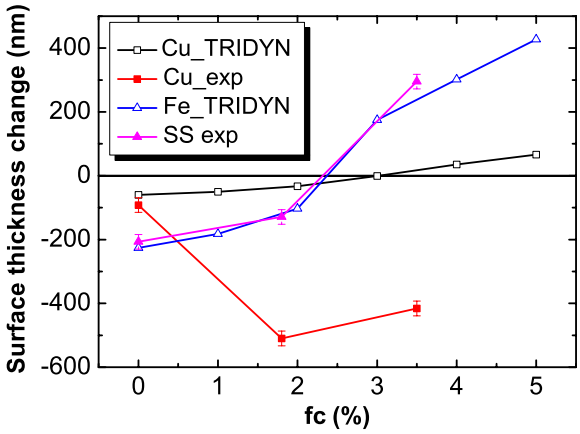

Figure 9.17: Comparison between the experimental results described in chapter 9.2.4 and the erosion/deposition calculated with TRIDYN.

have less chance to be deposited on copper and will rather contribute to the further sputtering of the surface.

Similar observations concerning enhanced sputtering of copper in presence of carbon ions have been made during carbon ion implantation in copper at high temperature [161]. According to the authors, carbon may enhance the sputtering not by direct sputtering of the material but rather by the precipitation of carbon at the near surface resulting in the creation of very weak Cu-C bonds. Copper surface atoms would be less attached to the bulk materials and sputtering by the plasma ions would be facilitated. Further experiments will be needed to check this assumption and clarify the precise role of carbon during the sputtering process.

9.4.4 Conclusions

The results presented here demonstrate that under similar exposure conditions, mirrors from different materials behave quite differently. Under simultaneous bombardment with deuterium and carbon ions, a copper mirror is damaged by physical sputtering from the plasma ions whilst a stainless steel mirror becomes coated with an a-C:H film. For both substrates the mechanism affecting the optical reflectivity is therefore different: sputtering of the copper surface increases the surface roughness and thus decreases the reflectivity, whilst the reflectivity of the SS mirror is modified by the absorption of light in the deposited layer. The different deposition rates measured on Si and Mo after exposure in TCV under similar conditions confirm that the erosion/deposition pattern is substrate dependent. Numerical simulations with TRIDYN have shown that the particle reflection coefficients onto different substrates could explain the behaviour observed for Mo, Si and SS. The case of copper remains, however, incompletely resolved. Several effects (surface chemistry, roughness...) may contribute to the observed increased erosion of the surface when carbon is present in the plasma. However the present data do not allow unambiguous conclusions and further experiments would be required to assess

these different hypotheses. It is clear, however, that in choosing diagnostic first mirror materials in ITER, both the resistance of a material to sputtering and the efficiency of deposition (eg. C, Be, W) must be considered with equal importance.

Part IV

Conclusions and perspectives

9.5 Conclusions

The question of the lifetime of the metallic mirrors in the diagnostic systems of ITER is of crucial importance for the success of the project. Any modifications of the mirror reflectivity caused by the intense plasma-wall interactions in the machine will affect the reliability of the spectroscopic signals. Although comparatively simple, the mirrors are the first element in very complex and expensive diagnostic systems and must function reliably through the life of the project. The basic questions to be answered are therefore: how long will the mirrors maintain the required optical properties, and how to maximize this duration ? The objective of this thesis was to improve the understanding of the effects of the plasma-wall interactions in a tokamak (material erosion, migration, and redeposition) on the optical properties of in-vessel metallic mirrors, with a view towards the parameters which may be optimized to extend their lifetime. Fig. 9.18 summarises the approach followed during this thesis and the main results obtained.

Two opposite effects are likely to contribute to the deterioration of the mirror reflectivity: erosion due to charge-exchange neutrals and deposition of impurities on the mirror surface.

Erosion of an initially polished polycrystalline material, proceeds with the removal of the polished layer and the progressive appearance of the different crystallographic grains, hence a progressive decrease of the specular reflectivity. On the contrary, as was confirmed by the exposure of single crystal and polycrystalline mirrors in the SOL of TEXTOR, a single crystal mirror is eroded homogeneously by the incoming particles and maintains a stable roughness. Single crystal mirrors thus appear as attractive solutions for mirrors likely to be subject to erosion. However, it remains very challenging from a technological point of view to manufacture a single crystal mirror with the size meeting ITER's requirements (for example 35 cm diameter for the mirrors in the Thomson Scattering system). A feasibility study is ongoing in Russia. The key parameter here is that the surface roughness remains negligible in comparison with the wavelength of the light during the erosion of the surface. An alternative to the use of single crystal may consist in the use of nano-crystalline films deposited on a metallic substrate. Two approaches are currently being investigated. The first one consists in the deposition of nanocrystalline molybdenum films deposited by magnetron sputtering on a polished molybdenum substrate. In addition, realization of rhodium layers by magnetron sputtering on different metallic substrates (copper, molybdenum, stainless steel) have been initiated during this work. The average crystallite size is about 30 nm, and the first tests with ion bombardment of the prepared mirrors are rather promising.

In ITER the use of carbon as plasma-facing material for the divertor targets together with the long range migration of carbon/hydrocarbon observed in present tokamaks raise the possibility that mirrors located at remote locations from the plasma may become coated with an amorphous hydrogenated carbon film. Exposure of molybdenum mirrors in the private-flux region of the DIII-divertor has evidenced a carbon deposition rate of 2 $nm.s^{-1}$ leading to strong modifications of the mirror reflectivity after 25 s of plasma. Estimates of the flux of carbon arriving on the mirrors located under the ITER dome indicate that a comparable deposition rate may be expected there. In addition to the protection of the mirror surface by baffle structure, mitigation methods will be necessary to prevent (or reduce) the extent of the problems caused by the deposition of carbon. One of such possible mitigation method was tested in DIII-D.

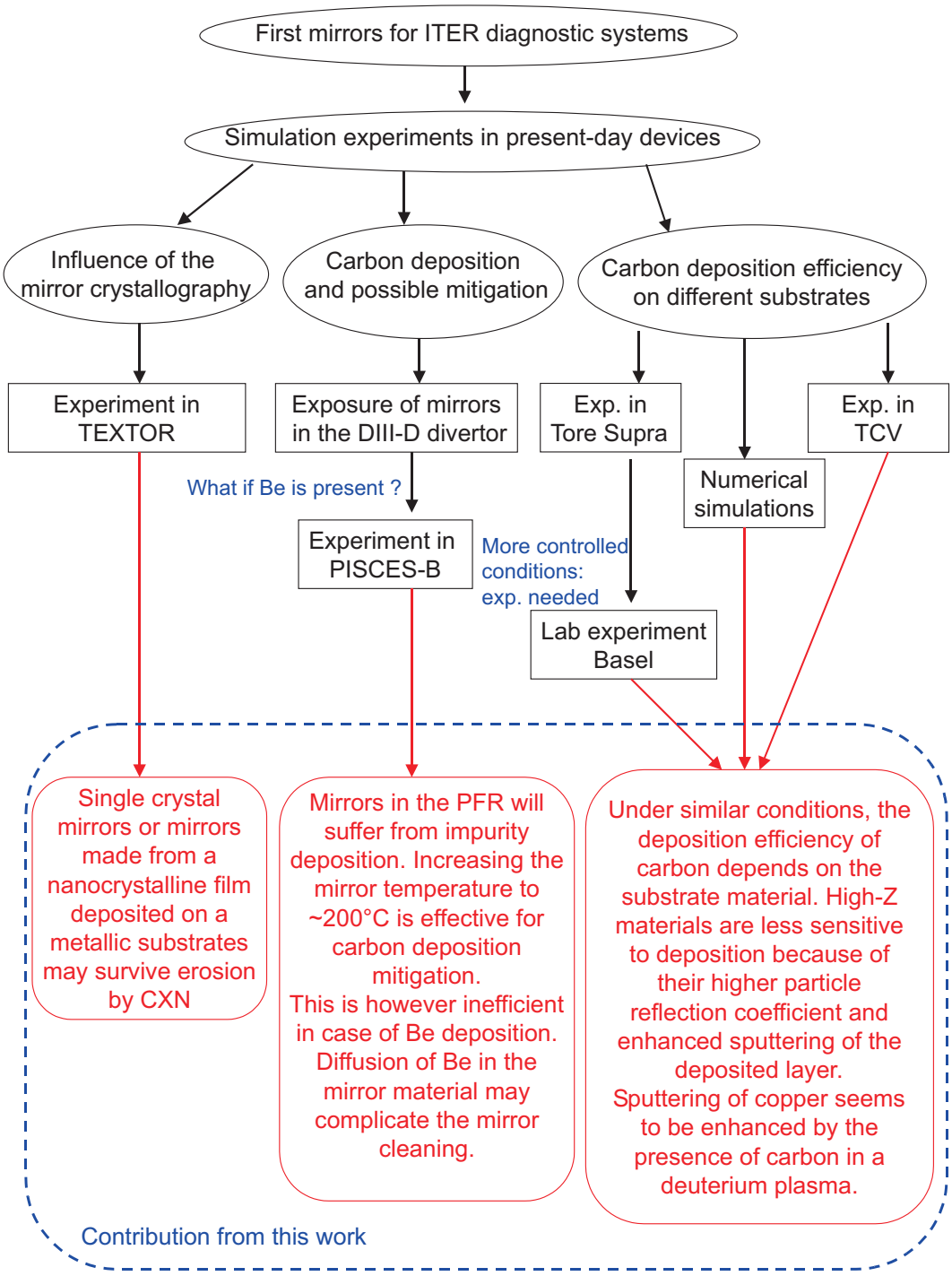

Figure 9.18: Summary of the main results obtained during this thesis.

Heating the mirrors to about 200°C, and thus thermally enhancing the chemical erosion yield of carbon, appeared to be sufficient to prevent carbon from being deposited on the mirrors. Though very encouraging, this result is affected by the relatively strong surface oxidation found on the surface of the heated mirrors. Although the origin of this oxidation remains unclear, its occurence puts the stress on the necessity of applying regular *in-situ* cleaning techniques to the mirrors in ITER even if mitigation methods are applied.

Of course, the problem of carbon deposition is intimately dependent on the presence of beryllium as a first wall material in ITER. Indeed experiments in PISCES-B have shown that the Be fraction present in the SOL plasma flow may lead to the formation of a Be coating on the graphite target thus reducing (and even suppressing) carbon erosion. In turn, the deposited beryllium may re-erode and lead to the formation of Be-rich deposited layers in line-of sight locations from the target. Experiments with metallic mirrors were carried out in PISCES-B with the aim of characterizing the effect of a Be/C layer on the mirror reflectivity and investigate the effect of the mirror temperature on the deposited layer. It was found that the reflectivity of the mirrors was drastically affected by the deposition of a Be/C layer. Except for experiments with very low Be fractions, the deposited layers mainly consist of Be. Increasing the mirror temperature mitigates carbon deposition as long as it has not been suppressed by the formation of a Be layer on the graphite target. The subsequent deposition of Be is not affected by the mirror temperature. Therefore in the case that beryllium is the main deposited impurity the temperature no longer acts as a mitigation agent. In-situ mirror cleaning may be complicated by the deposition of Be and dedicated investigations would be required to assess the effectivenes of the currently proposed cleaning techniques for Be-coated mirrors. Moreover the possible diffusion of Be into the mirror material (which was observed for the copper mirrors at $300°C$) may further complicate the cleaning issue because of the formation of Cu-Be alloy. These experiments were the first-ever investigation of the consequence of Be deposition on first mirrors.

The proper choice of the first mirror material should also take into account the fact the substrate material itself plays an important role. Experiments in Tore Supra and in the laboratory stand in Basel have shown that different materials behave very differently under simultaneous bombardment by carbon and deuterium. The presence of carbon in the plasma leads to a reduction of the effective sputtering yield of stainless steel while deposition of carbon occurs for a certain fraction of carbon. On the contrary the more carbon in the plasma the more erosion is experienced by a copper mirror. The presence of carbon as impurities in the deuterium plasma seems to enhance significantly the erosion of the surface. Moreover, the efficiency of carbon deposition on a given substrate also depends on the substrate material. A high Z material like Mo is much less sensitive than Si towards deposition of carbon. This was revealed by experiments carried out in the TCV tokamak where the deposition rate of carbon on silicon was found to be five times higher than on molybdenum. This is explained by the higher particle reflection coefficient on a high-Z material which implies that a larger fraction of the incoming particles will be backscattered by the surface, but also that reflected particles will do so with a significant energy and may sputter a deposited atom after its reflection by the surface.

This work has also contributed to the systemization of the experiments made with mirrors in various machines in the sense that a routine procedure has been established. Mirrors arrive

at the University of Basel after polishing and are first cleaned using a low temperature hydrogen plasma. After that detailed optical and surface characterizations are carried out. The mirrors are then sent back to be exposed and are returned for the same procedure after the experiment (except if the mirrors are coated with beryllium). This allows better comparison of the results obtained in different machines.

9.6 Perspectives and future experiments

Although a much better understanding of the first mirror problem has been gained during the last few years, more work is required before a solution can be found. From the results described in this thesis, it is clear that the material choice should be carefully made taking into account the location of the mirrors and the requirements in terms of optical properties and resistance to erosion/deposition. However, whatever the material, it is clear that the design of the diagnostic duct will have to be optimized to reduce the arrival rate of particles on the mirror surface. This may be done either by a special shaping of the duct as was proposed in [168] or by integrating a shutter system in the design which will only open when the diagnostic needs to be used [169]. This latter technique is however valid only for diagnostic which does not neet to work continuously during the shot and is therefore restricted to a few systems.

Since it seems very likely that a certain level of deposition on the mirrors will be impossible to mitigate completely, cleaning techniques will need to be applied regularly during the mirror lifetime. Several candidate techniques are being assessed. Amongst them are plasma-based techniques and laser ablation. Plasma-based techniques like hydrogen glow discharge have demonstrated a good efficiency for the removal of carbon-based deposits, however recent experiments made at the University of Basel have shown that they are unefficient for the removal of the interfacial carbide formed during the growth of a carbon film on a carbide-forming element [100]. The remaining carbide will likely affect the reflectivity [117] and prevent the recovery of the initial optical properties of the mirrors. Laser ablation is being tested as a technique for fuel removal on plasma-facing-components (to limit the tritium retention in ITER) [170] and may be a good candidate material for *in-situ* mirror cleaning. However, the use of appropriate cleaning techniques does not preclude the diagnostic design from planning the possible replacement of the mirrors. In the design of the charge-exchange recombination spectroscopy (CXRS) for example, it is planned to install mirrors in tubes which are independent from the diagnostic port and can be retracted as a whole for mirror replacement [171].

From an experimental point of view and keeping in mind the necessity of being predicitive for the conditions in ITER, future experiments with mirrors should aim at simulating as realistically as possible the situation to be faced in a real diagnostic system. This may be done either by designing real mock-ups of diagnostic systems and integrating them into present machines, or designing the experiments in such a way that they simulate this situation. Such an attempt in being pursued at TEXTOR where a periscope-like system has been designed and exposed in the SOL plasma [96]. However the mirrors were exposed in such a way that they faced the plasma, which is not realistic in the sense that first mirrors in ITER will not be exposed to plasma ions but more likely to charge-exchange neutrals. The system is being modified to provide a more

realistic approach.

Of course to improve the relevance of the experiments it is necessary not only to optimize the experiment but also to carry out the experiments in machines where conditions are as close as possible to those in ITER. That is why a comprehensive first mirror test has been initiated at the JET tokamak [110]. JET is the world's largest divertor tokamak, it has an ITER-relevant configuration, a beryllium environment and a comprehensive programme of erosion/redeposition studies working in parallel with the mirror exposures. Erosion and deposition processes are monitored using a set of dedicated tools amongst which are quartz microbalances (QMB) [172] for shot-by-shot measurements and erosion/deposition monitors for *ex-situ* studies. A total of 32 mirrors were installed during the 2005 shutdown at several locations of interest for ITER mirrors in stainless steel cassettes with a "pan-pipe" shape. The cassettes have been installed at 5 different locations inside the JET vacuum vessel: 3 in the divertor (outer, inner and base) and 2 on the first wall. Cassettes installed on the first wall are protected with magnetic shutters which open only when the magnetic field is on (so only during tokamak pulses). The cassettes are installed in the vicinity of deposition monitors for a better comprehension of what happened during the exposure. The experiments include the test of mirrors with different inclination angles and with different distances with respect to the plasma. It is therefore possible to study the consequences of geometrical effects on the optical properties of the mirrors. Optical characterizations of the mirrors prior to their installation were made at the University of Basel by means of spectrophotometry and spectroscopic ellipsometry. In addition, to overcome the non-negligible complications introduced by the possible contamination of the mirror surface with beryllium, special spectrometric equipment has been designed and installed at JET. Design of the system, purchase of the different components, tests and assembly of the system were realized in the framework of the present work and will be used to characterize the exposed mirrors. More details about the system may be found in [110]. Unfortunately due to delays in the experimental campaigns at JET, the mirrors could not be retrieved from the tokamak before completion of this thesis. Samples are now expected to be removed in the first semester of 2007 and detailed investigations on the exposed mirrors will be presented elsewhere. This experiment should provide very useful results, and discussions are now ongoing to continue this experiment in the next few years when JET operates with its new ITER-like wall [173].

Bibliography

[1] U. Bardi, Energy Policy, 33 (2005) 53-61.

[2] S. Latouche, *Survivre au developpement*, Ed. Mille et une nuits (in French), Essay.

[3] U.S. Department of Energy, International Energy Outlook 2004, April 2004. *http://www.eia.doe.gov/oiaf/ieo*

[4] J. D. Lawson, Proc. Physical society, B70 (1957) 6.

[5] J. A. Wesson, *Tokamaks*, Clarendon Press, Oxford, 2nd edition, 1997.

[6] P. C. Stangeby, Plasma Phys. Control. Fusion, 42 (2000) B271-B291.

[7] F. Wagner *et al*, Phys. Rev. Lett., 49 (1982) 1408.

[8] B. Unterberg, U. Samm, Trans. Fus. Sc. Tech., 45-2T (2004).

[9] R. Hawryluk, Rev. Mod. Phys. 70 (1997) 537.

[10] J. Jacquinot and the JET team, Plasma Phys. Control. Fusion, 41 (1993) A13-A46.

[11] ITER physics basis, Nucl. Fusion, 39-12 (1999) 2175.

[12] Y. Shimomura, R. Aymar, V.A. Chuyanov, M. Huguet, H. Matsumoto, T. Mizoguchi, Y. Murakami, A.R. Polevoi, M. Shimada, ITER Joint Central Team, and ITER Home Teams, Nucl. Fusion 41-3 (2001) 309.

[13] Y. Shimomura, for the ITER International Team and Participant Teams, Fus. Eng. Des. 81 (2006) 3-11.

[14] A.E. Costley, D.J. Campbell, S. Kasai, K.E. Young, and V. Zaveriaev, Fus. Eng. Des. 55 (2001) 331-346.

[15] A.E. Costley, A. Malaquias, T. Sugie, G. Vayakis, and C. Walker, Proc. of the 19th IAEA Fusion Energy Conference, Lyon, France, paper CT-5 (2002).

[16] ITER physics basis, Nucl. Fusion, 39-12 (1999) 2541.

[17] A.E. Costley, A.J.H. Donne, K. Ebisawa, G. Janeschitz, S. Kasai, A. Malaquias, G. Vayakis, C.I. Walker, S. Yamamoto, and V. Zaveriaev, Proc. of the 28th EPS conf. on Plasma Physics and Controlled fusion, Madeira, 2001.

[18] P.D. Morgan, R. Barnsley, C.W. Gowers, M.F. Stamp, K.D. Zastrow, and JET-EFDA contributors, Proc. of the 30th EPS conf. on Plasma Physics and Controlled Fusion, St Petersburg, ECA Vol. 27A, O-3.3c, 2003.

[19] P. Sigmund, Phys. Rev. 184 (1969) 383.

[20] W. Eckstein, *Computer simulation of ion-solid interaction*, Springer Series in Material Science, Vol. 10, Springer, 1991.

[21] W. Eckstein, C. Garcia-Rosales, J. Roth, W. Ottenberger, Sputtering data, Max-Planck-Institut für Plasmaphysik, Report IPP 9/82 (1993).

[22] G.F. Matthews, J. Nucl. Mat. 337-339 (2005) 1-9.

[23] Y. Yamamura, and J. Bohdansky, Vacuum 35 (1985) 561.

[24] M. Küstner, W. Eckstein, V. Dose, and J. Roth, Nucl. Inst. Meth. B 145 (1998) 320.

[25] M. Balden, A.F. Bardamid, A.I. Belyaeva, K.A. Slatin, J.W. Davies, A.A. Haasz, M. Poon, V.G. Konovalov, I.V. Ryzhkov, A.N. Shapoval, and V.S. Voitsenya, J. Nucl. Mater. 329-333 (2004) 1515-1519.

[26] M. Mayer, R. Behrisch, P. Andrew, and A.T. Peacock, J. Nucl. Mater. 241-243 (1997) 469-475.

[27] H. Verbeek, J. Stober, D.P. Coster, W. Eckstein, and R. Schneider, Nucl. Fusion, 38-12 (1998) 1789.

[28] R. Behrisch, G. Federici, A. Kukushkin, and D. Reiter, J. Nucl. Mater. 313-316 (2003) 388-392.

[29] J. Roth, and C. Garcia-Rosales, Nucl. Fusion, 36-12 (1996) 1647, with corrigendum Nucl. Fus. 37-6 (1997) 897.

[30] M. Wittmann, and J. Küppers, J. Nucl. Mater. 227 (1996) 186.

[31] J. Roth, J. Nucl. Mater., 266-269 (1999) 51-57.

[32] M. Balden, and J. Roth, J. Nucl. Mater., 280 (2000) 39-44.

[33] J. Roth, et al, Nucl. Fusion, 44 (2004) L21-L25.

[34] A. Loarte, in *Nuclear Fusion Research: Understanding Plasma-Surface Interactions*, Springer series in Chemical Physics, 2004.

[35] R.J. Groebner, Phys. Fluids, B5 (1993) 2343.

[36] A. Loarte, *et al*, Phys. Plasmas 11 (2004) 2668.

[37] D. Naujoks, J. Roth, K. Krieger, G. Lieder, and M. Laux, J. Nucl. Mater., 210 (1994) 43-50.

[38] G. Federici, *et al*, Nucl. Fusion, 41 (2001) 1967.

[39] D.G. Whyte, J.P. Coad, P. Franzen, and H. Maier, Nucl. Fusion, 39 (1999) 1025.

[40] R.A. Pitts, *et al*, Plasma Phys. Control. Fusion, 47 (2005) B303-B322.

[41] R.A. Pitts, *et al*, J. Nucl. Mater., 337-339 (2005) 146-153.

[42] J.P. Coad, *et al*, J. Nucl. Mater., 290-293 (2001) 224-230.

[43] J.P. Coad, *et al*, Nucl. Fusion, 46 (2006) 350-366.

[44] M.J. Rubel, *et al*, Proc. of the 32nd EPS Conf. on Plasma Physics, Tarragona, ECA Vol. 29C (2005) P2-004.

[45] M. Rubel, J.P. Coad, D. Hole, and JET-EFDA contributors, Vacuum, 78 (2005) 255-261.

[46] J.P. Coad, *et al*, Fus. Eng. Des., 74 (2005) 745-749.

[47] E. Gauthier, and G. Roupillard, J. Nucl. Mater., 313-316 (2003) 701-705.

[48] S.D. Harrisson, and D.G. Whyte, J. Nucl. Mater., in press.

[49] J. Winter, Plasma Phys. Contr. Fusion, 38 (1996) 1503-1542.

[50] ITER Technical Basis, ITER EDA Documentation Series No 24, IAEA, Vienna 2002.

[51] T. Burchell, Phys. Scr., T64 (1996) 17.

[52] G. Federici, and C.H. Skinner, in *Nuclear Fusion Research: Understanding Plasma-Surface Interactions*, Springer series in Chemical Physics, 2004.

[53] R.P. Doerner, M.J. Baldwin, and R.A. Causey, J. Nucl. Mat., 342 (2005) 63-67.

[54] V.S. Voitsenya, *et al*, Rev. Sc. Instrum., 72 (2001) 475.

[55] K. Ebisawa, *et al*, Rev. Sci. Instrum., 72 (2001) 545.

[56] T. Kakuta, *et al*, J. Nucl. Mater. 307-311 (2002) 1277.

[57] M. Decreton, T. Shikama, and E. Hodgson, J. Nucl. Mater., 329-333 (2004) 125-132.

[58] S.V. Sheludyakov, G.E. Shatalov, and K.Yu. Vukolov, Plasma Devices and Operations, 13-2 (2005), 111-122.

[59] T. Sugie, A. Costley, A. Malaquias, and C. Walker, J. Plasma Fusion Res. 79 (2003) 1051-1061.

[60] Y. Kawano, S. Chiba, and A. Inoue, Rev. Sci. Instrum., 72 (2001) 1068.

[61] A.J.H. Donné, *et al*, Rev. Sci. Instrum., 75 (2004) 4694.

[62] H. Salzmann, *et al*, Rev. Sci. Instrum., 59 (1988) 1451.

[63] T. Sugie, *et al*, Rev. Sci. Instrum., 70 (1999) 351.

[64] H. E. Bennet, and J. O. Porteus, J. Opt. Soc. America, 53 (1961) 1389.

[65] V.S. Voitsenya, *et al*, J. Nucl. Mater., 233-237 (1996) 1239-1243.

[66] A.F. Bardamid, *et al*, Surf. Coat. Technol., 103-104 (1998) 365.

[67] V.S. Voitsenya, *et al*, J. Nucl. Mater., 290-293 (2001) 336-340.

[68] A.J.H. Donné, *et al*, Proc. of the 19th IAEA Fusion Energy Conference, Lyon, France, paper CT/P-10 (2002).

[69] A. Bardamid, *et al*, Vacuum, 58 (2000) 10-15.

[70] D.H. McNeill, Rev. Sci. Instrum., 61 (1990) 1265.

[71] A. von Keudell, C. Hopf, T. Schwarz-Selinger, and W. Jacob, Nucl. Fusion, 39 (1999) 1451.

[72] B.W. Brown, C.G. Gowers, P. Nielsen, and B. Schunke, Rev. Sci. Instrum. 66 (1995) 3077.

[73] K. Narihara, and S. Hirokura, Rev. Sci. Instrum. 63 (1992) 3527.

[74] D. Reiter, in *Nuclear Fusion Research: Understanding Plasma-Surface Interactions*, Springer series in Chemical Physics, 2004.

[75] A.S. Kukushkin, 9th meeting of the ITPA TG on diagnostics, Daejon, South-Korea, 2005.

[76] A.S. Kukushkin, H.D. Pacher, V. Kotov, D. Reiter, D. Coster, and G.W. Pacher, Nucl. Fusion, 45 (2005) 608-616.

[77] N. Yoshida, *et al*, 9th meeting of the ITPA TG on diagnostics, Daejon, South-Korea, 2005.

[78] *Handbook of optical constants of solids ed. I and II*, ed. E.D. Palik, Academic Press, 1985 and 1991.

[79] A.F. Bardamid, *in press*.

[80] D. Naujoks, and W. Eckstein, J. Nucl. Mater., 230 (1996) 93-100.

[81] W.R. Weidner, J.J. Hsia, and B. Adams, Appl. Optics 24 (1985) 2225.

[82] A. Rothen, Rev. Sci. Instrum., 16 (1945) 26-30.

[83] R.M.A. Azzam, and N.M. Bashara, *Ellipsometry and polarized light*, Amsterdam: North Holland, 1986.

[84] T.E. Jenkins, J. Phys. D: Appl. Phys., 32 (1999) R45-R56.

[85] A. Röseler, *Infrared spectroscopic ellipsometry*, Akademie Verlag Berlin, 1990.

[86] G.E. Jellison, Thin Solid Films, 313-314 (1998) 33-39.

[87] M. Cardona, and L. Ley, *Photoemission in solids*, Spriger-Verlag, Berlin, 1975.

[88] J.F. Watts, in *Surface science techniques*, J.M. Walls and R. Smith (Ed.), Elsevier Science, Oxford, 1994.

[89] A. Schüler, C. Ellenberger, P. Oelhafen, C. Haug, and R. Brenn, J. Appl. Phys. 87 (2000) 4285.

[90] Y. Hirooka, *et al*, J. Vac. Sc. Technol. A, 8 (1990) 1790.

[91] R.P. Doerner, M.J. Baldwin, and K. Schmid, Phys. Scr., T111 (2004) 75-79.

[92] K. Schmid, M. Baldwin, R. Doerner, and A. Wilthner, Nucl. Fusion, 44 (2004) 815-819.

[93] M.J. Baldwin, K. Schmid, R.P. Doerner, A. Wiltner, R. Seraydarian, and C. Linsmeier, J. Nucl. Mater., 337-339 (2005) 590-594.

[94] D.G. Whyte, G.R. Tynan, R.P. Doerner, and J.N. Brooks, Nucl. Fusion, 41 (2001) 47.

[95] O. Neubauer, *et al*, Fus. Sci. Technol., 47 (2005) 76.

[96] P. Wienhold, *et al*, J. Nucl. Mater., 337-339 (2005) 1116-1120.

[97] B. Schweer, *et al*, Fus. Sci. Technol., 47 (2005) 138.

[98] A. Litnovsky, *et al*, Proc. of the 32nd EPS conference on Plasma Physics, Tarragona, 27 June-1 July 2005, ECA Vol. 29C, P4-099 (2005).

[99] A. Litnovsky, *et al*, Fus. Eng. Des., in press.

[100] G. De Temmerman, EFDA ref. TW5-TPDS-DIADEV, intermediate report, July 2005.

[101] J.L. Luxon, Nucl. Fusion, 42 (2002) 614-633.

[102] C.P.C. Wong, D.G. Whyte, R.J. Bastasz, J. Brooks, W.P. West, and W.R. Wampler, J. Nucl. Mater., 258-263 (1998) 433-439.

[103] D.L. Rudakov, *et al*, Rev. Sci. Instrum., in press.

[104] A. Litnovsky, *et al*, Fus. Eng. Des., in press.

[105] A. Litnovsky, *et al*, J. Nucl. Mater., in press.

[106] D. van Houtte, G. Martin, A. Bécoulet, J. Bucalossi, F. Saint Laurent, B. Saoutic and Tore Supra team, Fus. Eng. Des. 74 (2005) 651-658.

[107] M. Lipa, *et al*, Fus. Eng. Des. 81 (2006) 221-225.

[108] F. Hoffmann, *et al*, Plasma Phys. Control. Fusion, 36(1994) B277-B287.

[109] R.A. Pitts, R. Chavan, J.-M. Moret, Nucl. Fusion 39 (1999) 1433.

[110] M.J. Rubel, *et al*, Rev. Sci. Instrum., 77 (2006) 063501.

[111] R.A. Pitts, *et al*, J. Nucl. Mat., 241-243 (1997) 867-872.

[112] G. De Temmerman, M.J. Rubel, J.P. Coad, R.A. Pitts, J.R. Drake, and JET-EFDA contributors, Proc. of the 32nd EPS conference on Plasma Physics, Tarragona, 27 June-1 July 2005, ECA Vol. 29C, P1-076 (2005).

[113] G. De Temmerman, R.A. Pitts, V.S. Voitsenya, L. Marot, G. Veres, M. Maurer, and P. Oelhafen, J. Nucl. Mater., in press.

[114] A. Tabasso, G.F. Counsell, D. Hole, and J.P. Coad, J. Nucl. Mater., 306 (2006) 73-77.

[115] D.M. Turley, and L.E. Samuels, Metallography 14 (1981) 275-294.

[116] Y. Yamamura, and H. Tawara, Atomic Data and Nuclear Data Tables, 62 (1996) 149-253.

[117] G. De Temmerman, M. Ley, J. Boudaden, and P. Oelhafen, J. Nucl. Mater., 337-339 (2005) 956-959.

[118] P. Reinke, and P. Oelhafen, Surf. Sci., 468 (2000) 203.

[119] K.G. Tschersich, J. Nucl. Mater., 162-164 (1989) 887-891.

[120] L. Marot, G. De Temmerman, Fus. Eng. Des., in press.

[121] A. Malaquias, M. Von Hellermann, P. Lotte, S. Tugarinov, and V.S. Voitsenya, Proc. of the 30th EPS conf. on Plasma Physics and Controlled Fusion, St Petersburg, ECA Vol. 27A, O-3.4c, 2003.

[122] A. Szekeres, T. Ivanova, and K. Gesheva, J. Solid State Electrochem. 7 (2002) 17-20.

[123] G. De Temmerman, *et al*, Colloquium, Forschungszentrum Jülich, Germany, February 2004.

[124] T. Saburi, T. Suzuki, K. Kiuchi, and Y. Fujii, Thin Solid Films, 506-507 (2006) 331-336.

[125] V. Philipps, *et al*, Proc. of the 32nd EPS conference on Plasma Physics, Tarragona, 27 June-1 July 2005, ECA Vol. 29C, P1-024 (2005).

[126] M.J. Rubel, *et al*, J. Nucl. Mater., in press.

[127] C.H. Skinner, *et al*, Phys. Scr., T103 (2003) 34-37.

[128] M.J. Baldwin, and R.P. Doerner, Nucl. Fusion, 46 (2006) 444-450.

[129] D. Nishijima, M.J. Baldwin, R.P. Doerner, and R. Seraydarian, J. Nucl. Mater., in press.

[130] H. Kawamura, and M. Kato, Proc. 2nd IEA Int. Workshop Beryllium Technology for Fusion, Jackson Lake Lodge, WY, September 6-8, 1995, 204-211.

[131] B.C. Odegard Jr., C.H. Cadden, and N.Y.C. Yang, Fus. Eng. Des., 41 (1998) 63-71.

[132] B. Schunke, *et al*, Proc. of the 32nd EPS conference on Plasma Physics, Tarragona, 27 June-1 July 2005, ECA Vol. 29C, P4-082 (2005).

[133] P. Garin, Fus. Eng. Des., 49-50 (2000) 89-95.

[134] F. Sze, R. Doerner, S. Luckhardt, and R.W. Conn, J. Nucl. Mater., 246 (1997) 165-170.

[135] N. Bibic, N. Popovic, and V. Sapsig, Nucl. Inst. Meth., B2 (1984) 645-648.

[136] M. Tanemura, and F. Okuyama, Surface Sci., 181 (1987) L193-L199.

[137] D. Naujoks, R. Behrisch, V. Philipps, and B. Schweer, Plasma Phys. Control. Fusion, 36 (1994) 2021-2030.

[138] http://www.srim.org/SRIM/SRIM2003.htm

[139] W. Möller, and W. Eckstein, Nucl. Instr. and Meth., B2 (1984) 814-818.

[140] W. Möller, W. Eckstein, and J.P. Biersack, Comput. Phys. Commun., 51 (1988) 355-368.

[141] J.P. Biersack, and L.G. Haggmark, Nucl. Inst. Meth., 174 (1980) 257.

[142] W.D. Wilson, L.G. Haggmark, and J.P. Biersack, Phys. Rev. B, 15 (1977) 2458.

[143] J. Lindhard, and M. Scharff, Kgl. Danske Videnskab. Selskab. Mat. Fys. Medd., 27 (1953) 15.

[144] O.S. Oen, and M.T. Robinson, Nucl. Instrum. Meth., 132 (1976) 647.

[145] G. Veres, Private Communication.

[146] P.C. Stangeby, *The plasma boundary of magnetic fusion devices*, Institute of physics publishing, Bristol and Philadelphia, 2000.

[147] Y. Hirooka, Fus. Eng. Des., 37 (1997) 299-306.

[148] Y. Hirooka, J. Nucl. Mat., 258-263 (1998) 1045-1049.

[149] H. Maier, K. Schmid, and W. Eckstein, J. Nucl. Mater., 337-339 (2005) 480-484.

[150] A. Kreter, *et al*, Plasma Phys. Control. Fusion, 48 (2006) 1401-1412.

[151] S. Berg, B. Gelin, A. Svärdstrom, and S.M. Babulanam, Vacuum, 34 (1984) 969-973.

[152] S. Berg, C. Nender, and B. Gelin, Vacuum, 38 (1988) 621-625.

[153] B. Gelin, A.M. Barklund, C. Nender, and S. Berg, Vacuum (1990) 1074-1076.

[154] D. Naujoks, and W. Eckstein, J. Nucl. Mater., 220-222 (1995) 993-996.

[155] W. Eckstein, K. Krieger, and J. Roth, J. Nucl. Mater., 258-263 (1998) 912-916.

[156] K. Krieger, and J. Roth, J. Nucl. Mater., 290-293 (2001) 107-111.

[157] S. -Tong Lee, *et al*, Appl. Phys. Lett., 59 (1991) 785.

[158] B. Balamurugan, B.R. Mehta, and S.M. Shivaprasad, Appl. Phys. Lett., 82 (2003) 115.

[159] T. Cabioc'h, J.P. Riviere, J. Delafond, M. Jouen, and M.F Denanot, Thin Solid Films, 263 (1995) 162-168.

[160] T. Cabioc'h, A. Naudon, M. Jaouen, D. Thiaudiere, and D. Babonneau, Phil. Mag. B, 79 (1999) 501-516.

[161] T. Cabioc'h, Pivate communication.

[162] M. Mayer, V. Rohde, A. von Keudell, and ASDEX Upgrade team, J. Nucl. Mater., 313-316 (2003) 429-433.

[163] M. Wischmeier, PhD Thesis, CRPP-EPFL, LRP 799/05 (2005).

[164] M. Wykes, G. Counsell, D. McGlinchey, and C.H. Wu, Fus. Eng. Des., 56-57 (2001) 403-407.

[165] C. Arnas, *et al*, J. Nucl. Mater., 337-339 (2005) 69-73.

[166] J. Winter, and G. Gebauer, J. Nucl. Mater., 266-269 (1999) 228-233.

[167] V. Rohde, *et al*, J. Nucl. Mater., in press.

[168] C. Ingesson, 9th meeting of the ITPA TG on diagnostics, October 2005, Daejeon, Korea.

[169] C.I. Walker, *et al*, Rev. Sci. Instrum., 75 (2004) 4243.

[170] C. Grisolia, *et al*, J. Nucl. Mater., in press.

[171] M. von Hellermann, *et al*, Proc. of the 21st IAEA Fusion Energy Conference, Chengdu, China, paper IT/P1-26 (2006).

[172] H.G. Esser, *et al*, Fus. Eng. Des., 66-68 (2003) 855.

[173] J. Pamela, *et al*, J. Nucl. Mater., in press.

Publications

During doctoral studies

- M. von Hellermann, *et al* (incl. G. De Temmerman), **Pilot Experiments for the International Thermonuclear Experimental Reactor active beam spectroscopy diagnostic**, Rev. Sc. Instrum., 75 (2004) 3458.

- V.S. Voitsenya, *et al* (incl. G. De Temmerman), **The environment effect on operation of in-vessel mirrors for plasma diagnostics in fusion devices**, Proc. of the 12th International Congress on Plasma Physics, October 25-29, 2004, Nice, France.

- P. Wienhold, *et al* (incl. G. De Temmerman), **Exposure of metallic mirrors in the scrape-off layer of TEXTOR**, J. Nucl. Mater., 337-339 (2005) 1116-1120.

- G. De Temmerman, *et al*, **Study of optical properties of $\mathbf{Mo}_x\mathbf{C}_{1-x}$ films**, J. Nucl. Mater., 337-339 (2005) 956-959.

- G. De Temmerman, *et al*, **Mirror Test for ITER: Optical Characterisation of Metal Mirrors in Divertor Tokamaks**, Proc. of the 32nd EPS conference on Plasma Physics, 27 June-1 July, Tarragona, Spain, ECA Vol. 29C, P1-076 (2005).

- A. Litnovsky, G. De Temmerman, *et al*, **Direct comparative test of single crystal and polycrystalline diagnostic mirrors exposed in TEXTOR in erosion conditions**, Proc. of the 32nd EPS conference on Plasma Physics, 27 June-1 July, Tarragona, Spain, ECA Vol. 29C, P4-099 (2005).

- A. Schüler, *et al* (incl. G. De Temmerman), **Sol-Gel deposition and characterization of multilayered solicon oxide/titanium silicon mixed oxide thin films on solar collector glasses**, Proc. of the ISES World conference, August 2005, Orlando, USA.

- M. Lipa, *et al* (incl. G. De Temmerman), **Analyses of metallic first mirror samples after long term plasma exposure in Tore Supra**, Fus. Eng. Des., 81 (2006) 221-225.

- M.J. Rubel, G. De Temmerman, *et al*, **Mirror test for International Thermonuclear Reactor at the JET tokamak: an overview of the programme**, Rev. Sci. Instrum., 77 (2006) 063501.

- A. Schüler, *et al* (incl. G. De Temmerman), **Sol-GEl deposition and characterization of multilayered $SiO_2/Ti_{1-x}Si_xO_2$ coatings on solar colector glasses**, Sol. Energy Mater. Solar Cells, 90 (2006) 2894-2907.
- D.L. Rudakov, *et al* (incl. G. De Temmerman), **First tests of molybdenum mirrors for ITER diagnostics in DIII-D divertor**, Rev. Sci. Instrum., 77 (2006) 10F126.
- A. Litnovsky, *et al* (incl. G. De Temmerman), **Diagnostic mirrors for ITER: a material choice and an impact of erosion and deposition on their performance**, J. Nucl. Mater., in press.
- M.J. Rubel, G. De Temmerman, *et al*, **Fuel removal from plasma-facing components by oxidation assisted techniques: an overview of surface morphology after exposure**, J. Nucl. Mater., in press.
- G. De Temmerman, *et al*, **First mirror tests for ITER: influence of material choice on the erosion/deposition mechanisms affecting optical reflectivity**, J. Nucl. Mater., in press.
- A. Litnovsky, G. De Temmerman, *et al*, **Investigation of single crystal and poly-crystalline mirrors under erosion conditions in TEXTOR**, Fus. Eng. Des., in press.
- V.S. Voitsenya, *et al* (incl. G. De Temmerman), **The properties of contaminated films deposited on in-vessel mirrors in Large Helical Device, Tore Supra, TCV and TRIAM-1M**, Proc. of the 33rd EPS conference on Plasma Physics, June 19-23, Roma, Italy, P5-134 (2006).
- D.L. Rudakov, *et al* (incl. G. De Temmerman), **DiMES studies of temperature dependence of carbon erosion and re-deposition in the DIII-D divertor**, Phys. Scr., in press.
- A. Litnovsky, *et al* (incl. G. De Temmerman), **First dedicated tests of diagnostic mirrors in a tokamak divertor: an extended overview of experiments in DIII-D**, Fus. Eng. Des., in press.
- G. De Temmerman, *et al*, **Substrate-dependent deposition efficiency on samples exposed in the TCV divertor**, Nucl. Fusion, in preparation.
- L. Marot, G. De Temmerman, *et al*, **Rhodium coated mirrors prepared by magnetron sputtering for fusion applications**, Fus. Eng. Des., in preparation.

Earlier publications

- G. De Temmerman, *et al*, **In situ monitoring of the magnetization rotation of a soft layer using microwave permeability measurements**, J. Magn. Magn. Mater., 290-291 (2005) 1580-1583.

Gregory De Temmerman

2 RUE DE FISLIS • F-68480 WERENTZHOUSE
Phone: +33 6 16 24 84 68 • EMAIL: gregory.detemmerman@unibas.ch
16/02/1979 • FRENCH • Driving License

Chemical Engineer – PhD in experimental physics

Professionnal Experience

2003/ 2006 **PhD** at the **Physics Institute, University of Basel**
"On the lifetime of the First Mirrors in the diagnostic systems of the International Thermonuclear Experimental Reactor"

- *Physical and chemical characterizations of the damages induced on a metallic surface by the exposure to a tokamak plasma*
- *Multi scale approach of the problem : participation to the experiments carried out in different European and American tokamaks (JET, TCV, TEXTOR, TORE SUPRA, DIII-D) and laboratory simulation experiments in dedicated plasma chambers (Basel ,PISCES-B San Diego)*
- *Extensive international collaborations (UK, France, Switzerland, Germany, Ukraine, Russia, USA)*
- *Member of the « First Mirror Specialist Working Group », that resides under the wings of the ITPA (International Tokamak Physics Activities) Topical Group on diagnostics.*

2003 Training period at **Commissariat à l'Energie Atomique (CEA), Research Centre of Le Ripaut, Laboratory of Magnetic and Microwave Materials** - 6 months

Subject*:* Study of the thermomagnetic annealing of thin ferromagnetic films

- *Description of the evolution of the magnetic parameters during the annealing (rotation of the uniaxial anisotropy, permeability levels)*
- *Development of an in-situ diagnostic system for thermomagnetic annealing*
- *Development of a Kerr effect microscope allowing observation of the thin film magnetic structure at elevated temperatures (investigation of the transition para/ferromagnetic of a magnetic thin film)*

2002 Training period at **Ugine & Alz**, **ARCELOR group**, **Research Centre of Gueugnon** - 3 months

Subject : Deep drawing forming of ferritic stainless steel coated with dry lubricants

- *Development of the knowledge on the tribological behaviour of dry lubricants*

2001 **URGO S.A., Fournier Group,** Dijon - 2 months
Placement as a worker at the packaging department

1997/2000 Pose of flag tiles in concrete (realization of sundecks)
Waiter during the weekends and holidays in a bar

Skills and abilities

Surface analysis techniques	XPS/UPS, XRD, Raman, SIMS, SEM, AFM
Optical measurements	spectrophotometry (total and diffuse reflectivity), Variable Angle Spectroscopic Ellipsometry UV-VIS-MIR (FT)
Plasma/material interactions	sputtering (physical and chemical), deposition techniques, modelling
Vacuum techniques	Magnetron sputtering, evaporation (under UHV conditions), development and maintenance of a UHV system
Magnetic measurements	VSM, microwave measurements (single coil technique), longitudinal kerr effect microscope
Material Science	Ferrous alloys, Transition Metal (Mo, W, Rh) including carbides and oxides, Composites, Mechanism of deformation, Embrittlement and fracture, Corrosion Crystallography, Polishing.
Language:	English: *fluent: PhD made entirely in english, several experimental campaigns in english speaking countries (GB 10 weeks, USA 1 month)* German: *read, written and spoken*
Computer skills	MS Office, Origin, Linux, Latex, Monte Carlo code (TRIDYN)

Formation

2003/2006 **PhD at the Physics Institute, University of Basel (Switzerland)**
2003 **Graduate Chemical Engineer (French equivalent to Msc)** from ENSCL
2001/2004 Graduate School of Chemistry ENSCL (Ecole Nationale Supérieure de Chimie de Lille)

- Final year: Option Reliability and optimization of materials

1997/2000 3-year intensive preparation for the nationwide competitive entrance for french graduate schools of chemistry and physics

Interests and Activities

Guitar (electric and acoustic), sport (climbing, ski), reading